
Spontaneous Symmetry Breaking in Collective Neutrino Oscillations

David de Sousa Seixas



PROGRAMAS DE
DOUTORAMENTO
FCT

München 2014

Spontaneous Symmetry Breaking in Collective Neutrino Oscillations

David de Sousa Seixas

Dissertation
an der Fakultät für Physik
der Ludwig-Maximilians-Universität
München

vorgelegt von
David de Sousa Seixas
aus Lissabon

München, den 14. Oktober 2014

This thesis is based on the author's work partly published in

- S. Sarikas, D. de Sousa Seixas, G. Raffelt, *Spurious instabilities in multiangle simulations of collective flavor conversion*, Phys. Rev. D 86, 125020, 2012 (arXiv:1210.4557),
- G. Raffelt, S. Sarikas, D. de Sousa Seixas, *Axial symmetry breaking in self-induced flavor conversion of supernova neutrino fluxes*, Phys. Rev. Lett. 111, 091101, 2013 (arXiv:1305.7140),
- G. Raffelt, D. de Sousa Seixas, *Neutrino flavor pendulum in both mass hierarchies*, Phys. Rev. D 88, 045031, 2013 (arXiv:1307.7625),
- S. Chakraborty, A. Mirizzi, N. Saviano, D. de Sousa Seixas, *Suppression of the multi-azimuthal-angle instability in dense neutrino gas during supernova accretion phase*, Phys. Rev. D 89, 093001, 2014 (arXiv:1402.1767),

conducted from September 2010 until September 2014 at the Max-Planck-Institut für Physik (Werner-Heisenberg-Institut), München, under the supervision of PD Dr. Georg Raffelt.

This thesis was supported by Fundação para a Ciência e a Tecnologia under grant SFRH/BD/66264/2009.

Erstgutachter: PD Dr. Georg Raffelt

Zweitgutachter: Prof. Dr. Gerhard Buchalla

Datum der mündlichen Prüfung: 14.10.2014

Table of Contents

Abstract	vii
Introduction	xii
1 Neutrino flavor oscillations	1
1.1 Flavor oscillations	1
1.1.1 What is flavor?	1
1.1.2 Vacuum oscillations	6
1.1.3 Density matrices	10
1.1.4 Polarization vectors	11
1.1.5 Matter effect	14
1.2 Canonical variables and adiabatic transitions	17
1.3 MSW effect	19
1.4 Neutrino-neutrino interaction	23
1.5 Evolution of flavor in a neutrino ensemble	24
1.5.1 Neutrinos in a box	24
1.5.2 Flavor continuity equation	26
1.5.3 Continuity and initial conditions in flavor space	27
1.6 Self-consistent approach and EoMs	29
1.7 Summary	30
2 Collective oscillations	33
2.1 Energy spectrum	33
2.2 Co-rotating frame	35
2.3 Conserved quantities: Hamilton function and lepton number	38
2.4 Fixed configurations and synchronized oscillations	39
2.5 Spectral splits	41
2.6 Summary	42
3 Bipolar oscillations and spontaneous symmetry breaking	45
3.1 Flavor evolution of a uniform isotropic gas	45
3.1.1 Stability of the flavor eigenstate	46
3.1.2 Flavor pendulum	50
3.1.3 Bipolar oscillation	51

3.1.4	Beyond Rabi oscillations in Bose-Einstein condensates	52
3.1.5	Adiabatic invariants	54
3.2	Spontaneous symmetry breaking	55
3.2.1	Isotropic equations of motion with explicit velocity dependence	55
3.2.2	Departure from the symmetric solution	56
3.2.3	Chaotic behavior	64
3.3	Summary	65
4	Oscillations in a uniform isotropic ensemble	67
4.1	Flavor evolution in a uniform neutrino fluid	67
4.2	Stability of an isotropic distribution	71
4.3	Discretization of the angular distribution	73
4.4	Expansion in spherical harmonics	75
4.5	Summary	77
5	Core-collapse supernovae	79
5.1	Collapse of the progenitor	79
5.2	Core bounce and shockwave	82
5.3	Neutrino sphere	83
5.4	Accretion phase	83
5.5	Cooling	85
5.6	Summary	85
6	Collective oscillations in supernovae	87
6.1	Equations of motion for the flux of neutrinos	87
6.1.1	Stationarity	87
6.1.2	Isotropies	89
6.1.3	Angular variables and spectra	90
6.1.4	Equation of motion	91
6.2	General conditions for the stability of the flavor state	94
6.2.1	Eigenvalue equation	94
6.2.2	Spontaneous symmetry breaking in numerical simulations	100
6.3	Spurious instabilities	100
6.3.1	Single-angle vs. uniform distribution	102
6.3.2	Discrete approximation of the uniform spectrum	102
6.4	Summary	104
	Conclusions	109
	Bibliography	113
	Acknowledgments	118

Abstract

We explore the phenomenon of spontaneous symmetry breaking in the context of collective neutrino flavor oscillations. Namely, we investigate the spontaneous breaking of isotropy in a homogeneous gas of neutrinos and of azimuthal isotropy in the context of core-collapse supernovae. For the homogeneous gas, a simple one-dimensional model is analysed in order to demonstrate the phenomenon and understand the connection to the linearized stability analysis. The effect is then investigated in the context of isotropic emission from a supernova core. We show that an azimuthally isotropic flavor configuration is unstable under the differential equations of motion. We analyse the linear stability of propagation in the flavor state and the important consequences to the general prediction of collective flavor conversion. This symmetry-breaking instability is sensitive to the ordering of the neutrino masses.

Zusammenfassung

Wir untersuchen das Phänomen der spontanen Symmetriebrechung im Kontext kollektiver Neutrino-Flavour-Oszillationen. Insbesondere betrachten wir die spontane Brechung der Isotropie in einem homogenen Neutrinogas und die Brechung der azimuthalen Symmetrie im Kontext von Kernkollaps-Supernovae. Für das homogene Gas untersuchen wir ein einfaches eindimensionales Modell, um das Phänomen vorzuführen und die Verbindung zur linearisierten Stabilitätsanalyse herauszuarbeiten. Dann wird der Effekt im Kontext von isotroper Neutrinoausstrahlung aus einem Supernova-Kern angewandt. Wir zeigen, dass eine isotrope Flavour-Konfiguration unter den differentiellen Bewegungsgleichungen instabil ist. Wir analysieren die lineare Stabilität der Propagation im Flavour-Zustand und wichtige Konsequenzen für die allgemeine Vorhersage kollektiver Flavour-Konversion. Diese symmetriebrechende Instabilität wird von der Anordnung (“Hierarchie”) der Neutrinomassen beeinflusst.

Notation and acronyms

Acronyms:

- CC: charged current
- NC: neutral current
- SN: supernova
- MA: multi-angle
- MZA: multi-zenith-angle
- MAA: multi-azimuthal-angle
- SASI: Standing Accretion Shock Instability
- LESA: Lepton-number Emission Self-sustained Asymmetry

Vector notation:

Three-component vectors are denoted by bold-face letters \mathbf{P} . Three-component vectors in physical space are denoted by arrows \vec{v} . A boldface letter $\vec{\mathbf{A}}$ with an arrow means a vector of flavor vectors. Sometimes, vectors are denoted by a complex number and a real number $\mathbf{P} = (p, P_z)$, instead of the usual form of three real numbers $\mathbf{P} = (P_x, P_y, P_z)$, with the imaginary unit being the 90° rotation on the plane perpendicular to the z direction. This notation has been introduced as it distinguishes clearly the diagonal part P_z of the density matrix and the off-diagonal part p and p^* , in the basis where z is the direction of the diagonal Pauli matrix σ_z . The three-component form can be recovered by taking $P_x = \text{Re } p$ and $P_y = \text{Im } p$.

Introduction

‘[...] out of the hole came a mouse and, barely noticeable, it had caused a great stir in the dogs. So we looked at each other in understanding: we didn’t have a destination, yet we had walked with determination.’

Memoirs of a Gauge, A. Kabelschacht

The Standard Model of particle physics has had a resounding experimental success. With beautiful simplicity, it encompasses in a simple framework an extensive range of phenomena. But the true beauty of physics begins where one looks at the complexity of dynamical behavior such a simple set of particles can exhibit. From neutrinos to magnets to fireflies, it is with the outcome of their interactions that we weave the tapestry of nature and find common ground between distant phenomena. This work focuses on one such case in which a dense fluid of seemingly elusive particles behaves in new and puzzling ways.

For a long time scientists looked up at the stars hoping, with gargantuan detectors, to read in them the parameter space of neutrinos. It was from the atmospheric neutrinos that the first undeniable indication of neutrino masses came from. When Super-Kamiokande looked at the flux of neutrinos produced in our planet’s atmosphere, they noticed an asymmetry between the number of muon neutrinos coming from above (from the sky) and from below (through the Earth). These fluxes should be identical as the cosmic rays form a uniform directional spectrum. The results of this experiment showed that flavor was not conserved throughout the propagation of neutrinos, a feature which could best be explained by flavor oscillations, a consequence of neutrino masses. This proof cascaded through the theory and experimental divisions of the world, allowing physicists to finally explain another problem which stood unresolved at the time: the solar neutrino problem. Davis and his collaborators had captured a flux of solar neutrinos lower than the one computed from Bahcall’s model of nuclear processes in the Sun, which predicted a flux of electron-like neutrinos much higher than the measured one. The newly observationally-supported theory of neutrino oscillations led to a series of experiments – of which SNO and KamLAND are the most notable – that set out to test and eventually prove that the missing flux of electron neutrinos had transitioned into the two other flavors, muon and tau. Since then, well-controlled reactor and beam experiments have allowed the

scientific community to measure most of the fundamental parameters of the neutrino sector, such as the difference between the masses and the particular mixture of flavors involved in each mass state. A few parameters are still missing, which are difficult or even impossible to see in oscillation experiments. The absolute values of the masses, for example, cannot be determined by flavor oscillation experiments. On the other hand, the so-called mass hierarchy – the way the neutrino masses are ordered – should be soon determined in the next generation of oscillation experiments.

Nevertheless, this is not the end of the story for stellar neutrinos. While trying to explain the missing flux of electron neutrinos from the Sun, Mikheyev, Smirnov and Wolfenstein came to the conclusion that the interaction with the matter inside the star plays an important role in the neutrino dispersion relation, leading to visible effects in flavor oscillations. The phenomenon came to be known as the MSW effect and, to the best of our knowledge, is the dominating effect at neutrino energies higher than 5 MeV. The importance of this interaction led to further attention towards another puzzling phenomenon: collective flavor oscillations. If neutrinos are placed in an environment where their density is high enough, they can act as a refractive medium for their own oscillatory behavior. Such media are rare. In fact, there are only three known cases in which this effect might be of relevance: the dense and hot early universe, the merging of two neutron stars, and a core-collapse supernova.

Core-collapse supernovae release most of their energy in the form of neutrinos. This flux is high enough that neutrinos can feel each other's presence. The resulting equations are non-linear and produce a myriad of interesting effects which have just recently begun to be explored. For example, whole ranges of the energy spectrum can swap their flavor, in an effect known as a *spectral split*. There can also be synchronized oscillations, where all energy modes change flavor in sync in spite of their different oscillation frequencies in vacuum. Even a quantum analogue of a pendulum was discovered, when it was found that in a uniform isotropic gas, flavor changes from one state to another with the dynamics of a classical pendulum. A similar effect can actually be and has already been measured in the transitions of condensed Rubidium atoms between two traps, and is completely analogous to the collective oscillations of neutrinos.

Most of these effects still await a consistent analysis to sort out their right placement in the actual dynamics of a supernova. The difficulty lies in the often strenuous analytical treatment of the collective behavior, in its demanding numerical needs, and in not-quite-successful-yet supernova simulations. For the study of neutrino oscillations in a supernova requires tackling a seven-dimensional partial differential equation (one dimension for time, three dimensions for the position in space, three for the momentum). It requires keeping track of the countless local non-linear interactions between beams travelling in different directions, while simultaneously paying attention to the evolution of the supernova. This problem is very hard to solve both analytically and numerically and one eventually turns to assumptions of symmetry and approximations of the spectra that help to simplify the equations. Despite these assumptions, the problem is still difficult and requires great numerical power. On the one hand, the qualitative description of these phenomena (synchronized

oscillations, spectral splits) seem to be independent of the simplifications, so these investigations are very useful. On the other hand, the details and the region of parameter space in which the effects occur do seem to be sensitive to these assumptions, and the frequently over-simplistic models can grossly mispredict the final results. They can mistakenly predict the stability of the flavor states under propagation, when actually these become unstable and non-linear behavior is observed.

This thesis presents one such case in which a naive assumption of spatial symmetry erroneously dismissed nonlinear flavor conversion in a big part of parameter space. As a consequence, we found that an isotropic emission does not necessarily imply an isotropic flavor evolution. This is a classic case of spontaneous symmetry breaking.

In the first chapter of this thesis we will describe the basics of neutrino oscillations, including vacuum, matter and neutrino-neutrino interactions, while simultaneously introducing the polarization vector language, which amounts to describing the flavor content of the many momentum modes in terms of positions on a three-dimensional Bloch sphere. The second chapter introduces the phenomenon of collective oscillations and establishes the general equations that describe it. In the third chapter we analyse two simple models and expose the limitations of some of the assumptions made in the literature up until recently, namely, of isotropy. Which leads us to the fourth chapter, where we analyse the onset of flavor conversion when the many energy and direction modes are kept explicit and show how this “symmetry breaking” comes about in the full three-dimensional isotropic case. In the fifth chapter we will hand the reader the relevant information about the supernova dynamics and neutrino fluxes which will be required for the rest of the last chapter. Finally, in the sixth chapter, we develop the onset of flavor instabilities in supernovae, how they inherit the different instabilities and how these instabilities reveal themselves in closer-to-realistic models. We also analyse how these instabilities change when the modes are discretized. This is important for numerical simulations since discretization is a necessity. Discretized versions of the equations can lead to drastically different results. Finally, we summarize our findings in a short chapter of conclusions.

CHAPTER 1

Neutrino flavor oscillations

The phenomenon of neutrino flavor oscillations is a text-book example of quantum interference. It can be simply summarized by the fact that weak charged-current (CC) reactions mix different mass states, and that this mixture changes with propagation. This means we have in neutrinos a window into the interplay of interactions with the mass spectrum, the so-called *flavor mixing*. Thanks to this effect, neutrino oscillations have allowed us to measure many parameters of the neutrino sector.

In this chapter we will present the key points of the theory of neutrino oscillations. We explain the different refractive terms these particles are subjected to when they propagate in vacuum, in a medium, and in the presence of other neutrinos, and how these media alter the evolution of the flavor content of the ensemble. In a medium of neutrinos, the neutrinos themselves can become the very background medium that causes the flavor refraction. Because the background participates in the oscillation process, oscillations in – or rather of – this medium are called collective oscillations. We will also be introducing the reader to the formalism of polarization vectors, which appears in many other contexts as it allows for a very intuitive way to visualize the dynamics of the system as the interaction of many classical spins. We will end the chapter with the introduction of the neutrino-neutrino refractive effect.

1.1 Flavor oscillations

1.1.1 What is flavor?

A great part of contemporary particle physics is dedicated to understanding the fundamental origin of particle masses. Recently, the best candidate – the Higgs mechanism – has been validated to a certain extent, marking a milestone into solving this problem. However, many questions remain to be answered. One very puzzling, if not the most puzzling, is the so-called *flavor problem*. This problem is simply that each particle, defined by which interactions it takes part in, comes in several different masses. And even more astonishingly, one can create states in which a particle is in a superposition of different mass states, making mass look like any other quantum property, except

for the fact that we still cannot compute its spectrum from some more fundamental principles. We will in this section follow a simple physical example in which we show, to some extent, the basic features of flavor as they appear in the context of neutrino physics. We will use the decay of pions because of their practical role in experimental neutrino physics.

Charged pions, composed of a pair of an up and a down quark ($\pi^+ = u\bar{d}$ and $\pi^- = d\bar{u}$) decay into a charged lepton and a neutrino: $\pi^+ \rightarrow \ell^+ + \nu$ and $\pi^- \rightarrow \ell^- + \bar{\nu}$. Pions are produced in the laboratory by bombarding a graphite target with high-energy protons. The pions produced in these collisions are extracted electromagnetically and let to decay in a beam pipe. The charged-leptons are then absorbed in a layer of concrete and steel which filters the beam into a pure neutrino (or anti-neutrino) beam. We will use the decay of pions as a conceptual experiment to explain flavor.

In this thought experiment, we are not interested in creating a pure beam of neutrinos like it is commonly done in neutrino oscillation experiments, but instead we want to measure the mass of the product particles in the decay of charged pions. For that purpose, imagine we have developed charged-lepton detectors and neutrino detectors that can measure momentum and energy to such a precision that we can infer from those measurements the mass of the particle from the relativistic equation

$$m^2 = E^2 - p^2 \tag{1.1}$$

in natural units. Consider now that we have a beam of π^+ that decay into $\pi^+ \rightarrow l^+ + \nu$, a lepton of positive charge and a neutrino. We now place our mass detectors in front of the beam pipe where the pions decay and measure the mass of both charged lepton and neutrino. Say we look at the results of the measurement of the mass of the charged leptons. As depicted in figure 1.1, we would see two peaks in the mass spectrum. One high peak at the value of 105 MeV and a much smaller one at 511 keV. We call these peaks the muon (105 MeV) and the electron (511 keV). Now say that we select from our data only the events in which we measured a charged-lepton mass of 511 keV, i.e., in the terminology just introduced $\pi^+ \rightarrow e^+ + \nu$ and we look at the relative spectrum of the masses of the accompanying neutrinos. Then we would see three peaks in the mass spectrum of the neutrinos despite the fact that we selected events where the mass of the charged lepton was single valued. This part of the experiment is still impossible today and though we do know different neutrino masses exist, we still do not know their absolute values. If we then look at the rest of the data set, that is, events of the type $\pi^+ \rightarrow \mu^+ + \nu$ we would observe the same phenomenon, the same three peaks, but with different heights. This means that a precise measurement of the mass of the positively-charged lepton necessarily implies an indetermination in the mass of the neutrino.

Obviously, if we analyse the data set in the reverse order and discriminate events of specific neutrino mass, we would for each set find two peaks in the spectrum of charged-lepton masses. This unavoidably mixed correlation between the mass of the charged lepton and the neutrino is called *flavor mixing*. This experiment indicates that the pion decay always produces an entangled state of lepton masses. An accurate knowledge of the charged-lepton's mass implies an indeterminate

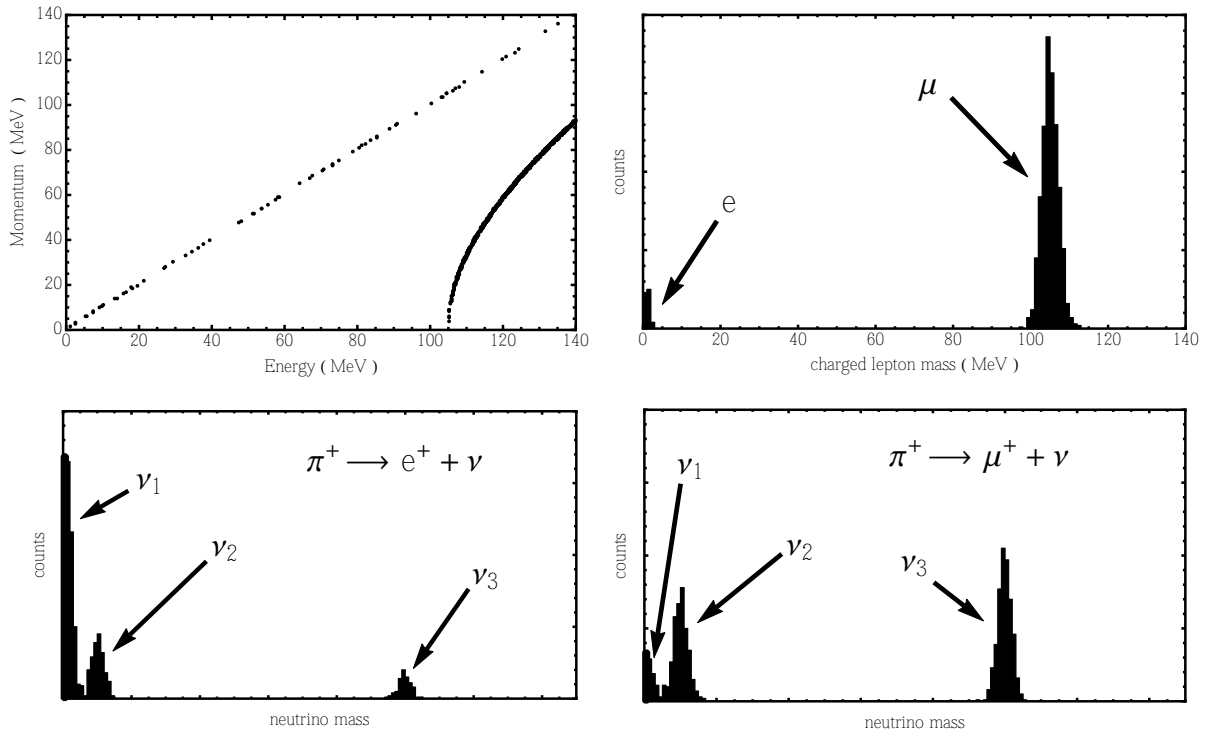


Figure 1.1: *Top left:* Schematic result of a statistical measurement of the charged-lepton's dispersion relation in the reaction $\pi^+ \rightarrow \ell^+ + \nu$. The electron line is drawn with fewer events representing the smaller decay rate of this mode. *Top right:* Corresponding mass spectrum of the measurement of the charged-lepton's dispersion relation. The lighter mode is called an electron (0.511 MeV) and the heavier mode is called a muon (105 MeV). The width of the peaks as depicted is arbitrary. *Bottom left:* Schematic result of an analysis performed on the subset of events $\pi^+ \rightarrow e^+ + \nu$. Three mass modes are visible for the neutrino. The height of the peaks is related to the mixing matrix terms $|U_{ei}|^2$, $i = 1, 2, 3$. This case corresponds to the normal hierarchy. *Bottom right:* Same for $\pi^+ \rightarrow \mu^+ + \nu$. Note that the peaks have different heights.

knowledge of the neutrino's mass and vice versa. In spite of many and diverse attempts, no one has yet successfully explained either the spectrum of masses that is observed, or why electroweak CC reactions like pion decay always produce a mix of mass states. These results apply to any CC process, i.e., where a charged W boson is involved. A coupling to the W^\pm always mixes the eigenstates of mass of the participating particles. It is important to point out that neutral-current (NC) reactions like Z^0 decay do not exhibit this peculiar feature. The neutral boson Z^0 decays into $Z^0 \rightarrow \text{particle} + \text{anti-particle}$. One still sees a mass spectrum but no mixing, that is, if one of the decay products is a 511 keV lepton, then so is the other one. This property is known as the absence of flavor-changing NCs.

According to measurements, charged leptons also have three masses. The largest mass of the

charged lepton, called the tau, does not appear in figure 1.1 because it is too heavy ($m_\tau = 1777$ MeV) to be produced in decays of charged pions with a mass of 140 MeV. The mass measurement operator, like any other measurement in quantum mechanics, can be described in terms of its eigenvalues and its eigenvectors. If we call e , μ and τ the eigenstates of a mass measurement performed on the charged lepton then the mass measurement operator can be described as

$$\begin{pmatrix} m_e & 0 & 0 \\ 0 & m_\mu & 0 \\ 0 & 0 & m_\tau \end{pmatrix} \quad (1.2)$$

in terms of the three eigenvectors of the mass measurement

$$|e\rangle = \begin{pmatrix} 1 \\ 0 \\ 0 \end{pmatrix}, \quad |\mu\rangle = \begin{pmatrix} 0 \\ 1 \\ 0 \end{pmatrix}, \quad |\tau\rangle = \begin{pmatrix} 0 \\ 0 \\ 1 \end{pmatrix}. \quad (1.3)$$

The same can be done for the neutrino with the three eigenvalues m_1 , m_2 and m_3 , and the three eigenvectors $|\nu_1\rangle$, $|\nu_2\rangle$ and $|\nu_3\rangle$.

Neutrino mixing is equivalent to saying that CC reactions like pion decay always produce an entangled combination of mass states. To see how this comes about, consider the resulting state vector in the eigenbasis of the charged-lepton mass:

$$\begin{aligned} & \mathcal{A}(\pi^+ \rightarrow e^+ + \nu) |e\rangle (U_{e1}|\nu_1\rangle + U_{e2}|\nu_2\rangle + U_{e3}|\nu_3\rangle) \\ & + \mathcal{A}(\pi^+ \rightarrow \mu^+ + \nu) |\mu\rangle (U_{\mu1}|\nu_1\rangle + U_{\mu2}|\nu_2\rangle + U_{\mu3}|\nu_3\rangle) \\ & \equiv \mathcal{A}(\pi^+ \rightarrow e^+ + \nu) |e\rangle |\nu_e\rangle + \mathcal{A}(\pi^+ \rightarrow \mu^+ + \nu) |\mu\rangle |\nu_\mu\rangle, \end{aligned} \quad (1.4)$$

where \mathcal{A} denotes the amplitude of each decay channel¹. The decay rate Γ , the square of the modulus of \mathcal{A} integrated over phase-space, scales roughly with $\Gamma \sim m_\ell^2$ which means the muon mass is measured about 10 000 times more often than the electron mass in a pion decay experiment. We have introduced the *neutrino flavor states* $|\nu_e\rangle$ and $|\nu_\mu\rangle$ defined as the superposition of neutrino mass states that one encounters when the mass of the charged lepton has been accurately measured.

¹Actually, we have neglected the dependence on momentum. The complete form of the final state is

$$\sum_{\vec{p}, \vec{q}_\ell, \vec{q}_\nu} \sum_{i,j} U_{ij} \mathcal{A}(\pi^+ \rightarrow \ell^+ + \nu) \langle \vec{q}_\ell | \ell_i \rangle \langle \vec{q}_\nu | \nu_j \rangle,$$

where one has to sum over the amplitude of obtaining different momenta and energies for the pion (\vec{p}), the charged lepton (\vec{q}_ℓ) and the neutrino (\vec{q}_ν) and over the different mass states for ℓ^+ and ν . In this way, if the momenta and energy of the pion and the charged lepton are perfectly known then so is the mass of the neutrino, simply because the only non-zero amplitude in that case is the one that preserves the conservation of energy and momentum.

In general, one defines the mixing matrix [1] as

$$\begin{pmatrix} |\nu_e\rangle \\ |\nu_\mu\rangle \\ |\nu_\tau\rangle \end{pmatrix} = U \begin{pmatrix} |\nu_1\rangle \\ |\nu_2\rangle \\ |\nu_3\rangle \end{pmatrix}. \quad (1.5)$$

This mixing is the same for any CC process because they all involve the intervention of a W^\pm boson. This matrix is unitary because of the experimental fact that charged leptons and neutrinos must be in one of the three known mass states. Searches for additional neutrino mass states are a present field of experiment. These neutrinos would only interact at very small rates with the known particles (otherwise we would have seen them already) and are therefore called *sterile neutrinos*.

A common parametrization of the mixing matrix factorizes the complete mixing into three rotations of two mass states [2]

$$U = \begin{pmatrix} 1 & 0 & 0 \\ 0 & c_{23} & s_{23} \\ 0 & -s_{23} & c_{23} \end{pmatrix} \begin{pmatrix} c_{13} & 0 & s_{13}e^{-i\delta} \\ 0 & 1 & 0 \\ -s_{13}e^{i\delta} & 0 & c_{13} \end{pmatrix} \begin{pmatrix} c_{12} & s_{12} & 0 \\ -s_{12} & c_{12} & 0 \\ 0 & 0 & 1 \end{pmatrix} \begin{pmatrix} 1 & 0 & 0 \\ 0 & e^{i\alpha_1} & 0 \\ 0 & 0 & e^{i\alpha_2} \end{pmatrix}. \quad (1.6)$$

The mass states are organized in decreasing mixing with the electron flavor. They are chosen that way so that a smaller mixing angle means an larger amount of electron flavor. For example, if only the $1 \leftrightarrow 2$ mixing is present and nothing else,

$$\begin{pmatrix} |\nu_e\rangle \\ |\nu_\mu\rangle \\ |\nu_\tau\rangle \end{pmatrix} = \begin{pmatrix} c_{12} & s_{12} & 0 \\ -s_{12} & c_{12} & 0 \\ 0 & 0 & 1 \end{pmatrix} \begin{pmatrix} |\nu_1\rangle \\ |\nu_2\rangle \\ |\nu_3\rangle \end{pmatrix}, \quad (1.7)$$

then a small θ_{12} means $|\nu_e\rangle \approx |\nu_1\rangle$, $|\nu_\mu\rangle \approx |\nu_2\rangle$. The numbering of the mass states does not indicate anything about the ordering of their masses.

All three angles θ_{12} , θ_{13} and θ_{23} were measured in the recent years, with θ_{13} , the smallest mixing angle, being measured only two years ago [3]. The CP-violating phase δ is still unknown, as are the two Majorana phases α_1 and α_2 , relevant only if neutrinos are of Majorana type. The current values of the parameters of the neutrino sector are summarized in table 1.1. For an in-depth review of present neutrino data see the report on neutrino masses, mixing and oscillation by the Particle Data Group [4]. For a review on what to expect from future reactor experiments see reference [5].

In practice, the conceptual experiment of mass entanglement of a charged lepton and a neutrino is very hard to realize, if even possible at all. The challenge stems from the fact that the masses of the neutrinos are much smaller than the masses of the charged leptons. Therefore, if one were to measure the energy and the momentum of the neutrino to a sufficient precision for the distinction of the different masses, one would have to run the detection mechanism for an enormous amount of time and over a gigantic distance, during which the charged lepton would have lost its coherence,

effectively measuring its mass. Because of this practical issue, one tends to study neutrino physics in terms of the charged-lepton mass states, or as it is generally referred to, the neutrino flavor states, since one can easily measure the mass of the charged lepton but not that of the neutrino [6].

1.1.2 Vacuum oscillations

We will now show the flavor of a neutrino can change as it propagates in vacuum. This phenomenon is an interference phenomenon called flavor oscillation. For that we need to first know what the properties of propagation of a mass state in vacuum are. In most cases, it is enough to consider an equation that tracks the evolution of the flavor of a neutrino of left-handed helicity (or an anti-neutrino of right-handed helicity).

In theory, being neutral fermions, neutrinos can obey either the Dirac or the Majorana equation [7], or a mixture of the two (see [8] for experimental attempts to determine which). These equations distinguish components of different helicity. The V – A nature of weak interactions makes it so that neutrinos always appear polarized with left-handed helicity and anti-neutrinos with right-handed helicity². But in vacuum, transitions between components of different spin are prevented by angular momentum conservation, so it is enough to consider each component separately.

Still, any process which breaks isotropy in the transverse direction to the motion of the neutrino can induce transitions between helicity states. This can happen, for example, in a strong magnetic field. For Dirac neutrinos, transitions between left and right helicity states can be induced through the neutrino’s dipole moment. For Majorana neutrinos, helicity transitions cause spin-flavor oscillations in a magnetic field between neutrinos of different helicity and flavor. These effects tend to be neglected because of the smallness of these transition moments. Nevertheless, there have been recent claims that this effect could become relevant in the context of collective oscillations in supernovae (see [9–11]). Whether these claims are sustained in future studies is one example of the on-going development of this field. For now, we assume that it is enough to study the evolution of left-helicity neutrinos, as that is how neutrinos are generally polarized when they are produced.

Going back to our example of a neutrino beam produced with pion decays, consider we have measured a positron in the charged-lepton detector. The accompanying neutrino is now in the state $|\nu_e\rangle$, which is a mixed state of different mass states. That means the neutrino propagates with three different dispersion relations! If we consider it to be emitted as a plane wave of exact energy E , the Klein-Gordon equation can be linearized to study the evolution of flavor with the distance x from the source. Denoting $\nu_i(x)$ for the amplitude of i -th mass state $|\nu_i\rangle$ as a function of x ,

$$-i\partial_x\langle x|\nu_i\rangle = p_i\nu_i(x) = \sqrt{E^2 - m_i^2}\nu_i(x) \approx \left(E - \frac{m_i^2}{2E}\right)\nu_i(x). \quad (1.8)$$

²Actually, the V – A nature polarizes neutrinos in chiral states but since chirality and helicity are approximately equal for ultrarelativistic states, such as the neutrinos masses, one may get away with this small abuse of language.

We have used the ultra-relativistic approximation $p \approx E - m^2/2E$. Each mass state has a different momentum computed from the relativistic dispersion relation. Over distance, the superposition of mass states evolves as

$$\begin{aligned} -i\partial_x \langle x | \nu_e \rangle &= -i\partial_x (U_{e1} \langle x | \nu_1 \rangle + U_{e2} \langle x | \nu_2 \rangle + U_{e3} \langle x | \nu_3 \rangle) \\ &= U_{e1} p_1 \nu_1(x) + U_{e2} p_2 \nu_2(x) + U_{e3} p_3 \nu_3(x) \\ &\approx E \nu_e(x) - \frac{1}{2E} [U_{e1} m_1^2 \nu_1(x) + U_{e2} m_2^2 \nu_2(x) + U_{e3} m_3^2 \nu_3(x)] . \end{aligned} \quad (1.9)$$

This in turn implies that the amplitude of the muon neutrino varies in distance as

$$\nu_e(x) = \sum_i U_{ei} e^{-i p_i x} \nu_i(0) \approx e^{-i E x} \sum_i U_{ei} e^{i (m_i^2/2E)x} \nu_i(0) . \quad (1.10)$$

The survival amplitude of this flavor state is

$$\begin{aligned} P_{ee}(x) &= \langle \nu_e | 0 \rangle \langle x | \nu_e \rangle \approx e^{-i E x} \sum_i U_{ei} e^{i (m_i^2/2E)x} \langle \nu_e | \nu_i \rangle \\ &= e^{-i E x} \sum_{i,j} U_{ei} e^{i (m_i^2/2E)x} U_{ej}^* \langle \nu_j | \nu_i \rangle \\ &= e^{-i E x} \sum_i |U_{ei}|^2 e^{i (m_i^2/2E)x} , \\ &= e^{-i (E - m_1^2/2E)x} \sum_i |U_{ei}|^2 e^{i x (m_i^2 - m_1^2)/2E} . \end{aligned} \quad (1.11)$$

The survival probability of the linear combination $|\nu_e\rangle$ of neutrino mass states is given by the square of the norm of this complex amplitude. We see right away that it is not conserved and that it depends on two oscillation frequencies that are related to the differences of the square of the neutrino masses $\omega_i \equiv (m_1^2 - m_i^2)/2E$, $i = 2, 3$. We call $m_2^2 - m_1^2 \equiv \Delta m_{\text{sol}}^2$ the solar mass difference and $|m_3^2 - m_1^2| \approx |m_3^2 - m_2^2| \equiv \Delta m_{\text{atm}}^2$ the atmospheric mass difference. We know that $\Delta m_{\text{sol}}^2 = 7.54 \pm 0.26 \times 10^{-5} \text{eV}^2$ and that $|\Delta m_{\text{atm}}^2| = 2.43 \pm 0.10 \times 10^{-3} \text{eV}^2$ [4]. The names *solar* and *atmospheric* refer to the type of experiments that are sensitive to these mass differences. The measured atmospheric mass difference is not a signed value which means we still do not know how to place the third mass state relative to the first and second (cf. figure 1.2). The neutrino masses are numbered according to their electron flavor content, i.e., 1 is the state with the largest mixing with the electron flavor, 2 the second largest and so on. Thanks to the study of neutrino oscillations in solar matter, we know that $m_2 > m_1$. The two remaining possible arrangements are called *mass hierarchies* or *mass orderings*. The *normal hierarchy* (NH) is defined as $m_3 > m_2 > m_1$ and the *inverted hierarchy* (IH) is defined as $m_2 > m_1 > m_3$. For a review on the experimental probes into the mass hierarchy, see [12, 13].

The complete 3×3 treatment can lead to very complicated interference patterns. Fortunately,

Parameters	NH	IH
Δm_{21}^2	$7.54^{+0.26}_{-0.22}$	$7.54^{+0.26}_{-0.22}$
$\Delta m_{31}^2 \mp \Delta m_{21}^2/2$	$2.43^{+0.06}_{-0.10}$	$2.42^{+0.07}_{-0.11}$
$\sin^2 \theta_{12}$	$0.307^{+0.018}_{-0.016}$	$0.307^{+0.018}_{-0.016}$
$\sin^2 \theta_{23}$	$0.386^{+0.024}_{-0.021}$	$0.392^{+0.039}_{-0.022}$
$\sin^2 \theta_{13}$	$0.0241^{+0.0025}_{-0.0025}$	$0.0244^{+0.0023}_{-0.0025}$

Table 1.1: Current status of neutrino oscillation parameters according to the Particle Data Group [4]. The values are the best-fits assuming $m_1 < m_2 < m_3$ (NH) or $m_3 < m_1 < m_2$ (IH). In NH, the second line reads $\Delta m_{31}^2 - \Delta m_{21}^2/2$ whereas in IH the second line reads $\Delta m^2 \equiv \Delta m_{31}^2 + \Delta m_{21}^2/2$.

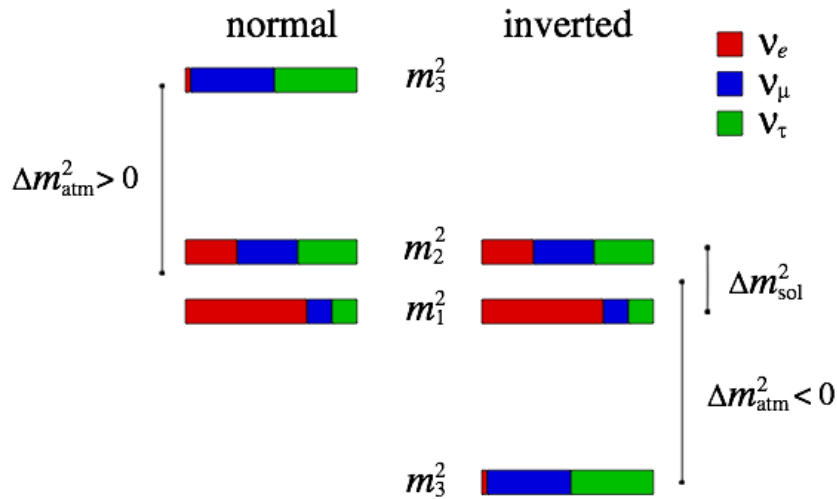


Figure 1.2: The different probabilities of a neutrino being in each of the interaction states when in a mass state. These numbers correspond to the relative probabilities of producing an electron, muon or tau through CC interaction in the ultrarelativistic limit.

one can very often treat the interference of only two states. For instance, since one mass squared difference is about 30 times larger than the other, one can very often treat the two oscillations as decoupled (cf. figure 1.3), because the solar oscillation ($1 \leftrightarrow 2$) happens over distances 30 times larger than the atmospheric oscillation ($1 \leftrightarrow 3 \approx 2 \leftrightarrow 3$). Also, the smallness of θ_{13} compared to the other two angles also means in many cases the approximation $\theta_{13} \approx 0$ leads to a defacto two-state interference. In fact, until recently, only two-flavor oscillations were observed until the small θ_{13}

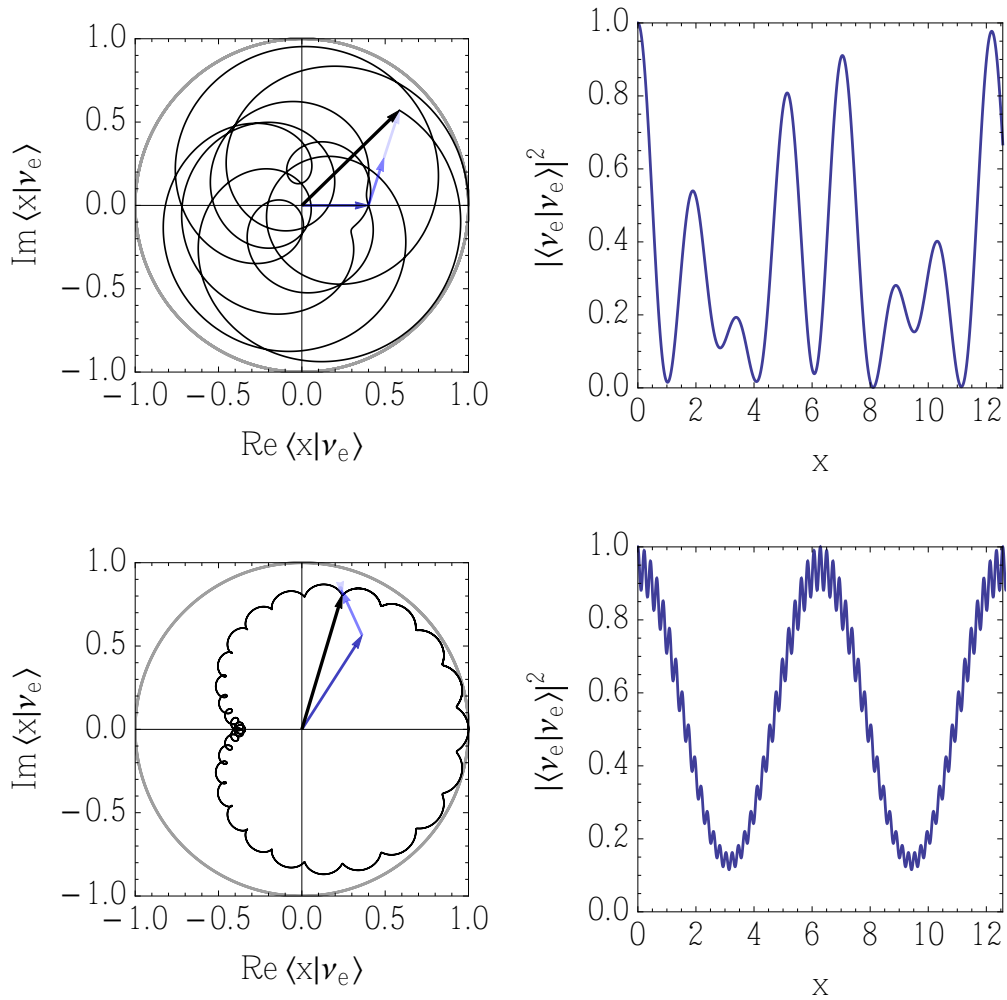


Figure 1.3: Visualization of the oscillation mechanism. The left-hand panels represent the pattern drawn on the complex plane, as a parametric function of distance, by the state $|\nu_e\rangle$ which is a combination of three eigenstates of propagation. The right-hand panels show the corresponding expectation value, which is the square of the norm of the amplitude drawn on the left-hand side panels. The upper panels show the case where the three masses are all spaced by roughly the same mass difference and the mixing angle are of similar order. The lower panels show the much simpler realization found in nature in which there are two characteristic scales of oscillation, one much larger than the other and one mixing angle which is much smaller than the other two.

was measured in 2012. Under the assumption $\theta_{13} \approx 0$, the mixing in eq. (1.6) can be rewritten as

$$\begin{pmatrix} 1 & 0 & 0 \\ 0 & c_{23} & -s_{23} \\ 0 & s_{23} & c_{23} \end{pmatrix} \begin{pmatrix} |\nu_e\rangle \\ |\nu_\mu\rangle \\ |\nu_\tau\rangle \end{pmatrix} = \begin{pmatrix} |\nu_e\rangle \\ c_{23}|\nu_\mu\rangle - s_{23}|\nu_\tau\rangle \\ s_{23}|\nu_\mu\rangle + c_{23}|\nu_\tau\rangle \end{pmatrix} = \begin{pmatrix} c_{12} & s_{12} & 0 \\ -s_{12} & c_{12} & 0 \\ 0 & 0 & 1 \end{pmatrix} \begin{pmatrix} |\nu_1\rangle \\ |\nu_2\rangle \\ |\nu_3\rangle \end{pmatrix}, \quad (1.12)$$

which tells us there will be an oscillation between the states $|\nu_e\rangle \leftrightarrow c_{23}|\nu_\mu\rangle - s_{23}|\nu_\tau\rangle \equiv |\nu_{\mu'}\rangle$ caused by the interference of $|\nu_1\rangle$ and $|\nu_2\rangle$, while state $s_{23}|\nu_\mu\rangle + c_{23}|\nu_\tau\rangle \equiv |\nu_{\tau'}\rangle$ remains as it is and propagates with the dispersion relation $E^2 - p^2 = m_3^2$. We have

$$\begin{pmatrix} |\nu_e\rangle \\ |\nu_{\mu'}\rangle \end{pmatrix} = \begin{pmatrix} \cos\theta_{12} & \sin\theta_{12} \\ -\sin\theta_{12} & \cos\theta_{12} \end{pmatrix} \begin{pmatrix} |\nu_1\rangle \\ |\nu_2\rangle \end{pmatrix} \quad (1.13)$$

Using formula (1.11), one gets,

$$\begin{aligned} P(\nu_e \rightarrow \nu_e) &= 1 - \sin^2 2\theta_{12} \sin^2 \frac{\omega x}{2}, \\ P(\nu_e \rightarrow \nu_{\mu'}) &= 1 - P(\nu_e \rightarrow \nu_e) = \sin^2 2\theta_{12} \sin^2 \frac{\omega x}{2}. \end{aligned} \quad (1.14)$$

Electron neutrinos can be distinguished from other species by a detector using a CC reaction. The former chlorine detector at Homestake [14] or the gallium detector of GALLEX [15] are examples of such detectors. These radiochemical devices count neutrinos thanks to the processes $\nu_e + {}^{37}\text{Cl} \rightarrow e^- + {}^{37}\text{Ar}$ and $\nu_e + {}^{71}\text{Ga} \rightarrow e^- + {}^{71}\text{Ge}$ respectively. A detector of this kind placed along the trajectory of the pure source of ν_e at various positions x would measure

$$\text{counts/week at distance } x = (\text{counts/week at distance } 0) \times P(\nu_e \rightarrow \nu_e). \quad (1.15)$$

This periodic pattern of length

$$l_{\text{osc}} = 2 \left| \frac{2\pi}{\omega} \right| = 8\pi \left| \frac{E}{\Delta m^2} \right| \quad (1.16)$$

is what is called vacuum flavor oscillation.

1.1.3 Density matrices

Of course in real neutrino beam experiments, one does not tag every neutrino by the mass of its partner lepton to filter out from the data muon neutrinos. The beam produced in pion decays is not a pure ν_μ or ν_e beam but a mixture of the two. Neither can one know, in fact, whether the neutrinos are emitted in plane waves or in some form of packet. However, these details become irrelevant once one makes the sum of expectation values over an incoherent set of events [16].

The system of a single neutrino of energy E studied in the previous section system contains altogether three observable quantities: $\langle \nu_e | \nu_e \rangle$, $\langle \nu_{\mu'} | \nu_{\mu'} \rangle$ and $\langle \nu_{\mu'} | \nu_e \rangle$. We can assemble them in a

density matrix:

$$\rho = \begin{pmatrix} \langle \nu_e | \nu_e \rangle & \langle \nu_e | \nu_{\mu'} \rangle \\ \langle \nu_{\mu'} | \nu_e \rangle & \langle \nu_{\mu'} | \nu_{\mu'} \rangle \end{pmatrix}. \quad (1.17)$$

One can study the system in either basis, flavor or mass. The results of one link to the results of the other according to

$$\begin{pmatrix} \langle \nu_1 | \nu_1 \rangle & \langle \nu_1 | \nu_2 \rangle \\ \langle \nu_2 | \nu_1 \rangle & \langle \nu_2 | \nu_2 \rangle \end{pmatrix} = \begin{pmatrix} \cos \theta_{12} & \sin \theta_{12} \\ -\sin \theta_{12} & \cos \theta_{12} \end{pmatrix} \begin{pmatrix} \langle \nu_e | \nu_e \rangle & \langle \nu_e | \nu_{\mu'} \rangle \\ \langle \nu_{\mu'} | \nu_e \rangle & \langle \nu_{\mu'} | \nu_{\mu'} \rangle \end{pmatrix} \begin{pmatrix} \cos \theta_{12} & -\sin \theta_{12} \\ \sin \theta_{12} & \cos \theta_{12} \end{pmatrix}. \quad (1.18)$$

One can easily prove that, in the mass basis, the density matrix obeys the equation of motion (EoM)

$$-i \frac{\partial \rho}{\partial x} = [\rho, H] \quad (1.19)$$

with $H_{ii} = p_i \approx E - m_i^2/2E$, i being a mass index. In the flavor basis, the equation is the same except for the mixing U :

$$H = E - \frac{1}{2E} \begin{pmatrix} \cos \theta_{12} & \sin \theta_{12} \\ -\sin \theta_{12} & \cos \theta_{12} \end{pmatrix} \begin{pmatrix} m_1^2 & 0 \\ 0 & m_2^2 \end{pmatrix} \begin{pmatrix} \cos \theta_{12} & -\sin \theta_{12} \\ \sin \theta_{12} & \cos \theta_{12} \end{pmatrix}. \quad (1.20)$$

By solving the EoM, one recovers the same results for the survival probability as in the previous section.

The density matrices of each neutrino in a set of many neutrinos can be added since they only contain linear observables such as the number of electron neutrinos. The density matrix of each neutrino, if it is not in a pure Fourier mode of energy E , must contain the transition amplitudes not only between flavor states but also between energy states. It will contain correlations between energy modes and therefore off-diagonal terms in the energy spectrum. However, these off-diagonal terms vary as $e^{i(E-E')t}$ and thus, if one sums the density matrices of many neutrinos over an incoherent set, these off-diagonal entries average away to zero. The sum over an incoherent set will give the matrix of densities in flavor space

$$\rho(x) = \begin{pmatrix} n_e(x) & \text{complex correlation} \\ \text{complex correlation}^* & n_{\mu'}(x) \end{pmatrix} \quad (1.21)$$

where n_e and $n_{\mu'}$ are the counts per unit volume per unit time of ν_e and $\nu_{\mu'}$ respectively, and $*$ denotes the complex conjugate.

1.1.4 Polarization vectors

Polarization vectors are a way to visualize a 2×2 Hermitian matrix in terms of a three-dimensional vector. This language has proven to be an exceptional tool, reducing the dynamics of the system to the mechanics of classical spins. The formalism also applies to systems with more levels but the

simple visualization properties are lost [17]. The density matrix may be written as

$$\rho = \frac{1}{2} \text{Tr} \rho + \tilde{\rho} \quad (1.22)$$

where we separated the trace of the density matrix from the rest of the physical quantities. It left us with a traceless matrix $\tilde{\rho}$. From equation (1.21), we see that the trace is equal to $\text{Tr} \rho = n_e(x) + n_{\mu'}(x)$ and is therefore conserved along the beam. The traceless matrix is (omitting the x dependence)

$$\begin{aligned} \tilde{\rho} &= \begin{pmatrix} c & a - bi \\ a + bi & -c \end{pmatrix} = c \begin{pmatrix} 1 & 0 \\ 0 & -1 \end{pmatrix} + a \begin{pmatrix} 0 & 1 \\ 1 & 0 \end{pmatrix} + b \begin{pmatrix} 0 & -i \\ i & 0 \end{pmatrix} \\ &= (a, b, c) \cdot (\sigma_x, \sigma_y, \sigma_z) \equiv \frac{1}{2} f(E) (\mathbf{P} \cdot \boldsymbol{\sigma}), \end{aligned} \quad (1.23)$$

where \mathbf{P} is a three-dimensional unit vector. We use boldface letters such as \mathbf{P} for vectors in flavor space and arrows for vectors in physical space, such as \vec{p} . We call $f(E)$ the length of the polarization vector. It can be determined when the density matrix is diagonal. If such a condition is valid at $x = 0$, then

$$\rho(0) = \begin{pmatrix} n_e(0) & 0 \\ 0 & n_{\mu'}(0) \end{pmatrix} = \frac{1}{2} [n_e(0) + n_{\mu'}(0) + f(E) \sigma_z] \Rightarrow f(E) = n_e(0) - n_{\mu'}(0). \quad (1.24)$$

If the total number of neutrinos is conserved, such as it is in a beam experiment, the study of the system is reduced to the study of the coefficients of the linear combination of the Pauli matrices. In this form, when the unit polarization vector \mathbf{P} points up along the z direction, the neutrino beam has maximal electron flavor. When it points down the neutrino beam has maximal μ' flavor. Intermediate positions indicate a mixed state. Namely, when the polarization vector is on the xy flavor plane, then the beam is maximally mixed, i.e., $n_e = n_{\mu'}$.

In vacuum, the Hamiltonian is diagonal for the mass states. To obtain it in the flavor basis, one just needs to perform the unitary transformation

$$\begin{aligned} H &= \begin{pmatrix} E & 0 \\ 0 & E \end{pmatrix} - \frac{1}{2E} \begin{pmatrix} \cos \theta_{12} & \sin \theta_{12} \\ -\sin \theta_{12} & \cos \theta_{12} \end{pmatrix} \begin{pmatrix} m_1^2 & 0 \\ 0 & m_2^2 \end{pmatrix} \begin{pmatrix} \cos \theta_{12} & -\sin \theta_{12} \\ \sin \theta_{12} & \cos \theta_{12} \end{pmatrix} \\ &= \begin{pmatrix} E - \frac{m_1^2 + m_2^2}{4E} & \\ & \end{pmatrix} \begin{pmatrix} 1 & 0 \\ 0 & 1 \end{pmatrix} - \frac{m_1^2 - m_2^2}{4E} \begin{pmatrix} \cos 2\theta_{12} & \sin 2\theta_{12} \\ \sin 2\theta_{12} & -\cos 2\theta_{12} \end{pmatrix} \\ &= \begin{pmatrix} E - \frac{m_1^2 + m_2^2}{4E} & \\ & \end{pmatrix} \begin{pmatrix} 1 & 0 \\ 0 & 1 \end{pmatrix} - \frac{m_1^2 - m_2^2}{4E} (\sin 2\theta_{12}, 0, \cos 2\theta_{12}) \cdot (\sigma_x, \sigma_y, \sigma_z). \end{aligned} \quad (1.25)$$

Since the total time variation of the density matrix is given by the commutator of the density matrix with the Hamiltonian, any terms proportional to the identity matrix do not play any part in it.

And since $[\sigma_i, \sigma_j] = 2i\epsilon_{ijk}\sigma_k$, the evolution equation acquires the much more appealing form

$$\frac{\partial \mathbf{P}}{\partial x} = \omega \mathbf{B} \times \mathbf{P}, \quad (1.26)$$

with

$$\begin{aligned} \mathbf{B} &= (\sin 2\theta_{12}, 0, \cos 2\theta_{12}), \\ \omega &= \frac{\Delta m^2}{2E}. \end{aligned} \quad (1.27)$$

Note that the mass basis, indicated by \mathbf{B} , is a basis rotated by twice the vacuum mixing angle θ_{12} in the space of polarization vectors. This comes from the fact that $SU(2)$ is a double cover on $O(3)$. Equation (1.26) is a simple precession equation of \mathbf{P} around \mathbf{B} . The trajectory followed by \mathbf{P} is a circle on the unit sphere centered around the direction of \mathbf{B} . Notice that when \mathbf{P} is aligned with \mathbf{B} , it remains that way in spite of propagation. Such a vector is thus an eigenstate of propagation, which in vacuum is the mass state. From this reasoning we conclude that a neutrino with a polarization vector pointing along \mathbf{B} is in a mass state. Which mass state depends on whether it is aligned or anti-aligned with \mathbf{B} . The mass state with positive z component is $|\nu_1\rangle$. The other one is either $|\nu_2\rangle$ or $|\nu_3\rangle$, depending on whether one is using the solar or the atmospheric mass difference.

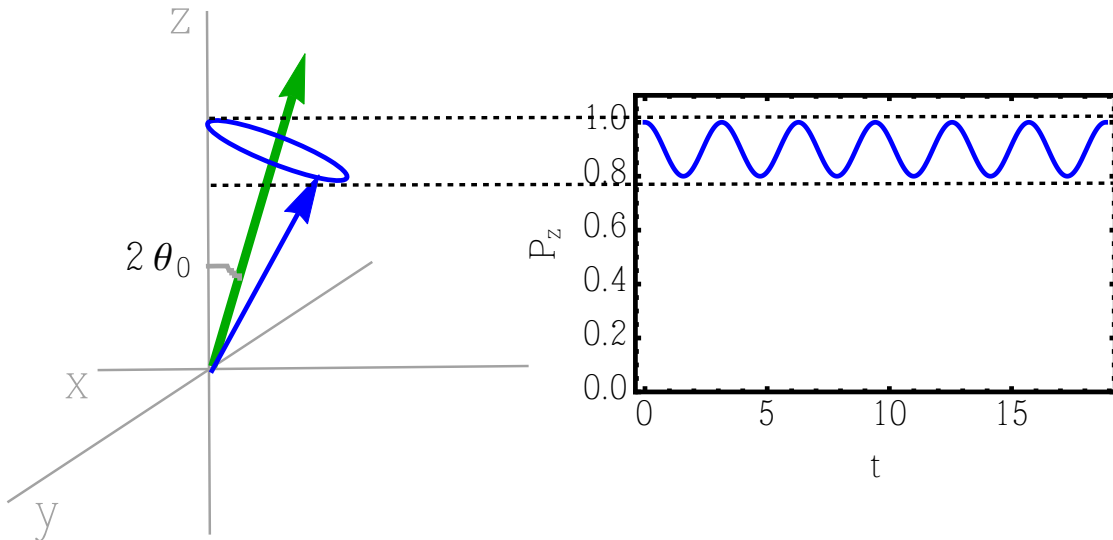


Figure 1.4: The vacuum precession of the flavor vector around \mathbf{B} . The projection of the trajectory onto the z axis gives the expectation value of flavor, which visibly describes an oscillation pattern.

According to eq. (1.26), \mathbf{P} performs a simple precession. The component $P_{\parallel} = \cos 2\theta_{12}$ along the mass direction is conserved. The transversal part \mathbf{P}_{\perp} varies as $\sin 2\theta_{12}e^{i\omega x}$, i being the 90 degree

rotation on the plane perpendicular to the mass direction. In the mass basis, the polarization vector is

$$\mathbf{P}_{\text{mass}} = \begin{pmatrix} \sin 2\theta_{12} \cos \omega x \\ \sin 2\theta_{12} \sin \omega x \\ \cos 2\theta_{12} \end{pmatrix}. \quad (1.28)$$

Reverting to the flavor basis,

$$\mathbf{P}_{\text{flavor}} = \begin{pmatrix} \cos 2\theta_{12} & 0 & \sin 2\theta_{12} \\ 0 & 1 & 0 \\ -\sin 2\theta_{12} & 0 & \cos 2\theta_{12} \end{pmatrix} \begin{pmatrix} \sin 2\theta_{12} \cos \omega x \\ \sin 2\theta_{12} \sin \omega x \\ \cos 2\theta_{12} \end{pmatrix}. \quad (1.29)$$

When the precession is projected onto the flavor z -direction, it results in an oscillation pattern. For a pure ν_e beam at the source, one recovers the previous result

$$P_z(x) = 1 - 2 \sin^2 2\theta_{12} \sin^2 \frac{\omega x}{2} = P(\nu_e \rightarrow \nu_e) - P(\nu_e \rightarrow \nu_{\mu'}) \quad (1.30)$$

This value gives the difference between the survival probability of ν_e and the transition probability into $\nu_{\mu'}$ as previously calculated.

Vacuum oscillation happens thanks to the interference between different mass states. Mass states – defined as the eigenstates of a measurement of mass – are the eigenstates of propagation in vacuum. One can think therefore of the vacuum as a medium where particles can move according to three relativistic dispersion relations $E^2 - p^2 = m^2$. Whatever the interactions at work in vacuum, we know experimentally that only three eigenstates of this type exist for each particle in the Standard Model. Our initial discussion on the flavor problem shows that the CC, however, does not operate in the same way: the states that participate in the electroweak interaction are superpositions of mass states. Therefore, the eigenstates of propagation in a medium are different from the eigenstates of propagation in vacuum. In the next sections, we will explore the effects of weak interactions on the evolution of flavor of neutrinos.

1.1.5 Matter effect

Neutrinos have two types of interactions: NC and CC. The NC interaction happens through the exchange of a Z^0 boson. This interaction is universal: all neutrinos of all flavors interact equally with all types of matter. It is similar to the electromagnetic interaction with the exception that it only couples to the left handed component of every particle involved and that it acts at a much shorter range because of the m_Z^2 suppression. We consider the case in which the energies of the neutrinos are too low to produce real heavy photons Z^0 , in which case one can use the effective Fermi Hamiltonian. We stress the interaction with neutrons even though neutrinos also interact with protons and electrons in the same way. However, the contributions of these two species are

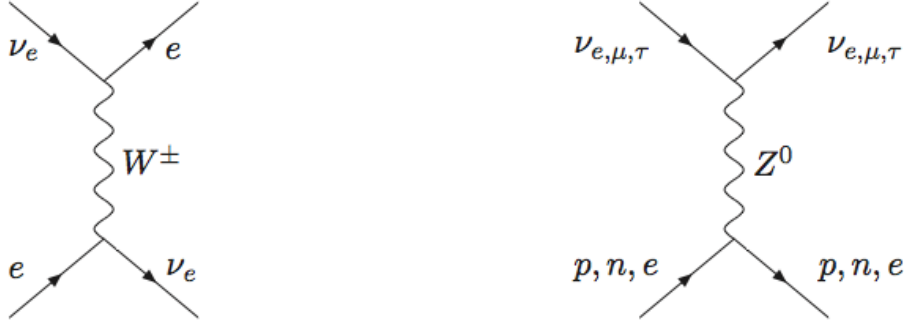


Figure 1.5: The two interactions a neutrino can have with matter. At low energies, of tenths of MeV as neutrinos acquire in a supernova, the gauge bosons are too heavy to be produced as real particles, having masses of $M_Z = 91 \text{ GeV}/c^2$ and $M_W = 80 \text{ GeV}/c^2$. Instead they suppress the cross-section of these processes by a factor of $1/M^2$. At low energies the vertex is infinitesimal because the heavy boson can only be produced off-shell. The cross-section of these processes varies roughly with the square of the energy at the center of mass. Note that whereas the NC interaction (right) interacts with all other particles, the CC requires the scattering on a charged lepton of the same flavor. This is actually what defines the flavor of a neutrino. NCs do not allow to figure out the flavor of a neutrino.

opposite and therefore, in an neutral medium, cancel.

$$H^{\text{NC}} = \frac{G_F}{\sqrt{2}} \sum_{i=e,\mu,\tau} \int \Psi_n^\dagger(\vec{x}) \gamma_0 \gamma_\mu (C_V^n - C_A^n) \Psi_n(\vec{x}) \Psi_{\nu_i}^\dagger(\vec{x}) \gamma^0 \gamma^\mu (1 - \gamma_5) \Psi_{\nu_i}(\vec{x}) d\text{vol} \quad (1.31)$$

where $G_F = 1.167 \times 10^{-5} \text{ GeV}^{-2}$ is Fermi's constant, Ψ_n is the field operator of the neutron field, Ψ_{ν_i} that of the neutrino field of flavor i , and C_V^n and C_A^n are the vector and axial effective couplings which for the neutrino-neutron interaction are -1 and -1.15 [18]. H^{NC} is diagonal in any basis.

The neutrinos also interact through CC (exchange of a charged W^\pm boson) with the charged leptons in the gas. This interaction can be described by the same effective Hamiltonian after a Fierz transformation. Nevertheless, this interaction is flavor dependent, relying on the density of charged leptons of each flavor. Therefore matter acts as a tri-refrangent medium to different flavors. The effective Hamiltonian is

$$H^{\text{CC}} = \frac{G_F}{\sqrt{2}} \sum_{\ell=e,\mu,\tau} \int \Psi_\ell^\dagger(\vec{x}) \gamma_0 \gamma_\mu (C_V^{\text{CC}} - C_A^{\text{CC}}) \Psi_\ell(\vec{x}) \Psi_{\nu_\ell}^\dagger(\vec{x}) \gamma^0 \gamma^\mu (1 - \gamma_5) \Psi_{\nu_i}(\vec{x}) d\text{vol} \quad (1.32)$$

Note that the vector and axial-vector couplings are different from those of the NC interaction with the neutrons: for instance, $C_V^{\text{CC}} \approx 1$ and $C_A^{\text{CC}} = 0.5$.

In the context of neutrino oscillations, one typically assumes that the neutrino beam flows collisionlessly, that is, the momentum of the neutrino is unchanged by the interactions with the

medium. The neutrino enters and exits the vertex of interaction with equal momenta and energy, but acquires a phase shift which averaged over many interactions changes the dispersion relation of its wave-function. The first-order perturbation potential is found by averaging the effective Hamiltonian over the wave-function of the system. The terms averaged over the neutron field represent familiar quantities

$$\begin{aligned} \langle n | \gamma_0 \gamma_\mu (C_V^n - C_A^n \gamma_5) | n \rangle &= \begin{cases} \langle n | (C_V^n - C_A^n \gamma_5) | n \rangle & \text{(time component)} \\ \langle n | \vec{\alpha} (C_V^n - C_A^n \gamma_5) | n \rangle & \text{(spatial components)} \end{cases} \\ &= \begin{cases} C_V^n n_n - C_A^n \left\langle \frac{\vec{\sigma}_n \cdot \vec{p}_n}{E_n} \right\rangle & \text{(time component)} \\ C_V^n \langle \vec{j}_n \rangle - C_A^n \langle \vec{\sigma}_n \rangle & \text{(spatial components)} \end{cases} \end{aligned} \quad (1.33)$$

The final four-potential depends on the neutron density n_n , the average helicity $\vec{\sigma}_n \cdot \vec{p}_n$, the current density of neutrons \vec{j}_n and the polarization of the gas $\vec{\sigma}_n$. In an unpolarized medium such as the one (for all practical purposes) found in supernovae, it can be expressed in the charged-lepton mass basis as

$$\begin{aligned} V_{\text{NC}} &= C_V \frac{G_F}{\sqrt{2}} (n_n - \vec{v}_\nu \cdot \vec{j}_n) \begin{pmatrix} 1 & 0 & 0 \\ 0 & 1 & 0 \\ 0 & 0 & 1 \end{pmatrix} \\ &= -\frac{G_F}{\sqrt{2}} (1 - \vec{v}_\nu \cdot \vec{v}_n) n_n \begin{pmatrix} 1 & 0 & 0 \\ 0 & 1 & 0 \\ 0 & 0 & 1 \end{pmatrix}, \end{aligned} \quad (1.34)$$

with the velocities \vec{v}_ν and \vec{v}_n of the neutrinos and of the neutrons. The unit matrix represents the fact that this potential acts on all three flavors equally. Furthermore, the neutrons tend to have negligible velocities, so one may disregard the velocity-dependent term.

The effective CC potential felt by the electron component of the beam in an unpolarized medium is, by similar arguments,

$$V_{CC} = \sqrt{2} G_F \begin{pmatrix} n_e & 0 & 0 \\ 0 & n_\mu & 0 \\ 0 & 0 & n_\tau \end{pmatrix}, \quad (1.35)$$

where $n_{e,\mu,\tau}$ stand for the density difference between the negative and positive charged leptons. In most media, of which stars and supernovae are an example, muon and taus are absent, which means we need only to consider the interaction of the electron neutrinos with the ambient electrons and positrons. In fact, any medium whose temperature is high enough to sustain a significant population of muons and taus is too hot to neglect the collision terms. Additionally, though the velocities of electrons can be highly directional in a supernova because of the complicated hydrodynamical motions inside the collapsing star, the average velocity is always small compared to the speed of light.

Therefore, like before, all terms are negligible except for the electron density. For anti-neutrinos, both CC and NC potentials are reversed by a minus sign.

Going back to the previous case $\theta_{13} \approx 0$, we wish to study solar flavor oscillations in a medium, i.e., the interference of states 1 and 2 under the influence of the electron potential. As discussed in the last paragraph, the density of muons and taus is zero in the Sun. Just like the vacuum Hamiltonian, the matter potential can be expressed as a 2×2 matrix

$$\begin{aligned} V &= \frac{G_F}{\sqrt{2}} \begin{pmatrix} n_n + 2n_e & 0 \\ 0 & n_n \end{pmatrix} = \frac{G_F}{\sqrt{2}} \left(\frac{n_n}{2} + n_e \right) \begin{pmatrix} 1 & 0 \\ 0 & 1 \end{pmatrix} + \frac{G_F}{\sqrt{2}} n_e \begin{pmatrix} 1 & 0 \\ 0 & -1 \end{pmatrix} \\ &= \frac{G_F}{\sqrt{2}} \left(\frac{n_n}{2} + n_e \right) + \frac{1}{2} \sqrt{2} G_F n_e (0, 0, 1) \cdot (\sigma_x, \sigma_y, \sigma_z) \\ &\equiv l_0 + \frac{1}{2} \lambda \mathbf{L} \cdot \boldsymbol{\sigma}. \end{aligned} \quad (1.36)$$

The EoMs are now

$$\partial_x \mathbf{P} = (\omega \mathbf{B} + \lambda \mathbf{L}) \times \mathbf{P} \equiv \mathbf{H}_\omega \times \mathbf{P} \quad (1.37)$$

with

$$\begin{aligned} \mathbf{H}_\omega &= \omega \mathbf{B} + \lambda \mathbf{L}, \\ \mathbf{B} &= (\sin 2\theta_{12}, 0, \cos 2\theta_{12}), \\ \mathbf{L} &= (0, 0, 1), \\ \omega &= \frac{\Delta m^2}{2E}, \\ \lambda &= \sqrt{2} G_F n_e. \end{aligned} \quad (1.38)$$

The NC term does not explicitly contribute to oscillations between flavors because the increase in frequency is the same irrespective of flavor. That is not the case however if one is studying oscillations between spin states, such as Dirac spin-flipping or Majorana particle-antiparticle oscillations. The interactions with the neutrons becomes relevant whenever one of the states interacts differently with the neutrons from the other one. For example, a right-handed Dirac neutrino is a sterile neutrino and thus does not refract in a neutron medium. In this case, the neutron medium does induce a bi-refringence between left-handed and right-handed states much like the electronic medium induces a bi-refringence between electron and heavy-lepton flavors.

1.2 Canonical variables and adiabatic transitions

We will show now how this system is equivalent to a classical system of a precessing spin [20]. We will use this analogy to show how the polarization vector can be dragged slowly along the propagation eigenstate leading, in some cases, to a complete inversion of the flavor content, in

what is called the Mikheyev-Smirnov-Wolfenstein (MSW) effect, described in the next section. The general EoMs (1.37) for a beam of neutrinos propagating in a weakly charged static medium are easy to understand. A neutrino whose flavor vector points along the direction of \mathbf{H}_ω remains in that state. Therefore the propagation eigenstates are determined by this direction. In matter ($\lambda \gg \omega$) this direction is the z direction, i.e., the eigenstates are the flavor states. In vacuum ($\omega \gg \lambda$) it is the \mathbf{B} direction, i.e., the mass states are the eigenstates of propagation. At intermediate densities these states are a mixture of both flavor and mass states. The EoMs describe the precession of \mathbf{P} around \mathbf{H}_ω . Because of the cross product, the component of the flavor vector along $\omega\mathbf{B} + \lambda\mathbf{L}$ is conserved:

$$\frac{\partial}{\partial x} [(\omega\mathbf{B} + \lambda\mathbf{L}) \cdot \mathbf{P}] = 0. \quad (1.39)$$

This property is no surprise. The EoMs simply state that the part of the amplitude of the system which is in the eigenstate of propagation is conserved, whereas the remaining part (perpendicular to \mathbf{H}_ω) continuously develops a phase. The projection of the wave-function onto the eigenstate of propagation

$$H(\mathbf{P}) = (\omega\mathbf{B} + \lambda\mathbf{L}) \cdot \mathbf{P} \quad (1.40)$$

can actually serve as a Hamiltonian function of the EoMs. If one describes \mathbf{P} in spherical coordinates, i.e., in the form $\mathbf{P} = (\sin \theta \cos \varphi, \sin \theta \sin \varphi, \cos \theta)$, the function is equal to

$$H = \omega \sin 2\theta_{12} \sin \theta \cos \varphi + (\omega \cos 2\theta_{12} + \lambda) \cos \theta \quad (1.41)$$

and

$$\begin{aligned} \frac{\partial H}{\partial \varphi} &= -\omega \sin 2\theta_{12} \sin \theta \sin \varphi = \dot{\theta} \sin \theta = -\frac{\partial}{\partial x}(\cos \theta) \\ \frac{\partial H}{\partial(\cos \theta)} &= -\omega \sin 2\theta_{12} \operatorname{ctg} \theta \cos \varphi + (\omega \cos 2\theta_0 + \lambda) = \dot{\varphi} \end{aligned} \quad (1.42)$$

which are of the form of canonical equations with canonical variable φ and canonical momentum $\cos \theta = P_z$. The dot here represents a derivative in respect to x . Lagrange's function L for this system is given by

$$L = P_z \dot{\varphi} + H = P_z \dot{\varphi} - (\omega\mathbf{B} + \lambda\mathbf{L}) \cdot \mathbf{P}. \quad (1.43)$$

One may use the EoMs to write down the Lagrangian in terms of φ and $\dot{\varphi}$ but the expression is rather complicated. The characteristic feature of this system is that P_z is the momentum associated with the variable φ . To make a more physical analogy, these features describe the properties of a system of classical spins. The vacuum term can be viewed as magnetic moment ω times the magnetic field \mathbf{B} . This "classical" system obeys the classical Halmilton-Jacobi EoMs

$$\frac{\partial f(\theta, \varphi)}{\partial x} = \{f, H\} \quad (1.44)$$

and the classical commutation relation – the Poisson bracket –

$$\{\varphi, \cos \theta\} = 1 \quad (1.45)$$

with

$$\{f, g\} = \frac{\partial f}{\partial \varphi} \frac{\partial g}{\partial(\cos \theta)} - \frac{\partial g}{\partial \varphi} \frac{\partial f}{\partial(\cos \theta)}. \quad (1.46)$$

The similarity with the spin algebra can be highlighted by noting that the three components of the polarization vector respect

$$\{P_i, P_j\} = \varepsilon_{ijk} P_k. \quad (1.47)$$

Indeed, using this identity

$$\begin{aligned} \partial_x P_i &= \sum_k \{P_i, (\omega B_k + \lambda L_k) P_k\} = \sum_k (\omega B_k + \lambda L_k) \{P_i, P_k\} \\ &= \sum_k (\omega B_k + \lambda L_k) \varepsilon_{ikj} P_j = [(\omega \mathbf{B} + \lambda \mathbf{L}) \times \mathbf{P}]_i \end{aligned} \quad (1.48)$$

one recovers the EoMs.

Despite the simplicity and the classical equivalence of these equations, the motion with varying λ is not quite so obvious to predict, unless the variation is adiabatic. Upon an adiabatic variation of the parameter, the following integral along a closed trajectory in phase space

$$I = \frac{1}{2\pi} \oint \cos \theta d\varphi = -\frac{1}{2\pi} \oint \varphi d(\cos \theta) = \frac{1}{2\pi} \iint d\varphi d(\cos \theta) \quad (1.49)$$

is invariant. The integral in its last form is the area enclosing a closed trajectory in phase space $(\cos \theta, \varphi)$, that is, the area described by the polarization vector on the unit sphere. This area is preserved when the relative variation of the parameter λ is much smaller than the frequency of oscillation

$$\frac{1}{\lambda} \frac{\partial \lambda}{\partial x} \ll \frac{\omega + \lambda}{2\pi}. \quad (1.50)$$

The adiabatic conservation of the area described on the Bloch sphere is a very powerful statement. Namely, if at some point the polarization vector coincides with \mathbf{H}_ω , then it sticks to it under slow changes of the parameters. This can allow complete inversions of the flavor content in the effect described in the next section.

1.3 MSW effect

It is fairly easy to understand how the presence of matter can lead to a near-complete inversion of the flavor content in the flux. As we pointed out in the previous section, the area described by the polarization vector is maintained when the variation of the matter density is slow compared to the

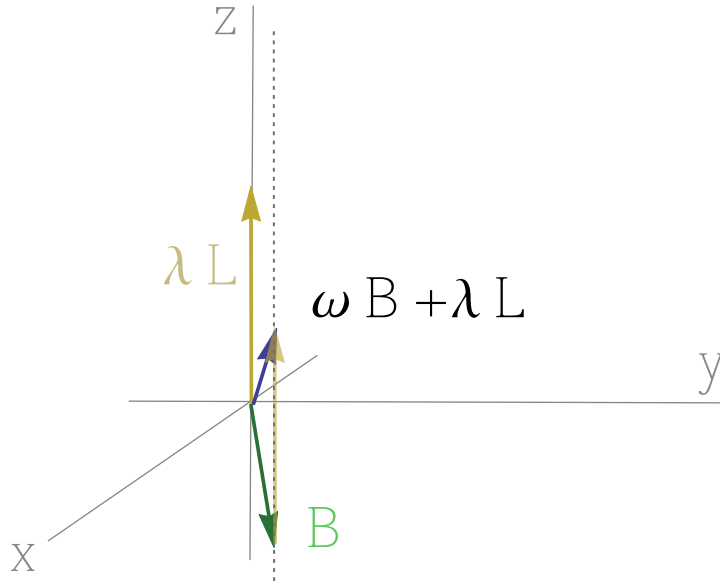


Figure 1.6: The flavor vectors, in the absence of neutrino-neutrino interactions, orbit around $\pm\omega\mathbf{B} + \mathbf{L}$ ($+\omega$ for neutrinos, $-\omega$ for anti-neutrinos). If $\omega\mathbf{B}$ is negative, i.e., $m_1^2 < m_2^2$ then a background of electrons and neutrons can invert the direction of the axis of precession along z .

oscillation length. This means that the trajectory, in the adiabatic regime, remains a circle centered around the varying vector \mathbf{H}_ω . When $\lambda \gg \omega$, this vector points along the z direction, coinciding with $\lambda\mathbf{L}$ whereas in the near vacuum case $\omega \gg \lambda$, the vector coincides with $\omega\mathbf{B}$. Neutrinos being produced in the electron state, \mathbf{P} coincides initially with $\mathbf{H}_\omega \approx \lambda\mathbf{L}$. As λ decreases adiabatically to zero, the flavor vector is dragged by \mathbf{H}_ω along all intermediate eigenstates of propagation until it reaches the eigenstate of propagation in vacuum, a mass state.

This effect is very important for solar and SN neutrinos, since the core of the Sun has a density of about [18] 150 g cm^{-3} , i.e., an oscillation length in matter of

$$l_{\text{osc}} = \frac{2\pi}{\lambda} = 1.63 \times 10^4 \text{ km} \frac{\text{g cm}^{-3}}{n_e} \approx 54 \text{ km}, \quad (1.51)$$

The solar oscillation length in vacuum for neutrinos of energy $E > 5 \text{ MeV}$ is

$$l_{\text{osc}} = \frac{2\pi}{\omega} = 4.96 \text{ km} \frac{E}{\text{MeV}} \frac{\text{eV}^2}{\Delta m^2} \approx 82 \text{ km}, \quad (1.52)$$

larger than the oscillation length in matter. Here, matter effects dominate ($\lambda \gg \omega$) for MeV neutrinos (and higher energies), and the flavor components are the eigenfunctions of propagation. They are generally free to stream out. This means the neutrinos – produced in the electron flavor –

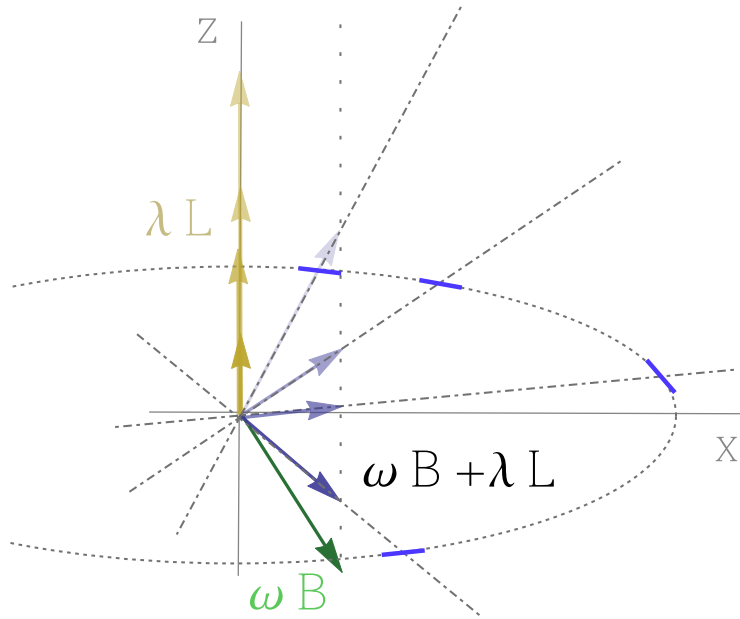


Figure 1.7: As the matter density thins, $\omega\mathbf{B} + \lambda\mathbf{L}$ moves from an upward position to a downward position, even though its x component remains always very small. If the change is adiabatic, the flavor vectors precess around $\omega\mathbf{B} + \lambda\mathbf{L}$ with a constant amplitude, the precession cone being slowly dragged down with it (represented by the blue dashes along the sphere of radius \mathbf{P}). This effect only happens for one hierarchy for neutrinos (and the other one for anti-neutrinos). In the other one both $\omega\mathbf{B}$ and $\lambda\mathbf{L}$ point in the same direction

in a region of high electronic density – start off in an eigenstate of propagation. As the neutrino travels to the outer envelopes and eventually reaches the empty space between the Sun and the Earth, the vector \mathbf{H}_ω slowly changes from the $\lambda\mathbf{L}$ to $\omega\mathbf{B}$. Vector \mathbf{P} , while keeping its alignment with \mathbf{H}_ω , is brought from the interaction state to the mass state. The electronic matter drags all the neutrinos onto the mass basis. No oscillations occur between the Sun and the Earth since the neutrino is already in the state of propagation in the vacuum. In fact, if one is precise, oscillations never occur, because the neutrino is always in a propagation eigenstate. It is born in the state of propagation at high density – the electron state – and is detected in the state of propagation at low density – a mass eigenstate. Being so, this adiabatic conversion allows us to directly measure the mixing angle between the interaction states and the mass states. We call a situation in which the less massive state contains a stronger electron flavor a *normal hierarchy* of masses (NH) and a situation in which the electron flavor is stronger in the more massive state an *inverted hierarchy* (IH) (cf. fig.1.8). It is easy to see that the two hierarchies lead to two distinct scenarios. Either the solar mass difference Δm^2 is negative, i.e., the more massive state contains the most electronflavor and $\omega\mathbf{B}$ on the hemisphere of positive z direction or the mass difference is positive and $\omega\mathbf{B}$ is on

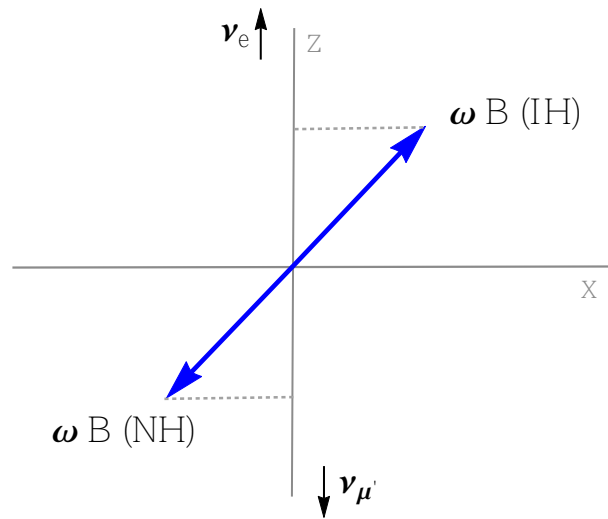


Figure 1.8: A schematic explanation of the difference between the two hierarchies. The dashed line indicates the flavor content of the vacuum state. In the IH this content is more electron flavored, whereas in the NH it is heavy-lepton flavored.

the southern hemisphere of the Bloch sphere, i.e., in the region of higher heavy-lepton component. In the first case, a thinning of the matter background from a high density to near vacuum means an inversion of the angle $\omega \mathbf{B} + \lambda \mathbf{L}$ makes with the z direction and therefore an inversion of the flavor polarization of the beam. The situation is reversed for anti-neutrinos (negative E). This is called an MSW resonance after the three scientists, S. Mikheyev, A. Smirnov and L. Wolfenstein, who first proposed it [21]. This effect was what ultimately led to explain the missing electron neutrino flux from the Sun [22], as measured by Super-Kamiokande [23] and SNO [24], who observed a resonant conversion for energies higher than 5 MeV. It also allowed the mixing angle θ_{12} and the signed value of the solar mass difference to be measured. KamLAND [25] then confirmed the existence of solar vacuum oscillations with its long baseline experiment.

Resonant flavor conversion happens when $\omega \sim \lambda$. In SN, with $Y_e \sim 0.3 - 0.5$, this condition is found in the outer layers at $\rho \sim 100 - 1000 \text{ g cm}^{-3}$ for the atmospheric mixing (H resonance) and at $\rho \sim 10 - 100 \text{ g cm}^{-3}$ for the solar mixing (L resonance). The simplest way to look at these resonances is to compute the dispersion relation of the propagation eigenstate as a function of the electron density. Figure 1.9 shows the energy of each of these states as a function of n_e in a three-flavor analysis. The transitions can be seen by following the solid lines for each flavor from high density to low density.

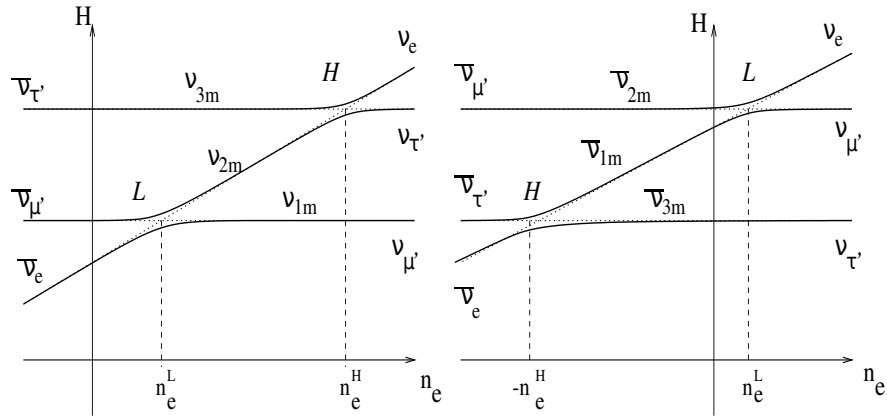


Figure 1.9: Energy as a function of the electron density for the three different eigenvalues of the propagation Hamiltonian [26]. The dashed lines represent the flavor states. Both μ and τ flavors do not respond to an increase of the electron density, whereas the energy of the electron flavor grows linearly. The left-hand panels shows NH, the right-hand panel IH. One can clearly witness the many transitions that happen as one decreases the density, by following the black solid lines. Negative densities represent how anti-neutrinos perceive the background of electrons.

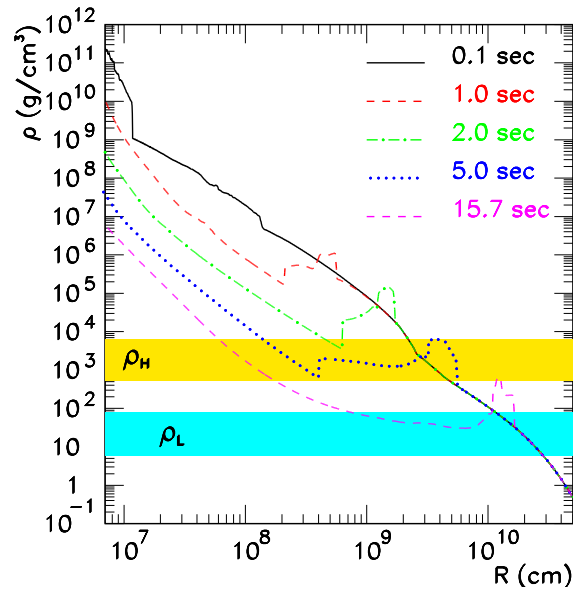


Figure 1.10: Density as a function of the distance to the core of the SN, at different time snapshots measured after the core bounce [27]. Of relevance are the two regions where MSW resonance might occur for the solar mass difference and the atmospheric mass difference, the so called H and L resonances. The atmospheric resonance happens before the solar one, as expected.

1.4 Neutrino-neutrino interaction

In most cases in the cosmos, the density of neutrinos is too small for neutrino-neutrino interactions to play any role of significance. There are however some cases in which neutrinos play a very

important role and are emitted in quantities great enough for the gas of neutrinos to cause a significant refractive effect on itself. Namely, the inner regions of a core-collapse supernova, the merging of two compact objects and the early universe around the time neutrinos decoupled from the primordial soup. The interaction that allows neutrinos to influence each other collisionlessly is the NC exchange of a Z^0 boson. Analogously to the interaction with neutrons

$$H_{ij}^{\nu\nu} = \frac{G_F}{\sqrt{2}} \sum_{i,j=1,2,3} \int \Psi_i^\dagger(\vec{x}) \gamma_0 \gamma_\mu (C_V^\nu - C_A^\nu) \Psi_i(\vec{x}) \Psi_j^\dagger(\vec{x}) \gamma^0 \gamma^\mu (1 - \gamma_5) \Psi_j(\vec{x}) d\text{vol} \quad (1.53)$$

For forward scattering, this evolution operator is

$$V^{\nu\nu} = \sqrt{2} G_F C_V^\nu (n_\nu + \vec{v} \cdot \vec{J}_\nu) \quad (1.54)$$

where n_ν and \vec{J}_ν are the density and current of the neutrino background. \vec{v} is the velocity of the test neutrino. The main difference between this term and the NC interaction with the neutrons is that, with neutrinos, the off-diagonal terms of the density matrix are present. In the language of polarization vectors this term is

$$V^{\nu\nu} = \frac{1}{2} \text{Tr} V^{\nu\nu} + \frac{\sqrt{2} G_F}{2} (\mathbf{N} - \vec{v} \cdot \vec{\mathbf{J}}) \cdot \boldsymbol{\sigma} \quad (1.55)$$

where \mathbf{N} and $\vec{\mathbf{J}}$ are the polarization vectors pertaining to n_ν and \vec{J}_ν respectively.

1.5 Evolution of flavor in a neutrino ensemble

1.5.1 Neutrinos in a box

In this section we will show how one can study the evolution of flavor in an incoherent fluid of neutrinos as a function of both space and time. Note that if both momentum and energy of a neutrino are known with a high enough precision, then so is the mass and the oscillations pattern is lost. To avoid this, we consider an ensemble of neutrinos, incoherent in space. This means we take a volume large enough so that the interference terms $\exp i(p - p')x$ between two modes of momentum between neutrinos average to zero. In such conditions, it is enough to consider the state of the neutrino ensemble by the occupation numbers of each state of momentum p . Let $|\Psi\rangle$ be the state of the neutrino ensemble and of the matter background. This state can be factorized into

$$|\Psi\rangle = |\nu\rangle \times |e\rangle \times \dots \quad (1.56)$$

where the first item in the product is the state of the neutrino ensemble and the following are the many-particle wave-functions of the different matter components. Anti-neutrinos are denoted by a wave-function of negative energy.

Each mode of the neutrino gas of momentum p contains additionally three flavor states. We can write the state of the neutrino ensemble as a continuum of momentum states:

$$|\nu\rangle = \begin{pmatrix} |\nu_e\rangle \\ |\nu_\mu\rangle \\ |\nu_\tau\rangle \end{pmatrix} = \begin{pmatrix} |w_e(\vec{p}_0), w_e(\vec{p}_0 + d\vec{p}), w_e(\vec{p}_0), w_e(\vec{p}_0 + 2d\vec{p}), \dots\rangle \\ |w_\mu(\vec{p}_0), w_\mu(\vec{p}_0 + d\vec{p}), w_\mu(\vec{p}_0), w_\mu(\vec{p}_0 + 2d\vec{p}), \dots\rangle \\ |w_\tau(\vec{p}_0), w_\tau(\vec{p}_0 + d\vec{p}), w_\tau(\vec{p}_0), w_\tau(\vec{p}_0 + 2d\vec{p}), \dots\rangle \end{pmatrix} \quad (1.57)$$

where $w_i(\vec{p})$ is the occupation number of state \vec{p} with flavor i . We call $a_i^\dagger(\vec{p})$ and $a_i(\vec{p})$ the operators that respectively add and subtract a particle at position \vec{p} and flavor i to the state vector. Because neutrinos are fermions and we assumed that all (anti-)neutrinos have a (right-)left-helicity, the occupation number of each state can only be either 0 or 1. We consider a volume of space big enough so that any quantum correlations between modes of different momentum vanish. However, one has enough time resolution that the evolution of flavor as a function of time is visible. This is the opposite case of the previous beam example, where one could not resolve time but could resolve space.

The density matrix is defined as the expectation value of the cross-flavor number operator $\rho_{ij}(\vec{p}) = \langle a_i^\dagger(\vec{p}) a_j(\vec{p}) \rangle$, $i = e, \mu, \tau$. Indeed, the expectation values of the entries of this operator give

$$\begin{aligned} \rho_{ij}(\vec{p}) &= \langle \Psi | a_i^\dagger(\vec{p}) a_j(\vec{p}) | \Psi \rangle \\ &= \begin{pmatrix} \langle \nu_e(\vec{p}) | & \langle \nu_\mu(\vec{p}) | & \langle \nu_\tau(\vec{p}) | \end{pmatrix} a_i^\dagger(\vec{p}) a_j(\vec{p}) \begin{pmatrix} |\nu_e(\vec{p})\rangle \\ |\nu_\mu(\vec{p})\rangle \\ |\nu_\tau(\vec{p})\rangle \end{pmatrix} \\ &= \begin{pmatrix} w_{\nu_e}(\vec{p}) & \langle \nu_e(\vec{p}) | \nu_\mu(\vec{p}) \rangle & \langle \nu_e(\vec{p}) | \nu_\tau(\vec{p}) \rangle \\ \langle \nu_\mu(\vec{p}) | \nu_e(\vec{p}) \rangle & w_{\nu_\mu}(\vec{p}) & \langle \nu_\mu(\vec{p}) | \nu_\tau(\vec{p}) \rangle \\ \langle \nu_\tau(\vec{p}) | \nu_e(\vec{p}) \rangle & \langle \nu_\tau(\vec{p}) | \nu_\mu(\vec{p}) \rangle & w_{\nu_\tau}(\vec{p}) \end{pmatrix}_{ij} \end{aligned} \quad (1.58)$$

The diagonal entries describe the occupation numbers of each flavor state with momentum \vec{p} . The off-diagonal terms carry the phase differences between the many-particle wave-functions of the different flavors, averaged over the volume of space. The trace of the density matrix gives the total number of neutrinos of any species in momentum state \vec{p} .

Because the operators for particle and anti-particles follow the same rules we will refer to them from now on as one operator with positive and negative energy. Because, in the ultrarelativistic limit, the energy $\pm E$ is roughly equal to the momentum $|\vec{p}|$, we will denote particles by a momentum of positive norm and anti-particles by a momentum of negative norm. Thus, when we denote \vec{p} , we mean a double valued vector on three-dimensional space. In simple terms, this means that in spherical coordinates the norm of the momentum must be integrated from $-\infty$ to $+\infty$. For an

ensemble of delocalized neutrinos, the number operator $a_i^\dagger(\vec{p}) a_j(\vec{p})$ obeys the equation

$$i \frac{d}{dt} a_i^\dagger(\vec{p}) a_j(\vec{p}) = [a_i^\dagger(\vec{p}) a_j(\vec{p}), H] \quad (1.59)$$

This Hamiltonian is composed of a vacuum term diagonal in the neutrino mass basis and a matter term diagonal in the charged-lepton mass basis. We can write a first order perturbation equation using the plane-wave amplitudes in vacuum yielding

$$i \frac{d}{dt} a_i^\dagger(\vec{p}) a_j(\vec{p}) = [a_i^\dagger(\vec{p}) a_j(\vec{p}), H_{\text{vac}}] + [a_i^\dagger(\vec{p}) a_j(\vec{p}), H_{\text{int}}] \quad (1.60)$$

This equation neglects collisional terms and higher order refractive effects. The Hamiltonian has been separated into a refractive term in vacuum and one under the interaction with the medium. We can convert this equation into an equation for the density matrix by taking its expectation value $\rho = \langle \Psi | a_i^\dagger, a_j | \Psi \rangle$. The calculation yields an evolution equation of the form

$$i \frac{d\rho}{dt} = [\rho, H_0] + [\rho, V]. \quad (1.61)$$

The calculation of these terms requires some algebraic work which we will not fully transcribe here. The details can be found in reference [28].

If the states are sparsely occupied, then one can take the average density of neutrinos in some volume of momentum space as the quantity of study. Take a small region of momentum space $V_{\vec{p}}$ containing many momentum modes near \vec{p} ; we will from now on study the quantity $\rho(\vec{p}t)$ which is the average flavor density matrix in $V_{\vec{p}}$. The diagonal entries of this matrix give

$$\begin{aligned} \rho_{ii}(\vec{p}, t) &= \frac{\text{number of neutrinos of flavor } i \text{ in } V_{\vec{p}}}{\text{unit momentum}} \\ &= \sum_{\vec{q} \text{ in } V_{\vec{p}}} \frac{w_i(\vec{q})}{\text{no. momentum states in } V_{\vec{p}}} \times \frac{\text{no. momentum states}}{\text{unit momentum}}. \end{aligned} \quad (1.62)$$

In the same way, the off-diagonal entries carry the average phase interference factors in around \vec{p} .

1.5.2 Flavor continuity equation

In practice, neutrinos are never completely delocalized. But we can assume that inside a big enough volume they are approximately delocalized and that it is effectively enough to consider momentum eigenstates. This volume must be large compared to the Compton wave-length of the neutrinos yet small compared to the whole region of space in which we wish to track the evolution of flavor. We then divide space into a collection of these small yet large volumes, and we label each one of them with a three-dimensional position vector \vec{r} whose infinitesimal variation $d\vec{r}$ is much bigger than the wavelength of the neutrinos present in that volume. Our EoMs will contain an explicit evolution

in time given by the evolution in time of each collection neutrinos of approximate momentum \vec{p} inside each box, and an explicit evolution in space given by the transfer of neutrinos between boxes. Hence, there is no contradiction in studying the evolution of the fluid's flavor in both position and time, and with definite momentum.

Since scattering is neglected, the gas of neutrinos is a collection of many free-streaming fluids. Each one of them respects the continuity equation

$$\frac{d\rho}{dt}(\vec{p}, \vec{r}, t) = \frac{\partial\rho}{\partial t}(\vec{p}, \vec{r}, t) + \nabla \cdot [\vec{v}\rho(\vec{p}, \vec{r}, t)] \quad (1.63)$$

which must be valid independently for each free stream with velocity $\vec{v} = \vec{p}/|p|$. The total density $D(\vec{x}, t)$ at that point follows the continuity equation obtained by the sum of all the individual equations

$$\begin{aligned} \frac{dD}{dt}(\vec{r}, t) &= \frac{\partial D}{\partial t}(\vec{r}, t) + \nabla \cdot \int \frac{d\vec{p}}{(2\pi)^3} \vec{v} \rho(\vec{p}, \vec{r}, t) \\ &= \frac{\partial D}{\partial t}(\vec{r}, t) + \nabla \cdot \vec{J}(\vec{r}, t) \end{aligned} \quad (1.64)$$

where $\vec{J}(\vec{r}, t)$ is the total neutrino current in the box at position \vec{r} and at time t . The momentum is integrated over positive and negative momenta in order to take into account anti-neutrinos. Although this last equation may seem very simple, the fact remains that each individual mode with momentum p and velocity \vec{v} evolves differently and the computation of the weighted sum \vec{J} requires the knowledge of each individual density profile $\rho(\vec{p})$. For a given stream, neglecting deflection and scattering, $\rho\nabla \cdot \vec{v}$ is zero. One is therefore generally confronted with the equation

$$\frac{d\rho}{dt} = \frac{\partial\rho}{\partial t} + \vec{v} \cdot \nabla\rho = i[H, \rho]. \quad (1.65)$$

It is important to remember that this equation describes the transfer of neutrinos between neighbouring boxes labelled by their position in space and time. In the next few sections we will deduce the various Hamiltonian terms involved in neutrino oscillations.

1.5.3 Continuity and initial conditions in flavor space

If one is only interested in studying the interference of two mass states and two flavors – the electron flavor ν_e and some linear combination of the two heavy lepton flavors ν_X – with vacuum mixing angle θ_0 , then each matrix $\rho(\vec{p}, \vec{r}, t)$ can be written as the sum of a trace and a linear combination of the Pauli matrices.

$$\rho(\vec{p}, \vec{r}, t) = \frac{1}{2} [\text{Tr} \rho(\vec{p}, \vec{r}, t) + f(\vec{p}, \vec{r}, t) \mathbf{P} \cdot \boldsymbol{\sigma}], \quad (1.66)$$

where $f(\vec{p}, \vec{r}, t)$ is the square-root of the determinant of $\rho(\vec{p}, \vec{r}, t)$ and \mathbf{P} is a unit polarization vector. Both trace and determinant of the matrix – as we have already shown earlier – do not change under

the evolution of flavor. The only source of change for them is the transport of fluid from one box to the next as described by the continuity equation. We have

$$\begin{aligned} \dot{\rho}(\vec{p}, \vec{r}, t) &= \frac{1}{2} \left[\frac{d}{dt} \text{Tr} \rho + \left(\dot{f} \mathbf{P} + f \dot{\mathbf{P}} \right) \cdot \boldsymbol{\sigma} \right] \\ &= i [H(\vec{p}, \vec{r}, t), \rho(\vec{p}, \vec{r}, t)] = \frac{1}{2} f(\vec{p}, \vec{r}, t) [\mathbf{H}(\vec{p}, \vec{r}, t) \times \mathbf{P}(\vec{p}, \vec{r}, t)] \cdot \boldsymbol{\sigma}. \end{aligned} \quad (1.67)$$

where

$$H(\vec{p}, \vec{r}, t) \equiv \frac{1}{2} [\text{Tr} H(\vec{p}, \vec{r}, t) + \mathbf{H}(\vec{p}, \vec{r}, t) \cdot \boldsymbol{\sigma}] \quad (1.68)$$

We know that $\text{Tr} \rho(\vec{p}, \vec{r}, t) = n_\nu(\vec{p}, \vec{r}, t)$ is the total neutrino density of momentum \vec{p} at position \vec{r} and at time t . Omitting the momentum, space and time dependencies, the EoMs are

$$\frac{1}{f} \dot{n}_\nu + \left(\frac{\dot{f}}{f} \mathbf{P} + \dot{\mathbf{P}} \right) \cdot \boldsymbol{\sigma} = (\mathbf{H} \times \mathbf{P}) \cdot \boldsymbol{\sigma}, \quad (1.69)$$

from where we deduce that

$$\dot{n}_\nu = \partial_t n_\nu + \vec{v} \cdot \nabla n_\nu = 0 \quad (1.70)$$

and

$$\frac{\dot{f}}{f} \mathbf{P} + \dot{\mathbf{P}} = \frac{1}{f} (\partial_t f + \vec{v} \cdot \nabla f) \mathbf{P} + (\partial_t \mathbf{P} + \vec{v} \cdot \nabla \mathbf{P}) = \mathbf{H} \times \mathbf{P}. \quad (1.71)$$

This equation contains another continuity equation in itself. This can be seen by projecting the equation onto the direction of \mathbf{P} :

$$\frac{\dot{f}}{f} \mathbf{P} \cdot \mathbf{P} + \dot{\mathbf{P}} \cdot \mathbf{P} = (\mathbf{H} \times \mathbf{P}) \cdot \mathbf{P} = 0. \quad (1.72)$$

Then,

$$\frac{\dot{f}}{f} = \frac{1}{f} (\partial_t f + \vec{v} \cdot \nabla f) = -\dot{\mathbf{P}} \cdot \mathbf{P} = 0, \quad (1.73)$$

since by definition $\mathbf{P}^2 = 1$. Therefore,

$$\partial_t \mathbf{P} + \vec{v} \cdot \nabla \mathbf{P} = \mathbf{H} \times \mathbf{P}. \quad (1.74)$$

This equation contains two physically different terms. The first one ($\partial_t \mathbf{P}$) describes the change in flavor due to its natural precession inside each local volume. The second ($\vec{v} \cdot \nabla \mathbf{P}$) describes the change in flavor due to the transport of neutrinos from one volume to the adjacent ones.

If we assume that we can define an initial condition where the neutrino gas is flavor-polarized, i.e., where the density matrix is diagonal in flavor space, then the diagonal entries are equal to the

local densities of electron and heavy-lepton neutrino flavor

$$\rho^0(\vec{p}) = \begin{pmatrix} n_e^0(\vec{p}) & 0 \\ 0 & n_X^0(\vec{p}) \end{pmatrix} \quad (1.75)$$

at the initial condition. The square-root of the determinant is

$$f^0(\vec{p}) = n_e^0(\vec{p}) - n_X^0(\vec{p}) \quad (1.76)$$

and

$$\mathbf{P}^0(\vec{p}) = (0, 0, 1). \quad (1.77)$$

To avoid having to deal explicitly with the transport terms, one often chooses the coordinate system in such a way that some symmetries are apparent and $f(\vec{p}, \vec{r}, t)$ does not change as the system evolves. For example, in a uniform fluid where $\rho(\vec{p}, \vec{r}, t) = \rho(\vec{p}, t)$ one would define f by its initial value $f(\vec{p}, \vec{r}, t = 0) = f(\vec{p}, t = 0)$, since in this case we have $\nabla f = 0$, then

$$\partial_t f + \vec{v} \cdot \nabla f = \partial_t f = 0 \Rightarrow f(\vec{p}, t) = f(\vec{p}, t = 0) \quad (1.78)$$

In the case of a supernova however, where one wants to study the change of flavor of a stationary emission of neutrinos as a function of the distance to the core, one must define f differently as to avoid its natural $1/r^2$ decay because of the continuity equation.

1.6 Self-consistent approach and EoMs

We highlight two important assumptions that we have made and that are common in the literature:

- We consider a volume of space big enough so that any quantum correlations between modes of different momentum vanish. Then we study the interaction of two of these volume as dictated by the EoMs. Some authors have claimed that in view of the non-linear nature of the neutrino-neutrino interaction, this assumption may be erroneous [29].
- Many-particle correlations are neglected. For a formalism to study the system taking into account two-body correlations see reference [30].

These assumptions are called the mean field approximation. One solves the equations as if each neutrino of momentum \vec{p} behaved like all the others of same momentum. Under this assumption, we can say that the background neutrino density and the background neutrino current in the neutrino-neutrino refraction term can be expressed as a sum of all the individual contributions of each mode

of momentum \vec{p}

$$\begin{aligned}\mathbf{N}(\vec{r}, t) &= \int f(\vec{p}, \vec{r}, t) \mathbf{P}(\vec{p}, \vec{r}, t) \frac{d\vec{p}}{(2\pi)^3}, \\ \vec{\mathbf{J}}(\vec{r}, t) &= \int f(\vec{p}, \vec{r}, t) \frac{\vec{p}}{|\vec{p}|} \mathbf{P}(\vec{p}, \vec{r}, t) \frac{d\vec{p}}{(2\pi)^3}.\end{aligned}\tag{1.79}$$

This goes to say that we assume that the background medium of neutrinos follows the same equations as the test neutrino. $\mathbf{P}(\vec{p}, x, t)$ is the unit polarization vector of mode \vec{p} of the box at position x and at time t and $f(\vec{p}, x, t)$ its length. Using the flavor continuity equation (1.65), we obtain the EoM for \mathbf{P}

$$\frac{\partial \mathbf{P}}{\partial t}(\vec{p}, \vec{r}, t) + \vec{v} \cdot \nabla \mathbf{P}(\vec{p}, \vec{r}, t) = \left\{ \omega \mathbf{B} + \lambda(\vec{r}, t) \mathbf{L} + \sqrt{2} G_F \left[\mathbf{N}(\vec{r}, t) - \vec{v} \cdot \vec{\mathbf{J}}(\vec{r}, t) \right] \right\} \times \mathbf{P}(\vec{p}, \vec{r}, t)\tag{1.80}$$

This equation is the main EoM that we will analyse through the rest of the thesis. Note that under the mean-field assumption it is non-linear due to the terms $\mathbf{N} \times \mathbf{P}$ and $(\vec{v} \cdot \vec{\mathbf{J}}) \times \mathbf{P}$. These terms will be the source of many new dynamics not encountered in the usual linear vacuum and matter flavor oscillations.

1.7 Summary

We saw throughout this chapter how phase differences evolve between interaction states of a neutrino and how they are influenced by the presence of electrons, neutrons and other neutrinos. We summarize the following points:

- Neutrino oscillations come from the interference of different mass wave-functions. These wave-functions have a relativistic dispersion relation between the energy and the momentum, $E^2 - p^2 = m^2$ in vacuum, which we then linearized in the ultra-relativistic limit. We neglected changes in the spin of the neutrinos which so far seems to be admissible given the insufficient strength of magnetic fields in core-collapse SN and in the early universe, where collective oscillation are susceptible to occur.
- We assumed the 3-flavor oscillation pattern to decouple into two effective 2-flavor patterns with different time/length-scales. This is often a good approximation though there are exceptions, such as the cooling phase of a SN.
- Neutrinos are produced and absorbed in interaction states. A high matter density causes the eigenstate of propagation to be asymptotically coincident with the interaction states. Therefore, if neutrinos are produced in a region of high matter density they stay in their original state for as long as matter remains dense.

In the next chapter we will explore the effects caused by the presence of neutrino-neutrino interactions. The neutrino-neutrino interaction is radically different from the one neutrinos have with matter because, whereas the collisionless passage of neutrinos through matter leaves matter unchanged, the refractive effect a particular beam of neutrinos inflicts on its fellow particles is just as great as the one that is inflicted upon it by the others. This means the background participates in the oscillation phenomenon, which is why these oscillations are called collective oscillations.

CHAPTER 2

Collective oscillations

In this chapter we will describe the phenomena most commonly encountered in collective neutrino oscillations. We will use the example of a fluid which in its initial state is uniform, that is, the flavor content and neutrino density is identical at every point. Despite this simplification, the qualitative results apply in general and the quantitative analysis is also easy to extrapolate, as we will see in chapter 6. Many novel dynamics were discovered in the study of the oscillations induced by neutrino-neutrino refraction. One finds that the neutrinos can evolve in synchronicity and that this behavior can result in complete inversions of the flavor content in certain regions of the energy spectrum. These inversions are called *spectral splits*.

2.1 Energy spectrum

As we saw in the previous chapter, the length of the polarization vector obeys the continuity equation for each mode of momentum \vec{p} :

$$\partial_t f(\vec{p}; \vec{r}, t) + \vec{v} \cdot \nabla f(\vec{p}; \vec{r}, t) = 0. \quad (2.1)$$

In this chapter we assume that the gas is initially uniform, i.e., that $\nabla \rho = 0$. This implies that $f(\vec{p}; \vec{r}, t) = f(\vec{p}; t = 0)$ and that $\mathbf{P}(\vec{p}; \vec{r}, t) = \mathbf{P}(\vec{p}; t = 0)$. In this case, the EoMs (1.80) are

$$\frac{\partial \mathbf{P}}{\partial t}(\vec{p}; t) = \left\{ \omega \mathbf{B} + \lambda(t) \mathbf{L} + \sqrt{2} G_F \left[\mathbf{N}(t) - \vec{v} \cdot \vec{\mathbf{J}}(t) \right] \right\} \times \mathbf{P}(\vec{p}; t) \quad (2.2)$$

We have also assumed that λ is independent of the position, that is, that there are no inhomogeneities in the electron background.

Because ω are the actual precession rates in vacuum, it is preferable to write the equations down

in terms of this variable exclusively. Under the mean-field approximation, we have

$$\begin{aligned}
\sqrt{2} G_F \mathbf{N} &= \sqrt{2} G_F \int f(\vec{p}) \mathbf{P}_{p,\vec{v}} \frac{d\vec{p}}{(2\pi)^3} \\
&= \sqrt{2} G_F \iint f\left(\frac{\Delta m^2}{2\omega}, \vec{v}\right) \left| \frac{\Delta m^2}{2\omega^2} \right| \left(\frac{\Delta m^2}{2\omega} \right)^2 \mathbf{P}_{\omega,\vec{v}} d\omega d\vec{v} \\
&\equiv \sqrt{2} G_F (n_{\bar{\nu}_e}^0 - n_{\bar{\nu}_X}^0) \iint g(\omega, \vec{v}) \mathbf{P}_{\omega,\vec{v}} d\omega d\vec{v}
\end{aligned} \tag{2.3}$$

with

$$g(\omega, \vec{v}) d\omega d\vec{v} = \frac{1}{n_{\bar{\nu}_e}^0 - n_{\bar{\nu}_X}^0} f(\vec{p}) \frac{d\vec{p}}{(2\pi)^3}. \tag{2.4}$$

In this last equation, we have defined the distribution function $g(\omega, \vec{v})$ in such a way that the integral over the anti-neutrino range of ω is normalized to -1 . We define the strength of the neutrino-neutrino refractive effect as the Fermi constant times the difference between the number of electron anti-neutrinos and the number of heavy-lepton anti-neutrinos:

$$\mu \equiv \sqrt{2} G_F (n_{\bar{\nu}_e}^0 - n_{\bar{\nu}_X}^0). \tag{2.5}$$

With this definition we normalize the distribution of function g to -1 for anti-neutrinos and to $1 + \epsilon$ for neutrinos. ϵ is called the neutrino-antineutrino asymmetry and is zero when $\bar{\nu}$ and ν are present in equal parts, it is -1 when the density of neutrinos is negligible in comparison to the density of antineutrinos and infinite when the density of antineutrinos is negligible in comparison with the density of neutrinos¹. In other words,

$$1 + \epsilon \equiv \frac{n_{\nu_e}^0 - n_{\nu_X}^0}{n_{\bar{\nu}_e}^0 - n_{\bar{\nu}_X}^0}. \tag{2.6}$$

In the inverted hierarchy ($\Delta m^2 > 0$), ω is positive for neutrinos and negative for anti-neutrinos, meaning

$$\begin{cases} \iint_0^{+\infty} g_{\text{IH}}(\omega, \vec{v}) d\omega d\vec{v} = 1 + \epsilon & (\text{neutrinos}), \\ \iint_{-\infty}^0 g_{\text{IH}}(\omega, \vec{v}) d\omega d\vec{v} = -1 & (\text{antineutrinos}). \end{cases} \tag{2.7}$$

On the other hand, in the inverted hierarchy ($\Delta m^2 > 0$), positive values of ω correspond to negative values of energy, thus calling for the definition

$$\begin{cases} \iint_0^{+\infty} g_{\text{NH}}(\omega, \vec{v}) d\omega d\vec{v} = -1 & (\text{antineutrinos}), \\ \iint_{-\infty}^0 g_{\text{NH}}(\omega, \vec{v}) d\omega d\vec{v} = 1 + \epsilon & (\text{neutrinos}), \end{cases} \tag{2.8}$$

In the absence of muons and taus, the processes producing the heavy-lepton neutrinos and the heavy-

¹Actually, to be strictly correct, by density of neutrinos we mean flavor difference density, that is, $n_{\nu_e}^0 - n_{\nu_X}^0$

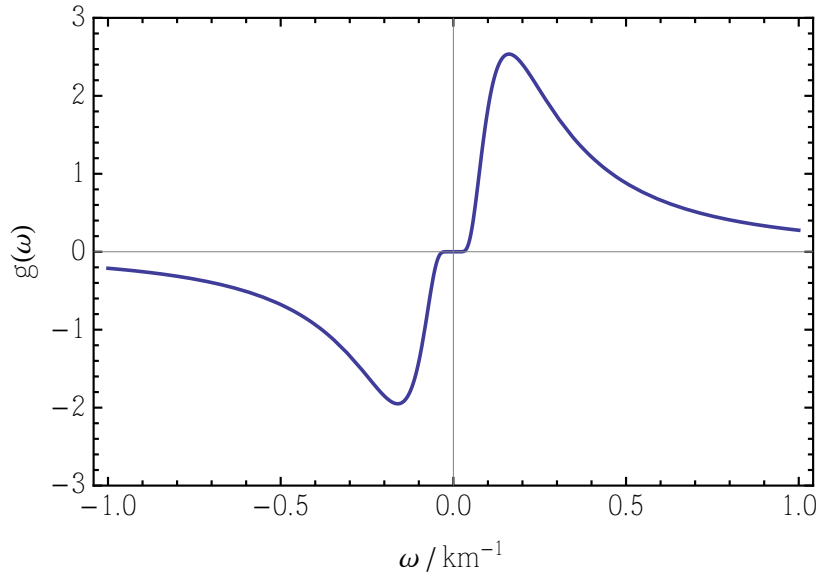


Figure 2.1: The corresponding omega spectrum for an energy distribution of the Fermi-Dirac type in the normal hierarchy $\Delta m^2 > 0$. Positive ω 's correspond to neutrinos while the negative values make up the anti-neutrino spectrum. The positive part normalizes to $1 + \epsilon$ and the negative one to -1 . After the peak, for higher values of $|\omega|$, the distribution decays roughly with ω^2 .

lepton anti-neutrinos are the same (NC) and, as a consequence, so are their number densities. Under this assumption, the definition of ϵ can be restated as

$$\epsilon \equiv \frac{n_{\nu_e}^0 - n_{\nu_X}^0}{n_{\bar{\nu}_e}^0 - n_{\bar{\nu}_X}^0} - 1 = \frac{n_{\nu_e}^0 - n_{\nu_X}^0 - n_{\bar{\nu}_e}^0 + n_{\bar{\nu}_X}^0}{n_{\bar{\nu}_e}^0 - n_{\bar{\nu}_X}^0} = \frac{n_{\nu_e}^0 - n_{\bar{\nu}_e}^0}{n_{\bar{\nu}_e}^0 - n_{\nu_X}^0} \quad (2.9)$$

2.2 Co-rotating frame

In the mean-field approximation (2.3), the non-linear term only depends on the cross-product of every pair of polarization vectors. Therefore, if every polarization vector is rotated by the same amount, this term is also rotated likewise. Because of this, one can simplify the equations by moving to a frame that rotates with the frequency induced by the electron background thanks to the fact that this contribution is identical for all vectors. Namely, in this case of a homogeneous gas of neutrinos, the effect of matter can be rotated away, leaving us with a system which is in practice equivalent to a system of many neutrinos in vacuum with a very small mixing angle.

Since the flavor vectors can only move on the unit sphere, it is often more intuitive to write down the equations in terms of spherical coordinates. We write the three component polarization as the combination of a vector on the xy plane – denoted by a complex number p of norm smaller

than 1 – and a real number indicating the component along the z axis:

$$\mathbf{P} = \begin{pmatrix} p \\ P_z \end{pmatrix}. \quad (2.10)$$

In this way, p describes ρ_{eX} and P_z , as usual, $\rho_{ee} - \rho_{XX}$. The off-diagonal components of the density matrix are given by p and p^* , i being the 90° rotation on the xy plane. In the flavor basis, the polarization vectors are, in spherical coordinates,

$$\mathbf{P}_{\omega, \vec{v}} = \begin{pmatrix} \sin \theta(\omega, \vec{v}) e^{i\varphi(\omega, \vec{v})} \\ \cos \theta(\omega, \vec{v}) \end{pmatrix}. \quad (2.11)$$

$\theta(\omega, \vec{v})$ and $\varphi(\omega, \vec{v})$ are functions that give the latitude and longitude on the Bloch sphere of each flavor mode defined by ω, \vec{v} . They also vary in time and spatial position. The neutrino-neutrino term is

$$\begin{aligned} \mathbf{R}(\vec{v}, t) &= R(\vec{v}, t) \begin{pmatrix} \sin \Theta(\vec{v}, t) e^{i\Phi(\vec{v}, t)} \\ \cos \Theta(\vec{v}, t) \end{pmatrix} \\ &\equiv \int (1 - \vec{v} \cdot \vec{v}') \mathbf{P}(\omega', \vec{v}'; t) d\Gamma \\ &= \mathbf{D}(t) - \vec{v} \cdot \vec{\mathbf{A}}(t), \end{aligned} \quad (2.12)$$

where

$$\int d\Gamma = \int_{-\infty}^{+\infty} d\omega \int d\vec{v} g(\omega, \vec{v}). \quad (2.13)$$

\mathbf{D} is the scalar component of the flavor vector and $\vec{\mathbf{A}}$ is a spatial vector of vectors in flavor space that sums up the vector part of the “order parameter”, whose components are

$$\begin{aligned} \mathbf{D}(t) &= \int \mathbf{P}(\omega, \vec{v}, t) d\Gamma, \\ \vec{\mathbf{A}}(t) &= \int \vec{v} \mathbf{P}(\omega, \vec{v}, t) d\Gamma \end{aligned} \quad (2.14)$$

are the scalar and vector parts of the order parameter.

We use the term order parameter as both \mathbf{D} and $\vec{\mathbf{A}}$ give us insight into the distribution of the polarization vectors:

- if all the polarization vectors are uniformly distributed along the energy spectrum, i.e., there is no correlation between the position of $\mathbf{P}(\omega)$ on the Bloch sphere and ω , then $\mathbf{D} = 0$;
- if all the polarization vectors are uniformly distributed along the velocity spectrum along some direction \vec{u} , i.e., there is no correlation between the position of $\mathbf{P}(\vec{v})$ on the Bloch sphere and $\vec{u} \cdot \vec{v}$, then $\vec{u} \cdot \vec{\mathbf{A}} = 0$;

- if the correlation between energy and velocity along some direction \vec{u} are identical, then $\mathbf{R}(\vec{u}) = \mathbf{D} - \vec{u} \cdot \vec{\mathbf{A}} = 0$. This is the case when all neutrinos stream in the same direction \vec{u} .

For now, we will analyse a situation in which there is no preferred direction, that is, $\vec{\mathbf{A}} = 0$ and $\mathbf{R} = \mathbf{D}$. In this case, the EoMs become

$$\begin{cases} \dot{\theta} = -\omega \sin 2\theta_0 \sin \varphi + \mu R \sin(\Theta) \sin(\varphi - \Phi) \\ \dot{\varphi} = \omega(\cos 2\theta_0 - \sin 2\theta_0 \cot \theta \cos \varphi) + \lambda + \mu R \cos(\Theta) - \mu R \sin(\Theta) \cot(2\theta) \cos(\varphi - \Phi) \end{cases} \quad (2.15)$$

It is noticeable that the matter term impacts all modes equally by adding a common precession rate λ around the z -axis. The neutrino-neutrino refractive effects come into play when the matter density is also high, with $\lambda \sim 10 - 1000$, which in any case is always much larger than the average value of ω . Because λ is a common precession rate, one can make the coordinate change $\varphi \rightarrow \varphi - \lambda t$. This in practice is the same as going to a frame of reference (in flavor space) that rotates with frequency $-\lambda$ around the flavor axis z . The order parameter is changed according to

$$\Phi \rightarrow \Phi - \lambda t \quad (2.16)$$

Since the self-interaction depends on $\varphi - \Phi$, it is unchanged by this change of frame. That was to be expected, as $\mathbf{R} \times \mathbf{P}$ does not vary if \mathbf{R} and \mathbf{P} are rotated by the same angle. The new EoMs are

$$\begin{cases} \dot{\theta} = -\omega \sin 2\theta_0 \sin(\varphi + \lambda t) + \mu R \sin \Theta \sin(\varphi - \Phi) \\ \dot{\varphi} = \omega[\cos 2\theta_0 - \sin 2\theta_0 \cot \theta \cos(\varphi + \lambda t)] + \mu R \cos \Theta - \mu R \sin(\Theta) \cot \theta \cos(\varphi - \Phi) \end{cases} \quad (2.17)$$

The matter term vanished, but it somehow reappeared in the vacuum term. The mass eigenstate direction now, which was stationary in the previous frame of reference, is given by a vector which rotates with frequency $-\lambda$:

$$\mathbf{B} = \begin{pmatrix} \sin 2\theta_0 e^{-i\lambda t} \\ \cos 2\theta_0 \end{pmatrix} \quad (2.18)$$

If, as we said, the initial condition comes accompanied by a high density matter background, then the terms $\cos(\varphi + \lambda t)$ and $\sin(\varphi + \lambda t)$ average out to zero over a very small period of time. Therefore the equations in this regime are

$$\begin{cases} \langle \dot{\theta} \rangle = \mu R \sin(\Theta) \sin(\langle \varphi \rangle - \Phi + \eta) \\ \langle \dot{\varphi} \rangle = \omega \cos 2\theta_0 + \mu R \cos \Theta - \mu R \sin \Theta \cot \theta \cos(\langle \varphi \rangle - \Phi + \eta) \end{cases} \quad (2.19)$$

where the average variations are taken over a period of $2\pi/\lambda t$. η is a small noise perturbation arising from the highly oscillatory xy part of \mathbf{B} . The EoMs in vector notation in this reference

frame, neglecting the noise and dropping the brackets to denote a short averaging

$$\dot{\mathbf{P}}(\omega; t) = \omega \langle \mathbf{B} \rangle \times \mathbf{P}(\omega; t) + \mu \mathbf{R} \times \mathbf{P}(\omega; t) \quad (2.20)$$

$\langle \mathbf{B} \rangle$ is a vector that points along the positive z direction. This vector has a norm $\cos 2\theta_0$. In the high density media in which neutrinos decouple from the weakly charged background, all polarization vectors propagate in the interaction eigenstate, as we argued in an earlier section. They point in the positive z direction, which serves the initial condition $P_z^0 = n_{\nu_e}^0(\vec{p}) - n_{\nu_X}^0(\vec{p})$. With this configuration, the order parameter is

$$\mathbf{R}^0 = (0, 0, \epsilon\mu) \quad (2.21)$$

because

$$\epsilon = \int d\Gamma \quad (2.22)$$

by definition. When all the polarization vectors are initialized in the positive z direction, $\dot{\mathbf{P}}$ vanishes because all the intervenient vectors are co-linear. Whether this configuration remains stable under the “shaking” caused by the neglected xy component of \mathbf{B} is one of the main questions adressed in this thesis.

Looking at the dynamics in this co-rotating frame leads one to a startling conclusion. The situation described in eq. (2.20) is similar to the situation in the non-co-rotating frame with $\lambda \rightarrow 0$ and $\omega \rightarrow \omega \cos 2\theta_0$. In the absence of neutrino-neutrino refraction, i.e., $\mu = 0$, the flavor vectors quickly distribute themselves on a narrow cone, as each of them precesses around z with a different frequency (cf. eq. 2.19). This phenomenon is known as *decoherence*. It is essential to develop the neutrino-neutrino term given that this one depends on \mathbf{R} being non-colinear with each \mathbf{P} . But considering this, if the vacuum angle is near maximum ($2\theta_0 \approx \pi/2$), then $\omega \cos 2\theta_0 \approx 0$ which means decoherence is prevented. And because of this, all flavors vectors stick together, preventing the neutrino-neutrino term from developing! We therefore come to the counter-intuitive conclusion that a large vacuum mixing suppresses collective oscillations. This suppression was observed numerically as reported in [31], where further details into the co-rotating frame can also be found.

It should be pointed out that neglecting the matter effects – or, in the co-rotating frame, the precessing transverse component of \mathbf{B} – can only be done in the regime where λ is much higher then ω . This is generally the case in a SN where the collective effects wither before the MSW conditions are reached for either mass differences.

2.3 Conserved quantities: Hamilton function and lepton number

As we already states before, the dynamics of the polarization vectors bear a striking similarity to the equations of an interacting collection of classical spins. We built on the results of section 1.2 where we deduced the Hamilton function of a polarization vector in a medium. The Hamiltonian

of the complete system is

$$H = \int \left[\omega \mathbf{B} + \lambda \mathbf{L} - \frac{\mu}{2} (\mathbf{D} - \vec{v} \cdot \vec{\mathbf{A}}) \right] \cdot \mathbf{P} d\Gamma. \quad (2.23)$$

The EoMs are recovered by using

$$\dot{\mathbf{P}}(\omega, \vec{v}, t) = \frac{1}{g(\omega, \vec{v})} \{ H, \mathbf{P}(\omega, \vec{v}, t) \} \quad (2.24)$$

and the fact that the Poisson bracket is

$$\{ P_i(\omega', \vec{v}'; t), P_j(\omega, \vec{v}, t) \} = \delta(\omega - \omega') \delta(\vec{v} - \vec{v}') \varepsilon_{ijk} P_k. \quad (2.25)$$

In the co-rotating frame at high λ , another quantity is also conserved:

$$L = \langle \mathbf{B} \rangle \cdot \mathbf{D} \quad (2.26)$$

which corresponds to the total lepton number of the ensemble. This can be verified by

$$\dot{L} = \frac{1}{g(\omega, \vec{v})} \{ H, \langle \mathbf{B} \rangle \cdot \mathbf{D} \}. \quad (2.27)$$

This is not true in cases when the matter effect has physical consequences (when $\lambda \sim \mu$ for example). Since $\langle \mathbf{B} \rangle$ is a pure z vector in the co-rotating frame, this means the total density $n_{\nu_e} - n_{\bar{\nu}_e}$ must be conserved which is equivalent to a lepton number conservation. This conservation law imposes constraints on the amount of flavor conversion due to collective oscillations. Indeed, if a part of the spectrum of antineutrinos changes its flavor content, then necessarily the neutrino spectrum must also change to compensate. This principle will be very useful in the next section.

2.4 Fixed configurations and synchronized oscillations

As we pointed out in section 1.2, in a high density background of matter, the configuration in which all vectors point along the z direction is fixed, whether in the positive or negative direction. That means that a system placed *exactly* in this configuration remains in that configuration. This is for example, the state in which neutrinos are when they decouple from the gas, when the density matrix is diagonal in the flavor basis. However, the noise induced by B_{\perp} in the co-rotating frame is moves at random the vectors slightly away from the z direction. In some cases, as we will prove in the next chapter, the neutrino-neutrino interaction can lead to an exponential motion away from the flavor direction. In other words, the propagation in the flavor state becomes unstable. Nevertheless, based on intuition gained from numerical simulations, another configuration has been found to be stable, to which the polarization vectors move after they leave the flavor states. This configuration

corresponds to all flavor vectors distributed on a common vertical plane and precessing with a common frequency. This phenomenon is called *synchronized oscillation* [32].

Consider now a uniform ensemble of neutrinos with $\vec{\mathbf{A}} = 0$ in the co-rotating frame. Denoting $\langle \mathbf{B} \rangle \rightarrow \mathbf{B}$ and $\omega \rightarrow \omega \cos 2\theta_0$ for the sake of conciseness, the EoMs read

$$\dot{\mathbf{P}}_\omega = (\omega \mathbf{B} + \mu \mathbf{D}) \times \mathbf{P}_\omega \equiv \mathbf{H}_\omega \times \mathbf{P}_\omega. \quad (2.28)$$

We have dropped the angular indexes for the polarization vectors since in the exact situation in which the vector order parameter is null, all of them follow the same trajectory. The order parameter receives a contribution of $g(\omega)$ from each of them – the integrated length spectrum. The configuration in which each \mathbf{P}_ω points along the direction of its own \mathbf{H}_ω is a fixed configuration. In other words, $\mathbf{P}_\omega = \mathbf{H}_\omega/|\mathbf{H}_\omega|$ (the polarization vectors are unit vectors). However, in this case the configuration is given by a self-consistent constraint:

$$\mathbf{D} \equiv \int \mathbf{P}_\omega d\Gamma = \int_{-\infty}^{+\infty} \frac{\mathbf{H}_\omega}{|\mathbf{H}_\omega|} g(\omega) d\omega = \int_{-\infty}^{+\infty} \frac{\omega \mathbf{B} + \mu \mathbf{D}}{|\omega \mathbf{B} + \mu \mathbf{D}|} g(\omega) d\omega \quad (2.29)$$

The equation remains valid for as long as the motion of \mathbf{D} is slow compared to the motion of each individual mode. One would somehow expect it to be so, since \mathbf{D} is a collective vector.

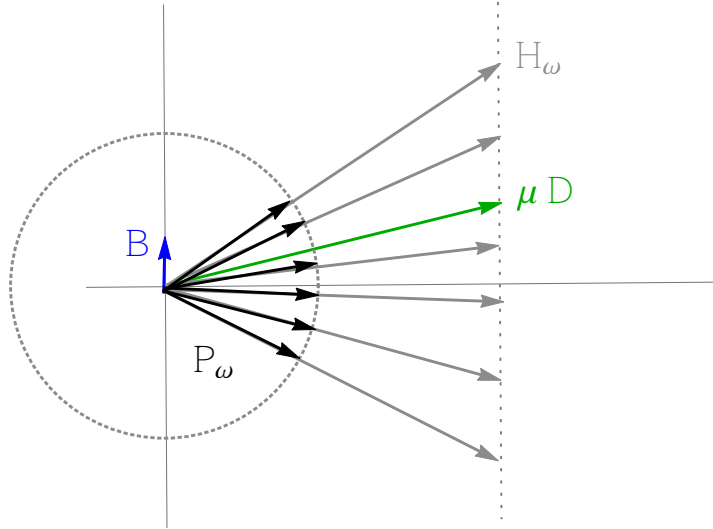


Figure 2.2: If μ is adiabatically decreased, the flavor vectors follow their individual \mathbf{H}_ω while \mathbf{D} describes a slow precession around \mathbf{B} . Its off-diagonal component increases at first and then decreases again, projecting a part of the spectrum onto the opposite flavor direction. The diagonal component of \mathbf{D} remains equal to ϵ whereas the off-diagonal part and its precession frequency are given by the self-consistency constraint (2.29).

It would appear, according to the simulations, that the stable configuration is one where all \mathbf{H}_ω distribute themselves on a vertical plane and precess with a common frequency ω_{sync} around the z axis as depicted in figure 2.2. An analytical proof of the stability of this configuration is, to this date, still missing.

2.5 Spectral splits

In a SN scenario, the interaction strength decreases with $1/r^4$. Leaving the proof for later, the interaction strength decreases with the usual spherical factor $1/r^2$, to which a factor of $1/r^2$ is added to make-up for the narrowing of the direction of the stream at large distances from the core. It is therefore interesting to study the outcome of the ensemble of polarization vectors when the self-coupling strength is adiabatically turned off. The numerical study of this scenario has led to the very interesting discovery of complete conversions on large portions of the energy spectrum, called *spectral splits* [33]. We observe a complete reversal of the flavor content up to a certain frequency ω_c . This frequency is actually easy to compute based on conservation arguments. In the final state, all flavor vectors end up in the fixed configuration with their directions pointing either up or down along the z axis, as shown in figure 2.4. The numerical observation is that there is a frequency that splits the modes into those that will collapse to the value $P_z = 1$ and $P_z = -1$. We mentioned earlier that the lepton number L is conserved by these equations. That puts certain restrictions on the flipping of flavor of large portions of the spectrum. In simple terms, the area under the spectrum must be conserved and equal to the neutrino-antineutrino asymmetry:

$$L = \mathbf{B} \cdot \mathbf{D} = \int_{-\infty}^{+\infty} g(\omega) \mathbf{B} \cdot \mathbf{P}_\omega^0 d\omega = \int_{-\infty}^{+\infty} g(\omega) d\omega = \epsilon \quad (2.30)$$

In the final configuration, once μ has decreased to zero, we find

$$L = \int_{-\infty}^{\omega_c} g(\omega) d\omega - \int_{\omega_c}^{+\infty} g(\omega) d\omega = \epsilon \quad (2.31)$$

This equation based on simple principles defines the parting frequency altogether. For example, if $\epsilon > 0$ then $\omega_c > 0$, and the split happens at the exact point at which the neutrino spectrum has same total weight as the anti-neutrino spectrum (cf. figure 2.3).

These splits are easy to understand in the adiabatic limit, as they actually correspond to an analogous effect to the MSW resonant conversion. As we said earlier, the configuration in which all the flavor vectors point along their own \mathbf{H}_ω is a fixed configuration. When the system is initialized, the \mathbf{H}_ω are all colinear with the z axis and so are the flavor vectors. This is the solution indicated by the self-consistency constraints (2.29) in the limit $\mu \rightarrow \infty$. But as μ is decreased, other solutions become possible. The collective vector \mathbf{D} begins to precess around \mathbf{B} is the frequency indicated by equation (2.31). One can go to a new coordinate frame that precesses with this collective frequency.

In this frame, all the \mathbf{H}_ω remain on a static plane. As figure 2.2 shows, $\mu\mathbf{D}$ first increases, dragging the individual modes along with it. But when μ vanishes the modes are brought back onto the vertical direction. In this reference frame, $\mathbf{H}_\omega = (\omega - \omega_c)\mathbf{B} + \mu\mathbf{D}$. The modes with $\omega > \omega_c$ fall back onto the positive direction whereas the others end up in the opposite direction.

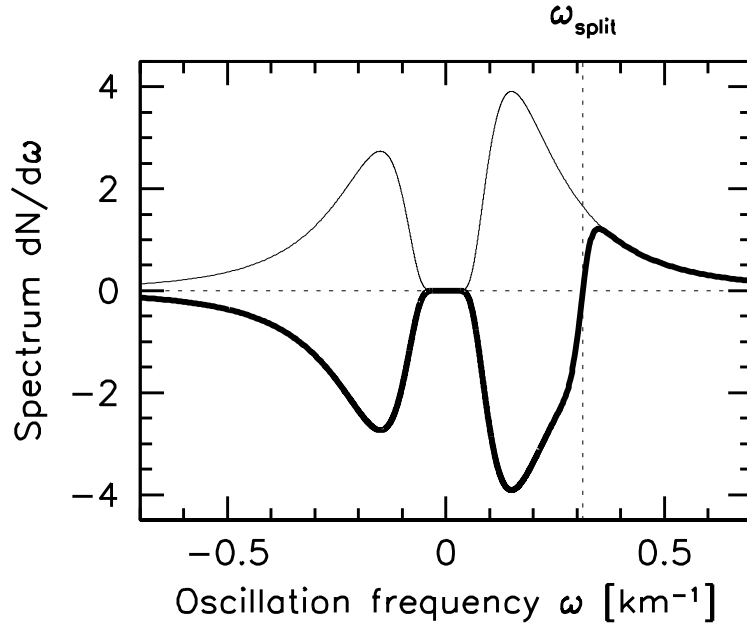


Figure 2.3: The final result of a spectral split phenomenon [34]. The vertical axis shows the z component of $|g(\omega)|\mathbf{P}_\omega$ for the initial (thin gray line) and final configurations (thick black line). The conservation of L demands that the area under the curve for positive frequencies minus the area for negative frequencies remains equal to ϵ , preventing the upper part of the spectrum from flipping its flavor.

2.6 Summary

In this chapter, we have deduced the equations of motion for an infinite collection of momentum modes. We have also seen that, for a uniform isotropic gas, these equations lead to spectral splits, caused by the dragging down of the flavor vectors on a common rotating plane. This can only happen when the original initial state – of all the flavor vectors pointing along the z direction – becomes unstable and the vectors shift to another other fixed state: the synchronized oscillation, whose stability has been numerically tested but never proven analytically.

One may question oneself on the importance of explicit angular modes. Figure 2.5 shows the difference between a single-angle treatment and a multi-angle simulation. Though the trajectories are a bit changed, the rough properties seem to be maintained. The initial configuration becomes unstable leading to spectral splits in the final state. In the next chapter we will show that angular modes can indeed lead to drastic differences when it comes to the stability of the initial configuration.

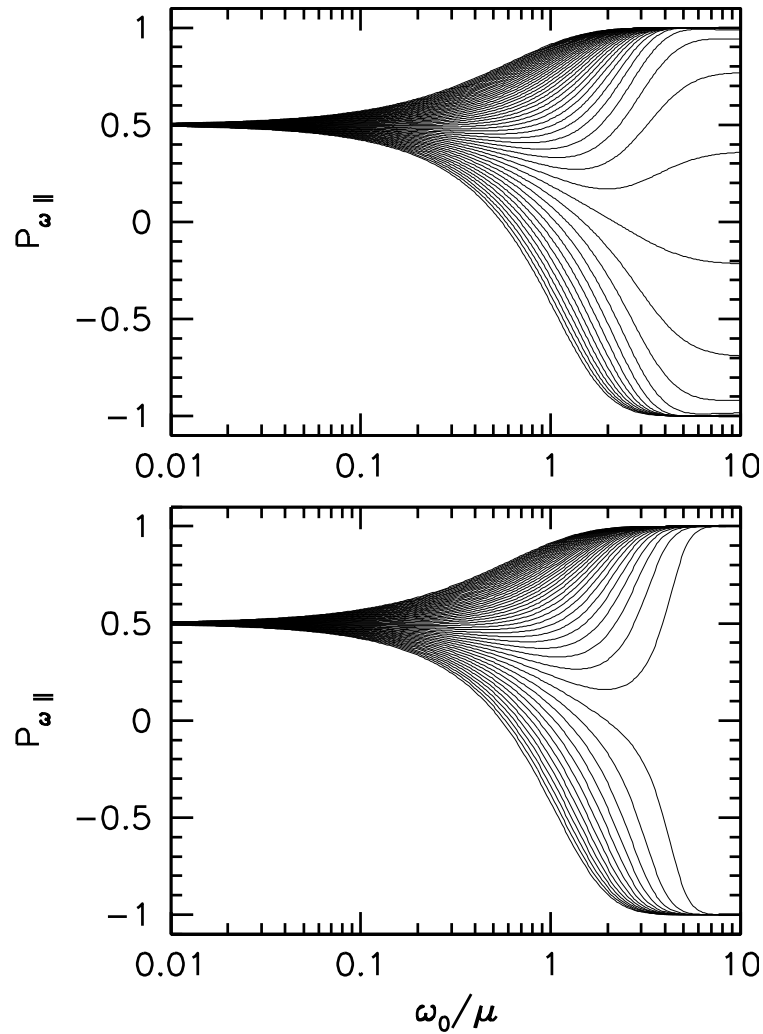


Figure 2.4: The diagonal component of each mode as a function of ω/μ . The lower panel shows the results computed according to the consistency constraint (2.29). The upper panel shows the actual result of a numerical simulation evolved in time with $\mu(t) \propto \exp -t/100$. Note that in this case the vectors were all initialized in a common direction different from $\hat{\mathbf{z}}$. The difference between the obtained, smeared spectral flip and the predicted sharp-split spectrum can be blamed on non-adiabaticities.

We will show the nature of these differences by studying the stability of a uniform isotropic gas and by comparing those results to a two-angular mode case. In addition, in solving these two cases, we will introduce a new phenomenon called *bipolar oscillations*.

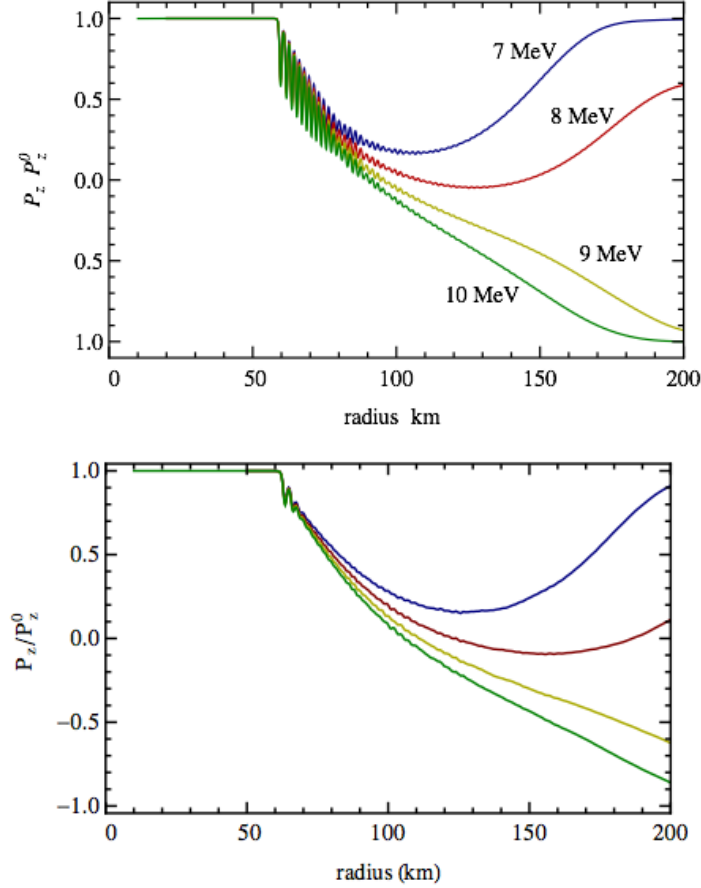


Figure 2.5: Evolution of the z component of different modes in a single-angle (upper panel) and multi-angle (lower panel) treatment in the context of SN [35]. Three distinct phases are discernible. A static phase when all self-interaction safeguards the initial configuration, followed by a phase of dampened bipolar oscillations and finally the splitting of the spectrum. In practice, one can never eliminate the non-adiabatic effects, which are visible in the strong oscillatory period following the instability of the initial conditions. As μ decreases and the two fixed configurations part, it takes a while before the vectors are drawn to the synchronized configuration. The motion towards this state is done half-abruptly causing small oscillations which cannot be eliminated. One can link the unavoidable non-adiabaticity to the discontinuity of the trajectories near the onset of flavor conversion. This discontinuity will be better understood in the next chapter.

CHAPTER 3

Bipolar oscillations and spontaneous symmetry breaking

Simulations of a free-streaming fluid of neutrinos interacting with each other and with matter led to the discovery of several new effects, which were presented partially in the last chapter. In this chapter we study an isotropic uniform gas of neutrinos as a simple model to understand both the onset of flavor conversion due to the self-coupling term and the oscillating behavior observed in the simulations. We will show that the oscillations in this case mimic the dynamics of a classical pendulum. In a second part, we will devote ourselves to understanding the solidity of the isotropy assumption. By that we mean the following question: if a the gas is almost symmetric, i.e., if $\vec{\mathbf{A}}$ is initially small, does it remain small or does it grow to non-neglegible proportions? This question was the main focus of the author's work during the development of this thesis. As we will see, the neglected current vector does grow exponentially in many situations, leading to radically different results. This is an example of *spontaneous symmetry breaking*.

3.1 Flavor evolution of a uniform isotropic gas

Let's recall the EoMs of the polarization vectors for an ensemble of neutrinos

$$\left(\frac{\partial}{\partial t} + \vec{v} \cdot \nabla\right) \mathbf{P} = \left[\omega \mathbf{B} + \lambda \mathbf{L} + \mu (\mathbf{D} - \vec{v} \cdot \vec{\mathbf{A}})\right] \times \mathbf{P}. \quad (3.1)$$

Though omitted, one must remember that \mathbf{P} is a function of the three spatial coordinates \vec{r} , of time t , of the energy (in the form of the vacuum oscillation frequency) ω and of the velocity. In this chapter we assume that:

- the fluid is uniform, i.e., $\nabla \mathbf{P}(\vec{r}, t) = 0$;
- the fluid is isotropic, i.e., $g(\omega, \vec{v}) = g(\omega)/4\pi$

Because of uniformity, $\mathbf{P}(\omega, \vec{v}; \vec{r}, t) = \mathbf{P}(t)$ is a function of time only. Also, isotropy implies that $\vec{\mathbf{A}} = 0$. Under this restriction, all flavor vectors with the same ω index, irrespective of the velocity, satisfy the same differential equation and therefore follow the same trajectories. We can therefore drop those indexes and work exclusively with the velocity integrated spectrum $g(\omega)$. This spectrum is the spectrum $g(\omega, \vec{v})$ integrated at every point in space over all directions, which then describes the initial difference of flavor density of the gas.

When neutrinos decouple from the gas, they possess a near-thermal Fermi-Dirac spectrum, which can be translated into a frequency spectrum (the frequency axis is inverted in the IH), as shown in the second chapter in fig. 2.1. To simplify the model as much as possible, we take only two frequencies, ω_0 and $-\omega_0$, computed from the average energies of the spectrum:

$$g(\omega) = -\delta(\omega + \omega_0) + (1 + \epsilon)\delta(\omega - \omega_0) \quad (3.2)$$

This approximation is often used in simulations that take into account the angular dependence of the modes. These simulations tend to be far more demanding, requiring the use of tens of modes to mimic the continuous case, a feature which will be explained in a later chapter of this thesis. In general, this single-energy approximation has its limits, though it captures some of the main dynamical features of the system. One can show that there is a system of discrete modes that relates by a linear combination to the continuous case. For further details, see [36].

The evolution of $\mathbf{P}_{+\omega_0} = \mathbf{P}$ and of $\mathbf{P}_{-\omega_0} = \bar{\mathbf{P}}$ obeys the equations

$$\begin{aligned} \partial_r \mathbf{P} &= \{+\omega_0 \mathbf{B} + \lambda \mathbf{L} + \mu [(1 + \epsilon)\mathbf{P} - \bar{\mathbf{P}}]\} \times \mathbf{P}, \\ \partial_r \bar{\mathbf{P}} &= \{-\omega_0 \mathbf{B} + \lambda \mathbf{L} + \mu [(1 + \epsilon)\mathbf{P} - \bar{\mathbf{P}}]\} \times \bar{\mathbf{P}}, \end{aligned} \quad (3.3)$$

where

$$\omega_0 = \frac{\Delta m^2}{2|E_0|}, \quad (3.4)$$

3.1.1 Stability of the flavor eigenstate

Assuming the absence of resonant matter effects, we can safely go to the co-rotating frame introduced earlier. For convenience, we denote $\mathbf{B}_z \rightarrow \mathbf{B}$ and $\cos 2\theta_0 \omega_0 \rightarrow \omega_0$. Our present aim is to understand if the noise introduced by \mathbf{B}_\perp can tip the system out of the interaction eigenstate in which neutrinos are when they propagate in very dense media. The initial condition is $\mathbf{P}(t = 0) = (0, 0, 1)$ and $\bar{\mathbf{P}}(t = 0) = (0, 0, 1)$. We wish to know whether this configuration remains stable under the small perturbations induced by the neglected off-diagonal component of \mathbf{B} . We therefore study the behavior of small perturbations around this state.

For $\mu = 0$ the system simply follows the vacuum oscillation. Neutrinos and anti-neutrinos precess around \mathbf{B} in opposite directions. There is no growth of the perturbations for $\mu = 0$. For finite self-coupling strengths, the differential change due to the non-linear term proportional to

$\mathbf{P} \times \bar{\mathbf{P}}$. This vector is a vector perpendicular to the plane formed by \mathbf{P} and $\bar{\mathbf{P}}$ and proportional to the area spanned by the two vectors. Since both polarization vectors have extremely small xy components, we can approximate them by a constant vertical vector of unit length and a small vector on the horizontal plane¹. In this regime the equations are linear. Following the notation clarified in Fig. 3.1, let us denote by p and \bar{p} the vector components perpendicular to \mathbf{B} :

$$\mathbf{P} = \begin{pmatrix} p \\ P_z \end{pmatrix} \quad \text{and} \quad \bar{\mathbf{P}} = \begin{pmatrix} \bar{p} \\ \bar{P}_z \end{pmatrix}, \quad (3.5)$$

The product of two three-dimensional vectors is

$$\bar{\mathbf{P}} \times \mathbf{P} = \begin{pmatrix} i(P_z \bar{p} + \bar{P}_z p) \\ \text{Im}\{p \bar{p}^*\} \end{pmatrix} \quad (3.6)$$

and

$$\mathbf{B} \times \mathbf{P} = \begin{pmatrix} i p \\ 0 \end{pmatrix}. \quad (3.7)$$

The previous equations show that the change of P_z is of order $|p|^2$, as was expected because the flavor vector is very near the top of the sphere where the variation of the latitude is of second order. The rate of change of p is nevertheless of first order. Setting $P_z \approx 1$ and $\bar{P}_z \approx 1$ to order θ , near the zenith, the dynamics are described by

$$-i \begin{pmatrix} \dot{p} \\ \dot{\bar{p}} \end{pmatrix} = \begin{pmatrix} \omega_0 - \mu & (1 + \epsilon) \mu \\ -\mu & -\omega_0 + (1 + \epsilon) \mu \end{pmatrix} \begin{pmatrix} \dot{p} \\ \dot{\bar{p}} \end{pmatrix}. \quad (3.8)$$

For the rest of this section we will proceed under the assumption that neutrinos and anti-neutrinos are found in equal mixtures $\epsilon = 0$. The differential equations look much simpler now:

$$-i \begin{pmatrix} \dot{p} \\ \dot{\bar{p}} \end{pmatrix} = \begin{pmatrix} \omega_0 - \mu & \mu \\ -\mu & -\omega_0 + \mu \end{pmatrix} \begin{pmatrix} \dot{p} \\ \dot{\bar{p}} \end{pmatrix} \quad (3.9)$$

Being a linear system of ordinary differential equations on the complex plane, only two possible behaviors can happen: precession around the origin and exponential growth or decline. From the trace of the matrix we see that the sum of the eigenvalues is null, which means the eigenvalues point in opposite directions on the complex plane. Their product is a real number, which implies that either both are real or both are imaginary: if a growing solution exists, there is always one that shrinks at the same rate. Therefore, given any initial perturbation of the polarization vectors, either we will eventually see only the growing solution (given by the matching eigenvector) or we

¹If $\mathbf{P}(\omega; t) = |\mathbf{P}(\omega; t=0)|(\sin \theta(\omega; t) e^{i\phi(\omega; t)}, \cos \theta(\omega; t))$ where $\theta(\omega; t)$ and $\phi(\omega; t)$ are the usual spherical coordinates as measured from the z direction then, for small θ , the xy component is linear in θ whereas the vertical one is constant.

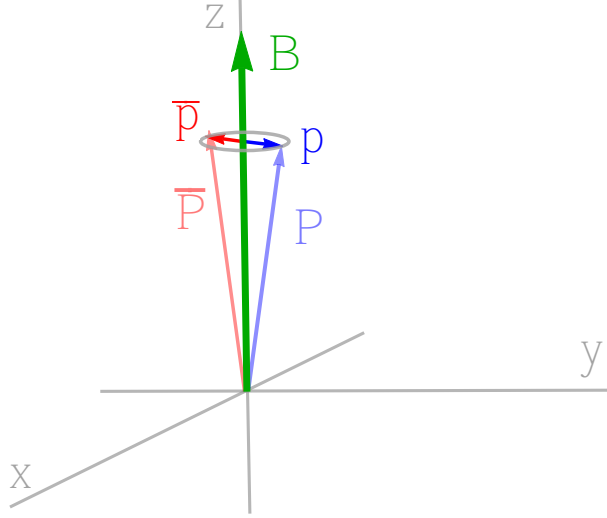


Figure 3.1: Illustration of the linearization scheme. Since \mathbf{B} is coincident with the z direction, both flavor vectors will be situated somewhere around \mathbf{B} on a narrow cone. We take therefore their component along \mathbf{B} to be near maximum and consider only the motion of their perpendicular component \mathbf{p} and $\bar{\mathbf{p}}$.

will see nothing at all (both polarization vectors remain approximately aligned with the z direction and the beam is stable in the eigenstate of flavor). The explicit eigenvalue equation is

$$\det \begin{pmatrix} \omega_0 - \mu & \mu \\ -\mu & -\omega_0 + \mu \end{pmatrix} = 0 \quad (3.10)$$

which yields the two solutions

$$\Omega_{\pm} = \pm |\omega_0| \sqrt{1 - 2\zeta \frac{\mu}{|\omega_0|}}. \quad (3.11)$$

The ω_0 presently used is defined as $\cos 2\theta_0 \Delta m^2 / 2|E|$. ζ stands for the sign of ω_0 . If the vacuum angle is smaller than $\pi/2$ then the sign indicates the hierarchy that one assumes: $\zeta = 1$ for IH, $\zeta = -1$ for NH. The eigenvectors are the configurations of p and \bar{p} which evolve as $\exp(-i\Omega r)$. The eigenstate of interaction loses its stability for imaginary Ω and flavor conversion occurs. The condition for instability requires $1 - 2\zeta\mu/|\omega_0| < 0 \Leftrightarrow \zeta\mu > |\omega_0|/2$. Since $\mu > 0$, neutrinos can only leave the flavor eigenstate if $\zeta = 1$, i.e., if the neutrino masses are organized according to the IH.

The eigenvectors are

$$p^{\pm} = \begin{pmatrix} \left(1 - \frac{\omega_0}{\mu} \mp \frac{\Omega}{\mu}\right) p + \bar{p} \\ \bar{p} \end{pmatrix} \quad (3.12)$$

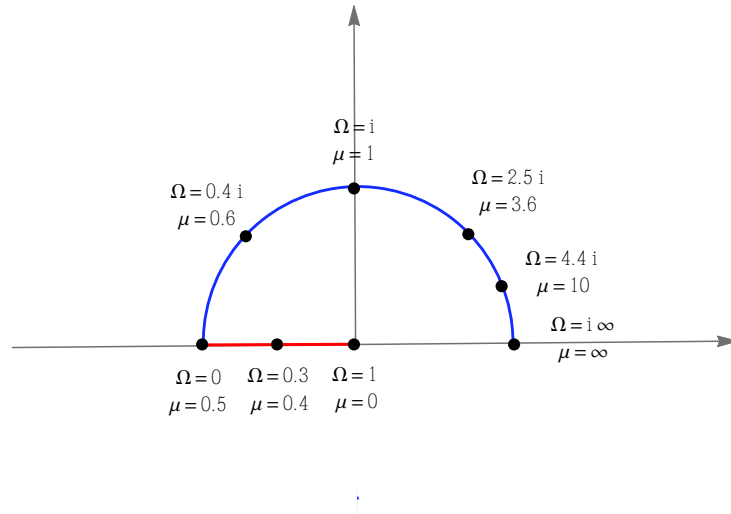


Figure 3.2: Visualization of the eigenpositions of the system in the linear regime on the plane perpendicular to $\omega\mathbf{B}$ (which is pointing out of the page towards you, the reader). We chose for this example $\omega = 1$. p is chosen to be the point $(1, 0)$ on this plane. In red are shown the initial settings of \bar{p} of the system for which it just spins around the central axis. As $\mu = 1/2$ the two vectors point in opposite direction on this plane and the system is locked in this position. As μ keeps growing the system has one growing solution and one shrinking solution. The two look the same on the plane: in both \mathbf{P} describes the unit circle, but in two different directions. In one case $\omega\mathbf{B} \times \mathbf{P} + \mu\bar{\mathbf{P}} \times \mathbf{P}$ points inwards on this plane, in the other outwards (leading to a growing solution). In the actual non-linear system, the onset of the growing effect will depend on how similar the initial conditions are to this configuration. Eventually all we will see is this configuration since the part that looks like the other one will shrink down.

which means that the whole system, as long as p and \bar{p} remain small, evolves as

$$p^\pm(t) = \begin{pmatrix} \left(1 - \frac{\omega_0}{\mu} \mp \frac{\Omega}{\mu}\right) p(0) + \bar{p}(0) \\ \bar{p}(0) \end{pmatrix} \exp(-i\Omega t). \quad (3.13)$$

In the NH the system remains neutrally stable. On the other hand, in the IH, there being one unstable ($i\Omega > 0$) and one stable configuration ($-i\Omega > 0$), the instability is a saddle-point instability. That means that in the unstable region of parameter space all configurations converge to the eigenvector with positive growth factor. After a while and for as long as the off-diagonal terms of the density matrix are not too big, \mathbf{P} and $\bar{\mathbf{P}}$ will be arranged according to the growing configuration, no matter what the initial state was. A growing solution necessarily means that one eventually has to move away from the linear equations. Once the modulus of p becomes large one has to consider the full non-linear system.

Before we move on to the treatment of the non-linear dynamics, we should point out what the effects of a neutrino-antineutrino asymmetry are on the stability of the flavor state. By computing

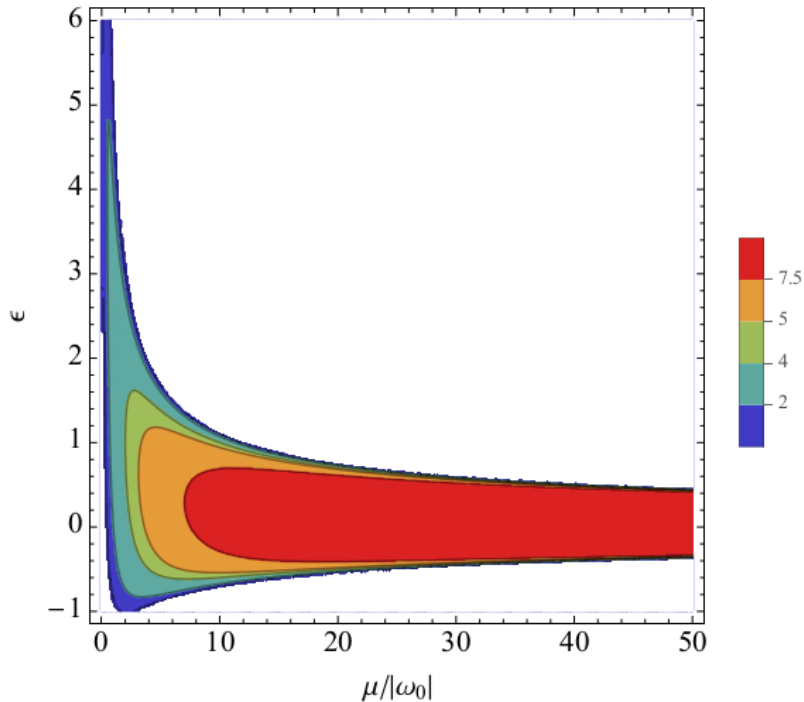


Figure 3.3: Contours of equal growth factor in the parameter space (ϵ, μ) . The instability becomes restricted to a narrower and narrower region when one moves away from the equal mixture case ($\epsilon = 0$). The scale of ϵ goes from no neutrinos ($\epsilon = -1$) to $n_{\nu_e} \gg n_{\bar{\nu}_e}$ ($\epsilon = +\infty$). During the prompt burst the asymmetry reaches very high values. It does so again in the cooling phase and reaches its minimum during the accretion phase ($\epsilon \sim 0.2 - 0.5$).

the eigenvalues of the linear equations, one can make a parametric plot in the space $(\epsilon, \mu/|\omega_0|)$ of the region in which instabilities occur. This plot is shown in fig. 3.3 and it reveals how even a small asymmetry greatly reduces the unstable region and the value of the growth factor. This feature is common to all models. For example, in the emission of neutrinos from a core-collapse SN, there is an initial burst of neutrinos produced in CC reactions that lasts about 10 ms. These are electron neutrinos which means the burst carries a high lepton number, i.e., a low ϵ . Thus we do not expect to see any collective oscillations in the early signal of a SN.

3.1.2 Flavor pendulum

So what happens after the off-diagonal components of the density matrix (x and y components of the flavor vectors) become too large for the linear approximation? The equations are anti-symmetric for the vacuum term and symmetric in the self-interaction. Therefore one expects the variables

$$\begin{aligned} \mathbf{S} &= (1 + \epsilon)\mathbf{P} + \bar{\mathbf{P}}, \\ \mathbf{D} &= (1 + \epsilon)\mathbf{P} - \bar{\mathbf{P}}, \end{aligned} \tag{3.14}$$

to be somewhat more physical. Using these new definitions to rewrite the equations

$$\begin{aligned}\dot{\mathbf{S}} &= \omega_0 \mathbf{B} \times \mathbf{D} + \mu \mathbf{D} \times \mathbf{S} = \mu \mathbf{D} \times \left(\mathbf{S} - \frac{\omega_0}{\mu} \mathbf{B} \right) \quad , \\ \dot{\mathbf{D}} &= \omega_0 \mathbf{B} \times \mathbf{S} \quad .\end{aligned}\tag{3.15}$$

Since the left-hand sides of the equations can always absorb a constant term such as $-(\omega_0/\mu)\mathbf{B}$ and since the addition of this term doesn't change the right-hand side of the second equation the simpler form of equations (3.3) becomes

$$\begin{aligned}\dot{\mathbf{Q}} &= \mu \mathbf{D} \times \mathbf{Q} \quad , \\ \dot{\mathbf{D}} &= \omega_0 \mathbf{B} \times \mathbf{Q} \quad ,\end{aligned}\tag{3.16}$$

where

$$\mathbf{Q} = \mathbf{P} + \bar{\mathbf{P}} - \frac{\omega_0}{\mu} \mathbf{B}.\tag{3.17}$$

From these equations, we deduce that the length Q is conserved and equal to

$$Q = |\mathbf{Q}(0)| = \sqrt{2 + \epsilon - \frac{\omega_0}{\mu}}.\tag{3.18}$$

These EoMs are the EoMs of a gyroscopic pendulum.

3.1.3 Bipolar oscillation

Given the initial conditions $\mathbf{P}(0) = \bar{\mathbf{P}}(0) = (0, 0, 1)$ and $\epsilon = 0$, i.e., according to the previous equations, $\mathbf{D}(0) = \mathbf{0}$, the motion of \mathbf{Q} is confined to the xz plane: $\mathbf{Q}(t) = Q (\sin \theta(t), 0, \cos \theta(t))$. We find

$$\begin{aligned}\dot{\theta} &= \mu D, \\ \dot{D} &= -\omega_0 Q \sin \theta,\end{aligned}\tag{3.19}$$

Equations (3.19) can be grouped together into

$$\ddot{\theta} = -\kappa^2 \sin(\theta)\tag{3.20}$$

where

$$\kappa^2 = \omega_0 \mu Q.\tag{3.21}$$

This is the same equation as that of a pendulum [37]. For $\kappa^2 > 0$ or $\omega_0 > 0$ (normal hierarchy) the system performs small oscillations around \mathbf{B} . However for $\omega_0 < 0$ (inverted hierarchy) it is as if the pendulum was initially set in an inverted position. As a consequence, \mathbf{Q} executes large

oscillations, during which the ensemble changes completely its neutrino content. This maximum amplitude oscillation is suppressed when $\epsilon \neq 0$, as shown in figure 3.4).

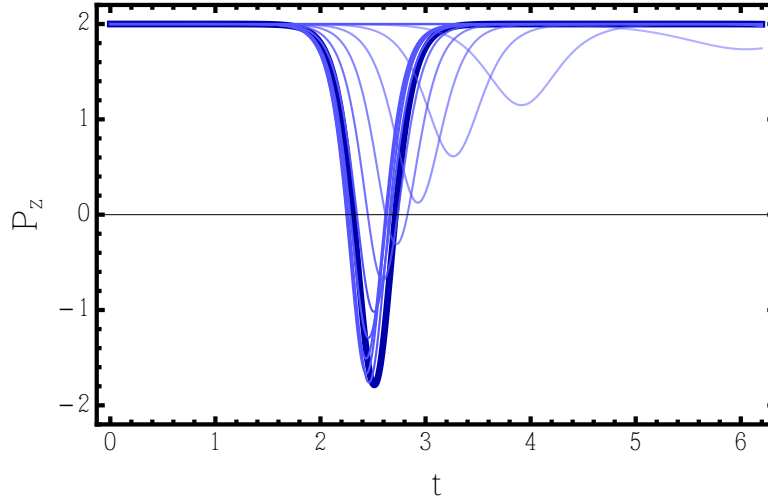


Figure 3.4: The z component of \mathbf{P} for several values of ϵ . The oscillations are strongly suppressed as ϵ increases. The dark blue curve shows $\epsilon = 0$. The pale blue curves show the trajectories for values of ϵ ranging from 0.1 to 2 in step intervals of 0.1.

3.1.4 Beyond Rabi oscillations in Bose-Einstein condensates

If one looks back at the assumptions that were made, one realizes that one is looking at a fairly general self-interacting quantum system. Proof of that is the discovery of similar behavior in trapped Bose-Einstein condensates (BEC). When a condensate is placed in an double-well potential, it can tunnel across the potential barrier. If the trap is symmetric, the eigenstates of the Hamiltonian are the symmetric and the anti-symmetric states. Each eigenstate having a specific energy a phase difference grows constantly between the macroscopic wave-function of a BEC placed in either of them. If one places an excess of particles in the first pit, the expectation value of the number of particles will oscillate in both pits, conserving the total number. This phenomenon is completely akin to the vacuum oscillation of neutrinos and in this context is known as Rabi oscillations. The condensate being prepared initially in a non-diagonal state, a phase difference develops between the two frequencies of the symmetric ($E = E_+/\hbar$) and of the anti-symmetric ($E = E_-/\hbar$) states. The analogy is even more striking if one considers the inter-particle interaction between the elements of the condensate. Assuming this interaction depends linearly on the density of particles, one finds the same non-linear equations that give rise to the pendulum-like behavior of the neutrino gas [38]. This phenomenon was confirmed experimentally using LASER-cooled Rubidium atoms to form a Josephson junction [39]. Figure 3.5 shows the density of atoms in each potential pit. The anharmonic oscillations are clearly visible.

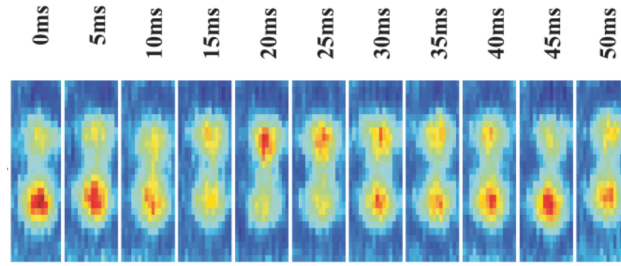


Figure 3.5: Evolution of the density of Rubidium atoms in a double-well LASER trap [39]. The states in each potential correspond to our flavor states whereas the symmetric and anti-symmetric states correspond to the mass eigenstates. These Josephson oscillations are the equivalent of our bipolar oscillations.

The pendulum dynamics, being an anharmonic phenomenon, requires a high occupation number. With few modes, only a handful of frequencies are available, and one observes at most complicated harmonic oscillations. Only in the limit of many particles can one observe a smooth anharmonic motion. For example, a pair of rubidium atoms placed in the double well potential do not oscillate like a pendulum. In this case, the energy of the system can only take the values $2E_-$, $E_+ + E_-$, $2E_+$ which leads to only a handful of frequencies that the system can exhibit. Instead, one needs a continuum of frequencies to emulate the pendulum.

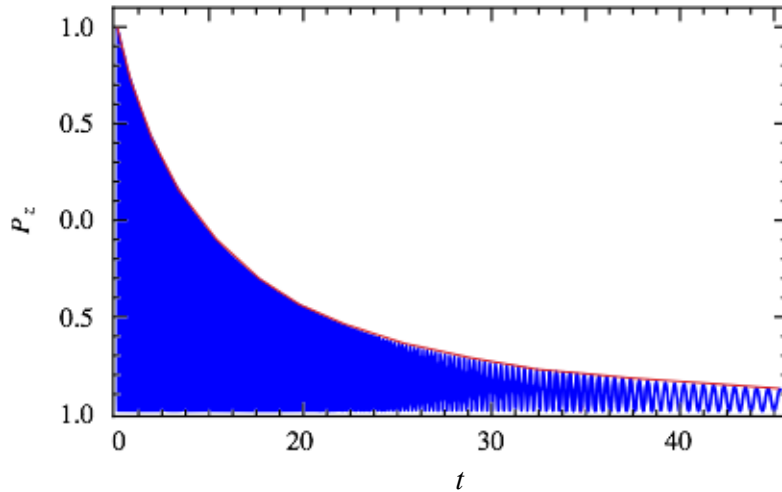


Figure 3.6: The z component of \mathbf{P} during an adiabatic decrease of $\mu \propto \exp(-t/20)$. The rate of change is kept much smaller than the period of oscillation. With each swing the pendulum loses energy, slowly decreasing the amplitude of its motion (shown as the red line).

3.1.5 Adiabatic invariants

In this section we study the pendulum system when μ is gradually decreased. This intends to mimic the decrease in the strength of the interaction as neutrinos stream out of a SN or in the early universe as the density of neutrinos decreases. Figure 3.6 shows how this can lead to a complete inversion of flavor by slowly decreasing the amplitude of the bipolar oscillations. The following quantity

$$\begin{aligned} H &= \frac{\mu}{2} \mathbf{D}^2 + \omega \mathbf{B} \cdot \mathbf{Q} \\ &= \omega_0 Q \cos \theta + \frac{\mu}{2} D^2, \end{aligned} \quad (3.22)$$

is conserved throughout the motion. The quantities θ and D follow the identities

$$\begin{aligned} \dot{D} &= -\frac{\partial H}{\partial D} \\ \dot{\theta} &= \frac{\partial H}{\partial \theta} \end{aligned} \quad (3.23)$$

which means (3.22) serves the purpose of a Hamilton function with (θ, D) as its canonical variables. These respect

$$\{\theta, D\} = \frac{\partial \theta}{\partial \theta} \frac{\partial \theta}{\partial D} - \frac{\partial D}{\partial \theta} \frac{\partial D}{\partial D} = 1 \quad (3.24)$$

The adiabatic invariant is the phase space area enclosed in a closed trajectory

$$I = \iint d\theta dD \quad (3.25)$$

If μ 's rate of change is slow compared to the period of oscillation, then I is conserved. The coordinates make up in phase space the trajectory defined by

$$H = \omega_0 Q \cos \theta + \frac{\mu}{2} D^2, \quad (3.26)$$

The closed trajectories are symmetrical in D as the formula for H indicates. That means that the extreme positions of θ are determined by

$$\cos \theta_{max} = \frac{H}{\omega_0 Q} \quad (3.27)$$

With this definition in mind, the area of phase space enclosed by the trajectory is given by

$$I = 2 \int_{\theta_{max}}^{2\pi - \theta_{max}} \sqrt{\frac{2}{\mu} (H - \omega_0 Q \cos \theta)} d\theta \equiv -4 \times \sqrt{\frac{2\omega_0 Q}{\mu}} \times F(\theta_{max}) \quad (3.28)$$

where

$$F(x) = \int_0^x \sqrt{\cos x - \cos \theta} d\theta \quad (3.29)$$

For an initial condition of $\mathbf{D} = 0$ and $\mathbf{Q} = (0, 0, Q)$, the pendulum makes a full amplitude oscillation between $2\theta_0 < \theta < 2(\pi - \theta_0)$. As μ decreases, the trajectory in phase space shrinks while maintaining the area it encloses. This forces $F(\theta_{max})$ to vary with $\sim \sqrt{\mu}$ to compensate for the change of I due to the factor $\mu^{-1/2}$. Therefore the extreme values of the angle are given by

$$\frac{F(\theta_{\max}(\mu))}{\sqrt{\mu}} = \frac{F(2\theta_0)}{\sqrt{\mu_0}} \Leftrightarrow \theta_{\max}(\mu) = F^{-1} \left[\sqrt{\frac{\mu}{\mu_0}} F(2\theta_0) \right] \quad (3.30)$$

where μ_0 is the initial value of μ . The adiabatic evolution of the average energy over a period follows

$$H(\mu) \approx \omega_0 Q \cos[\theta_{\max}(\mu)] \quad (3.31)$$

Simulations show that for small μ the predictions of these previous calculations fail. That is probably due to the μ -dependence of the length Q which was not taken into account. Though for $\omega_0 \ll \mu$ the difference between \mathbf{S} and \mathbf{S} can be neglected, that approximation becomes worse and worse as the neutrino density vanishes. See [40] for further details.

3.2 Spontaneous symmetry breaking

3.2.1 Isotropic equations of motion with explicit velocity dependence

The analysis done in the last sections, albeit simple, neglects the details of the velocity dependent interaction by integrating it out with the assumption of exact isotropy. To assess how sound this assumption is, let us suppose that we have two streams flowing in opposite directions with velocities \vec{v} and $-\vec{v}$. Their flavor is defined by two velocity modes, 1 and 2, each with positive energy, \mathbf{P}_1 and \mathbf{P}_2 , and negative energy, $\bar{\mathbf{P}}_1$ and $\bar{\mathbf{P}}_2$. This is a one-dimensional single-energy system. We wish to assess the impact of the explicit inclusion of velocity dependence. We have

$$\mathbf{D} = \mathbf{P}_1 + \mathbf{P}_2 - \bar{\mathbf{P}}_1 - \bar{\mathbf{P}}_2, \quad (3.32)$$

and

$$\vec{\mathbf{A}} = \vec{v}(\mathbf{P}_1 - \bar{\mathbf{P}}_1) - \vec{v}(\mathbf{P}_2 - \bar{\mathbf{P}}_2) = \vec{v}(\mathbf{P}_1 - \bar{\mathbf{P}}_1 - \mathbf{P}_2 + \bar{\mathbf{P}}_2) \equiv \vec{v}\mathbf{A}. \quad (3.33)$$

We see that in this case, the component of $\vec{\mathbf{A}}$ along the velocity is just the anti-symmetric version of \mathbf{D} in respect to the 1, 2 indexes. In computing the vector order parameter we still have assumed isotropy between the two existing modes, in the sense of $g(\omega, \vec{v}) = g(\omega, -\vec{v})$.

From eq. (3.33), the four flavor vectors obey the EoMs

$$\begin{aligned}
\partial_t \mathbf{P}_1 &= [+\omega_0 \mathbf{B} + 2\mu (\mathbf{P}_2 - \bar{\mathbf{P}}_2)] \times \mathbf{P}_1, \\
\partial_t \bar{\mathbf{P}}_1 &= [-\omega_0 \mathbf{B} + 2\mu (\mathbf{P}_2 - \bar{\mathbf{P}}_2)] \times \bar{\mathbf{P}}_1, \\
\partial_t \mathbf{P}_2 &= [+\omega_0 \mathbf{B} + 2\mu (\mathbf{P}_1 - \bar{\mathbf{P}}_1)] \times \mathbf{P}_2, \\
\partial_t \bar{\mathbf{P}}_2 &= [-\omega_0 \mathbf{B} + 2\mu (\mathbf{P}_1 - \bar{\mathbf{P}}_1)] \times \bar{\mathbf{P}}_2.
\end{aligned} \tag{3.34}$$

We will from this point on write $2\mu \rightarrow \mu$. As our goal is to study the impact of adding another directional mode, we choose again the simpler system with $\epsilon = 0$.

3.2.2 Departure from the symmetric solution

One important question must be asked now: are the $1 \leftrightarrow 2$ symmetric solutions stable? Namely and most importantly, we saw earlier that the isotropic version of this system performed bipolar oscillations in the IH whereas in the NH it was stuck in the flavor state. Do these features remain true if the symmetry imposition is relaxed? If $\vec{\mathbf{A}} \approx 0$ in the initial instant, does it remain small through the evolution? Using $\mathbf{D}_i = \mathbf{P}_i - \bar{\mathbf{P}}_i$ eqs. (3.34) are equivalent to

$$\begin{aligned}
\partial_t \mathbf{P}_1 &= (+\omega_0 \mathbf{B} + \mu \mathbf{D}_2) \times \mathbf{P}_1, \\
\partial_t \bar{\mathbf{P}}_1 &= (-\omega_0 \mathbf{B} + \mu \mathbf{D}_2) \times \bar{\mathbf{P}}_1, \\
\partial_t \mathbf{P}_2 &= (+\omega_0 \mathbf{B} + \mu \mathbf{D}_1) \times \mathbf{P}_2, \\
\partial_t \bar{\mathbf{P}}_2 &= (-\omega_0 \mathbf{B} + \mu \mathbf{D}_1) \times \bar{\mathbf{P}}_2.
\end{aligned} \tag{3.35}$$

If the two pairs of vectors 1 and 2 are initially prepared in the exact same position, they will follow the same trajectory and we are back in the previous case: there is a threshold $\mu > \omega_0/2$ above which the flavor content behaves like a pendulum. This threshold is only valid for $\omega_0 = \Delta m^2/2|E| < 0$, allowing us to distinguish the ordering of the neutrino masses. The threshold of stability was found to be the value of μ for which the precession caused by \mathbf{B} is stalled² by $\mathbf{P} \times \bar{\mathbf{P}}$. This condition can only be achieved for one hierarchy. On the other hand, once the second mode is explicitly taken into account, the threshold condition can now be satisfied in both hierarchies because the orientation of the non-linear term for $1 - \mu \mathbf{D}_2 \times \mathbf{P}_1$ - can now be chosen independently of the position of \mathbf{P}_1 and $\bar{\mathbf{P}}_1$ by an appropriate placement of \mathbf{P}_2 and $\bar{\mathbf{P}}_2$. As figure 3.7 shows, the variation of the transversal component of the perturbations can satisfy the threshold condition for any hierarchy.

By taking once again the perpendicular part of all vectors to \mathbf{B} to be very small, one gets, using

²This is not true in general but is valid in this simple case.

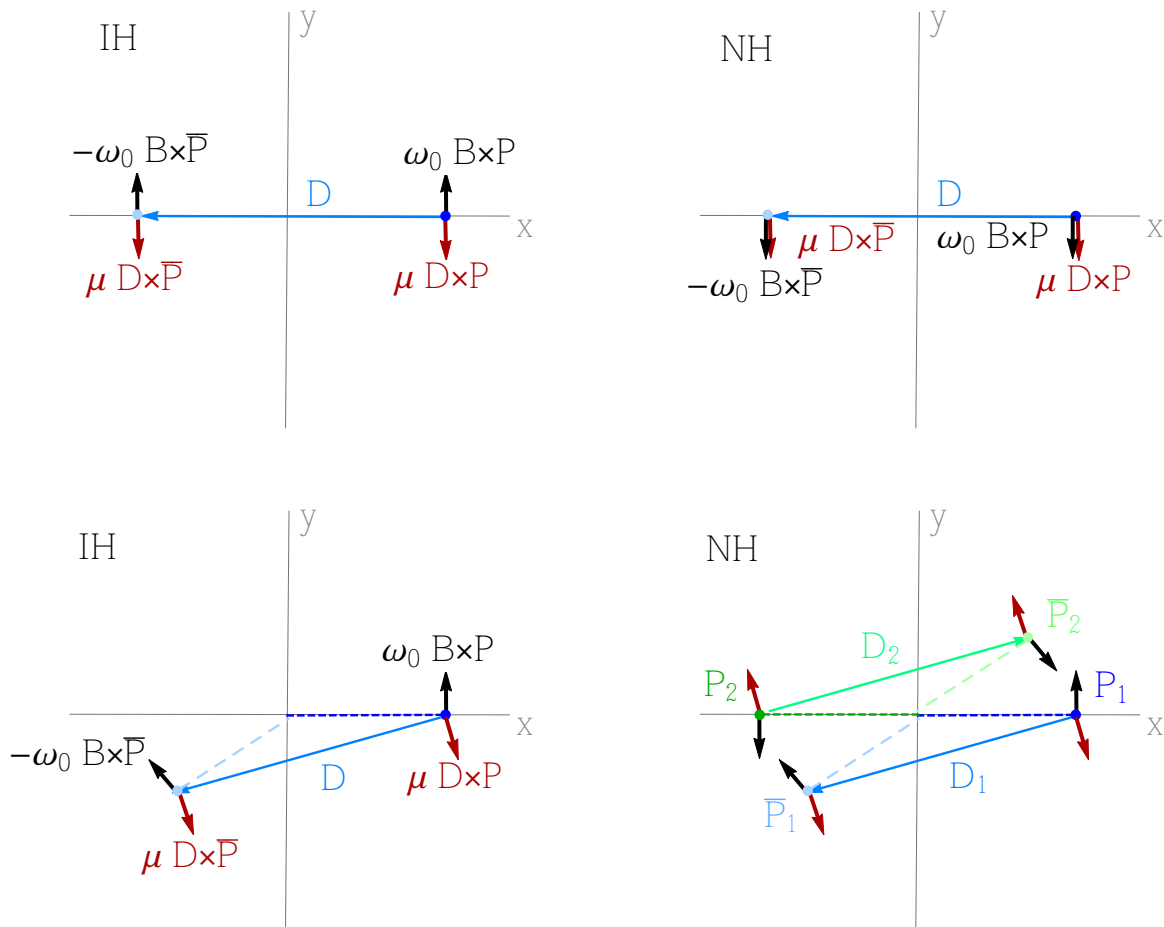


Figure 3.7: Eigenvectors in the linear regime we look for configurations which under an infinitesimal change remain the same up to a scaling and a rotation about the z axis (shown as vector pointing at the reader). In the two-vector system, there is an inherent limitation on the way the different contributions to the change of each vector can be arranged. In the 4-vector system these limitations are overcome. *Top left:* The threshold situation between growing and precession, in the two-vector system. In the IH the collective term counters the vacuum terms. *Top right:* Same system, but different hierarchy. The vacuum terms now collaborate with the collective term and this configuration is no longer an eigenconfiguration. There is never a way to make these vectors cancel: one can only find eigenconfigurations that lead to precession. *Bottom left:* Same system, again in the IH, showing an unstable eigenconfiguration. The components of the infinitesimal change transversal to the vectors cancel, leaving a small part that points outwards, stretching the vectors on the xy plane. The resulting change is identical relative to each vector, which is why this is an eigenconfiguration. There is also another solution which shrinks by the same amount, which can be visualized by reflecting this one on the x axis. *Bottom right:* New system and the instability that was previously unreachable. Because the neutrino-antineutrino pair vectors feel only the effect of the other mode, one can arrange the two modes opposite of each other as to flip the sign of the collective term, which now points again in the opposite direction to the vacuum contribution.

a similar notation

$$\begin{aligned}
 \dot{p}_1 &= i\omega_0 p_1 + i\mu(\bar{p}_2 - p_2), \\
 \dot{\bar{p}}_1 &= -i\omega_0 \bar{p}_1 + i\mu(\bar{p}_2 - p_2), \\
 \dot{p}_2 &= i\omega_0 p_2 + i\mu(\bar{p}_1 - p_1), \\
 \dot{\bar{p}}_2 &= -i\omega_0 \bar{p}_2 + i\mu(\bar{p}_1 - p_1),
 \end{aligned} \tag{3.36}$$

This is a linear system with solutions of the type

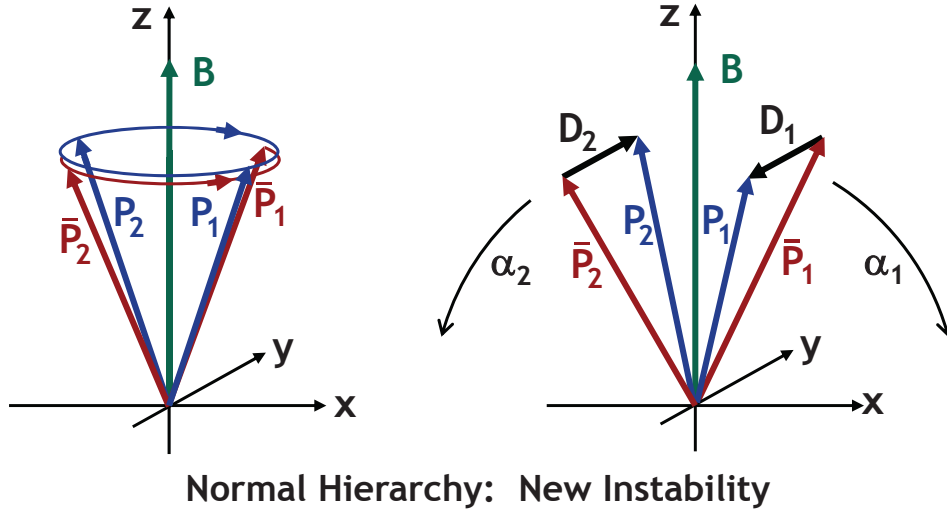


Figure 3.8: Visualization of flavor oscillations and the new instability as described in the text. The left panel shows, in the absence of the self-consistent interaction, the precession of the polarization vectors with modes of negative frequency (in red) precessing in the opposite direction of the modes of positive frequency (in blue). The right panel shows the self-consistent interaction and how mode 1 feels the effect of mode 2, and vice versa.

$$p(r) = \text{eigenvector} \exp(i\Omega r) \tag{3.37}$$

or linear combinations of them. The eigenvalues of the system are given by

$$\det \begin{pmatrix} \omega_0 - \Omega & 0 & -\mu & \mu \\ 0 & -\omega_0 - \Omega & -\mu & \mu \\ -\mu & \mu & \omega_0 - \Omega & 0 \\ -\mu & \mu & 0 & -\omega_0 - \Omega \end{pmatrix} = 0 \tag{3.38}$$

which has the four solutions

$$\Omega = \pm \sqrt{\omega_0(\pm 2\mu + \omega_0)} \tag{3.39}$$

where the two \pm signs are independent of each other. Two of these eigenvalues are identical to the

ones found in the previous section. It is therefore not surprising that the corresponding eigenconfigurations are the same as before:

$$\begin{pmatrix} \left[1 - \frac{\omega_0}{\mu} \mp i \sqrt{\frac{\omega_0}{\mu} \left(2 - \frac{\omega_0}{\mu} \right)} \right] p_1 \\ \bar{p}_1 \\ \left[1 - \frac{\omega_0}{\mu} \mp i \sqrt{\frac{\omega_0}{\mu} \left(2 - \frac{\omega_0}{\mu} \right)} \right] p_2 \\ \bar{p}_2 \end{pmatrix} \quad (3.40)$$

with the two pairs of vectors 1 and 2 being exactly equal. This mode grows for positive $\omega_0 < 2\mu$. However, another mode exists this time which grows for negative $\omega_0 > -2\mu$:

$$\begin{pmatrix} \left[1 - \frac{\omega_0}{\mu} \mp i \sqrt{\frac{\omega_0}{\mu} \left(2 - \frac{\omega_0}{\mu} \right)} \right] p_1 \\ \bar{p}_1 \\ - \left[1 - \frac{\omega_0}{\mu} \mp i \sqrt{\frac{\omega_0}{\mu} \left(2 - \frac{\omega_0}{\mu} \right)} \right] p_2 \\ \bar{-p}_2 \end{pmatrix} \quad (3.41)$$

whose eigenvalue is the same as the other one with $\omega_0 \rightarrow -\omega_0$ and the eigenconfiguration the same but with the two pairs arranged exactly in opposite directions now. From the third panel in figure 3.7 one easily gleans the resulting directions of \mathbf{D}_1 and \mathbf{D}_2 . The key point is that mode 1 feels the refractive effect caused by mode 2, and the other way round. Therefore, the precession around the respective $\mathbf{D}_{1,2}$ vectors leads to motions away from \mathbf{B} and subsequently to a pendulum with the 1 and 2 modes swinging in opposite directions (cf. figure 3.8). This configuration is unstable in NH.

To sum up the results:

- symmetric $1 \leftrightarrow 2$ configurations are stable in NH and unstable in IH (henceforth referred to as the *bimodal instability*);
- anti-symmetric $1 \leftrightarrow 2$ configurations are unstable in NH and stable in IH (henceforth referred to as the *multi-angle (MA) instability*).

Because a general perturbation to the flavor state will always result in a partly symmetric, partly antisymmetric configuration, one of the instabilities is likely to be excited, no matter what the hierarchy. Of course, if the system is prepared *precisely* such that initially all polarization vectors are the same, then only the traditional bimodal instability can occur. The smallest deviation from this exact initial symmetry causes an admixture of the anti-symmetric mode. The exponentially growing mode always wins. Therefore, any realistic initial condition provides a seed for a run-away solution in both hierarchies. The unstable region of parameter space when one includes $\epsilon \neq 0$ is

shown in figure 3.9.

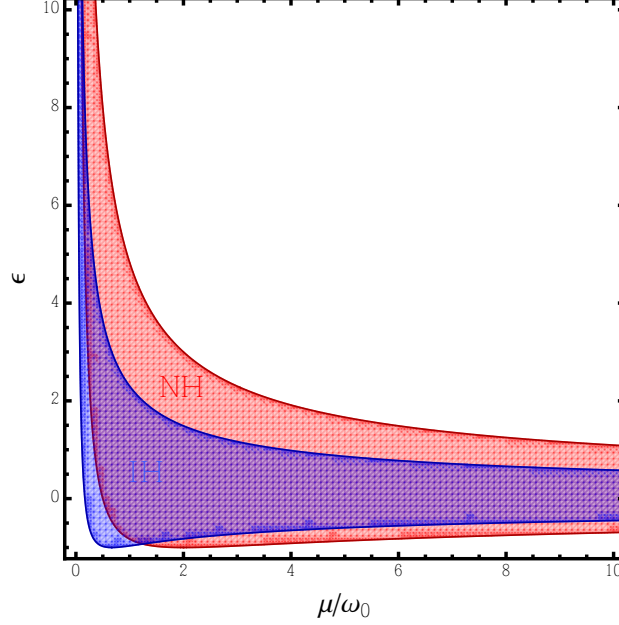


Figure 3.9: Suppression of the two instabilities – bimodal (blue) and MA (red) – as a function of ϵ .

We now turn to the non-linear analysis of the two-beam example. To this end we write the EoMs somewhat more symmetrically by introducing the sum vectors $\mathbf{S}_i = \mathbf{P}_i + \bar{\mathbf{P}}_i$ with $i = 1$ or 2 and find from Eq. (3.35)

$$\begin{aligned}
 \dot{\mathbf{S}}_1 &= \mu \mathbf{D}_2 \times \mathbf{S}_1 + \omega_0 \mathbf{B} \times \mathbf{D}_1, \\
 \dot{\mathbf{S}}_2 &= \mu \mathbf{D}_1 \times \mathbf{S}_2 + \omega_0 \mathbf{B} \times \mathbf{D}_2, \\
 \dot{\mathbf{D}}_1 &= \omega_0 \mathbf{B} \times \mathbf{S}_1 + \mu \mathbf{D}_2 \times \mathbf{D}_1, \\
 \dot{\mathbf{D}}_2 &= \omega_0 \mathbf{B} \times \mathbf{S}_2 + \mu \mathbf{D}_1 \times \mathbf{D}_2.
 \end{aligned} \tag{3.42}$$

We simplify further as in the previous section and assume exact particle-antiparticle symmetry. We also assume that all polarization vectors are initially in the x - z plane and that the corresponding particle and anti-particle vectors are prepared identically. The system then evolves symmetrically such that the \mathbf{S}_i vectors move in the x - z plane, whereas the \mathbf{D}_i vectors are oriented along the y direction. Therefore, the terms $\mathbf{D}_1 \times \mathbf{D}_2$ drop out.

We can now easily identify two solutions that are symmetric or anti-symmetric under $1 \leftrightarrow 2$. In the symmetric case, all polarization vectors are initially prepared identically. Then $\mathbf{D}_2 = \mathbf{D}_1$ and

we find two pairs of decoupled equations, with

$$\text{symmetric eigenconfiguration: } \begin{cases} \mathbf{D}_S &= \mathbf{D}_1 + \mathbf{D}_2 = 2\mathbf{D}_{1,2} \\ \mathbf{A}_S &= \mathbf{D}_1 - \mathbf{D}_2 = 0 \end{cases} \quad (3.43)$$

This eigenmode corresponds to the equation

$$\begin{aligned} \dot{\mathbf{S}}_1 &= \mu \mathbf{D}_1 \times \mathbf{S}_1 + \omega_0 \mathbf{B} \times \mathbf{D}_1, \\ \dot{\mathbf{D}}_1 &= \omega_0 \mathbf{B} \times \mathbf{S}_1, \end{aligned} \quad (3.44)$$

as written exclusively with mode 1; mode 2 follows the same equation (these equations are invariant under $1 \leftrightarrow 2$ transformations). Likewise, if the 1 and 2 modes are prepared with opposite x components, we have $\mathbf{D}_2 = -\mathbf{D}_1$, and

$$\text{anti-symmetric eigenconfiguration: } \begin{cases} \mathbf{D}_A &= \mathbf{D}_1 + \mathbf{D}_2 = 0 \\ \mathbf{A}_A &= \mathbf{D}_1 - \mathbf{D}_2 = 2\mathbf{D}_1 = -2\mathbf{D}_2 \end{cases} \quad (3.45)$$

which allows us to write

$$\begin{aligned} \dot{\mathbf{S}}_1 &= -\mu \mathbf{D}_1 \times \mathbf{S}_1 + \omega_0 \mathbf{B} \times \mathbf{D}_1, \\ \dot{\mathbf{D}}_1 &= \omega_0 \mathbf{B} \times \mathbf{S}_1, \end{aligned} \quad (3.46)$$

as written in terms of mode 1; mode 2 follows the same equations (these equations are invariant with a sign change under $1 \leftrightarrow 2$ transformations). The two regimes, symmetric and anti-symmetric, follow the same equations with the sign of μ flipped. The stability of the initial state requires the opposite signs between ω_0 and μ for the two contributions to cancel at the threshold, which is why the symmetric configurations become stable in the IH and anti-symmetric ones in the NH.

These pure symmetric or anti-symmetric solutions can each be brought to the form of a pendulum equation by introducing the vector $\mathbf{Q}_i = \mathbf{S}_i \mp (\omega_0/\mu) \mathbf{B}$. The EoMs are then $\dot{\mathbf{Q}}_i = \pm\mu \mathbf{D}_i \times \mathbf{Q}_i$ and $\dot{\mathbf{D}}_i = \omega_0 \mathbf{B} \times \mathbf{Q}_i$. However, the vector \mathbf{Q}_i is defined differently for the two cases. Still, if we go to the limit $\mu \gg \omega_0$ we can approximately equal \mathbf{S}_i with \mathbf{Q}_i and the motion of each \mathbf{S}_i is approximately a circle in the x - z plane with its center at the origin. We thus seek solutions of the form

$$\mathbf{S}_i(t) = S_i \begin{pmatrix} \sin \alpha_i(t) \\ 0 \\ \cos \alpha_i(t) \end{pmatrix} \quad \text{and} \quad \mathbf{D}_i(t) = \begin{pmatrix} 0 \\ D_i(t) \\ 0 \end{pmatrix} \quad (3.47)$$

leading to $\dot{\alpha}_1 = \mu D_2$, $\dot{\alpha}_2 = \mu D_1$, and $\dot{D}_i = \omega_0 S_i \sin \alpha_i$. Taking the second derivative then leads to the oscillator equations $\ddot{\alpha}_1 = \omega_0 \mu S_2 \sin \alpha_2$ and $\ddot{\alpha}_2 = \omega_0 \mu S_1 \sin \alpha_1$. With $S = S_1 = S_2$ and

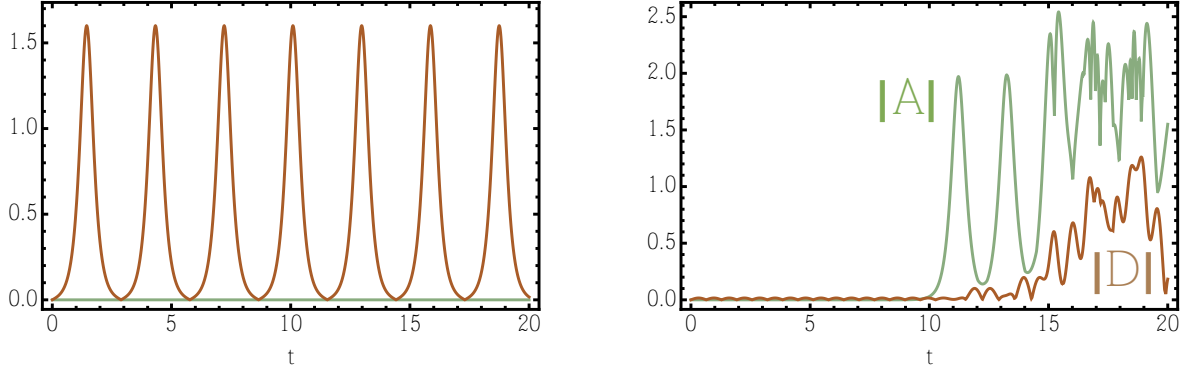


Figure 3.10: *Left:* Bimodal solution in IH. The non-linear behavior arises because of a growth of the scalar order parameter \mathbf{D} while $\vec{\mathbf{A}}$ remains zero. *Right:* In the NH, the MA instability comes from the growth of the vector part of the order parameter. After some time, the asymmetric mode excites the symmetric mode \mathbf{D} leading to the subsequent chaos.

$\kappa^2 = \omega_0 \mu S$ we finally have

$$\begin{aligned}\ddot{\alpha}_1 &= \kappa^2 \sin \alpha_2, \\ \ddot{\alpha}_2 &= \kappa^2 \sin \alpha_1.\end{aligned}\tag{3.48}$$

Our simplified system is therefore equivalent to two maximally mixed anharmonic oscillators.

The eigenmodes of this system consist of a symmetric solution with $\alpha_1(t) = \alpha_2(t)$ and an anti-symmetric one with $\alpha_1(t) = -\alpha_2(t)$. In the former case, with $\alpha = \alpha_1 = \alpha_2$, the EoMs reduce to the single equation $\ddot{\alpha} = \kappa^2 \sin \alpha$. We always assume that initially $\mathbf{D}_i = 0$, i.e., the particle and anti-particle modes begin in the same flavor state so that $\dot{\alpha}(0) = 0$. If the initial angle is small, $\alpha(0) \ll 1$, the symmetric solution corresponds to an inverted pendulum, i.e., an anharmonic oscillator beginning near the maximum of the potential. Switching the hierarchy amounts to $\omega_0 \rightarrow -\omega_0$ and thus $\kappa^2 \rightarrow -\kappa^2$. In this case, the symmetric solution corresponds to a harmonic oscillator with a small initial amplitude.

For the anti-symmetric solution we write $\alpha = \alpha_1 = -\alpha_2$ so that the EoMs reduce to $\ddot{\alpha} = -\kappa^2 \sin \alpha$. Therefore, the original case of inverted hierarchy now corresponds to the small-amplitude harmonic oscillator. Switching the hierarchy changes $\kappa^2 \rightarrow -\kappa^2$ and we are back to the inverted pendulum. In other words, switching the hierarchy and switching between the symmetric and anti-symmetric solution each causes a sign change in $\ddot{\alpha} = \pm \kappa^2 \sin \alpha$.

We may prepare the system initially such that both modes have exactly equal particle densities in exact flavor eigenstates. In this case $\alpha_1(0) = \alpha_2(0)$ and only the symmetric mode is excited. This is the traditional case where the solution was assumed to inherit the symmetry of the initial condition and small deviations from that symmetry were assumed to remain small.

However, the latter assumption is unjustified in the case of normal hierarchy where the traditional solution is stable, whereas the anti-symmetric solution is unstable. The smallest deviation of the initial state from perfect symmetry provides a seed for the exponentially growing solution which then eventually dominates.

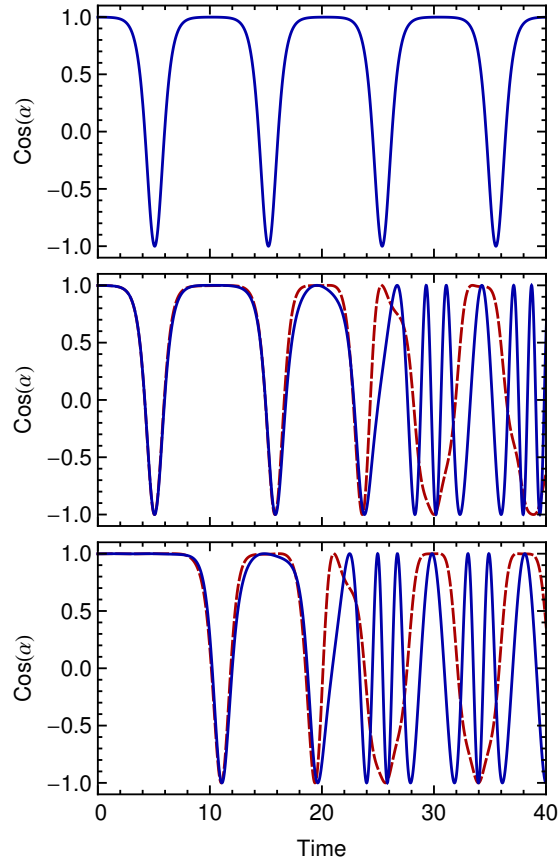


Figure 3.11: Solution for α_1 (blue solid line) and α_2 (red dashed line) with $\kappa = 1$ and $\alpha_1(0) = \alpha_2(0) = 0.05$. *Top:* Bimodal solution in IH. *Middle:* Same with 1% difference in κ^2 in the two EoMs. *Bottom:* Same in NH, showing the new instability.

We illustrate this behavior with a simple example in Fig. 3.11. We use $\kappa = 1$ and the initial angles $\alpha_1(0) = \alpha_2(0) = 0.05$. In IH we then find the usual bimodal solution with pendulum-like periodic flavor conversion (top panel). To disturb the perfect initial symmetry we can either make the initial angles slightly different or assume slightly different particle fluxes in the two beams. We choose the latter approach, implying that S_1 is slightly different from S_2 , i.e., κ^2 in the two equations is a bit different. If we use a 1% difference, which we shall assume henceforth, the bimodal solution at first proceeds as before, but it is now coupled to the harmonic oscillator of the anti-symmetric solution. Therefore, after a few pendulum dips, $\alpha_1(t)$ and $\alpha_2(t)$ get out of step, resulting in chaotic behavior.

Switching the hierarchy (bottom panel) would provide the traditional stable solution if the initial conditions were perfectly symmetric. Implementing our small mismatch has at first no effect, but the unstable admixture of the anti-symmetric mode quickly grows enough to take over and again we get pendulum like behavior that also becomes chaotic.

Even for exact initial symmetry, numerical noise is enough to trigger the run-away solution in normal hierarchy. This can be seen, for instance, when using Mathematica to solve the equations with standard settings. In our example, the first dip triggered by numerical noise was roughly at $t = 45$.

Our example was constructed to be perfectly symmetric between particles and antiparticles, restricting the motion to the x - z plane and assuming $\mu \gg \omega$. Numerical examples solving the full EoMs of Eq. (3.42) in various cases show analogous effects. In other words, if we relax further the symmetry assumptions this does not prevent the new instability, but also does not introduce yet other qualitatively new effects. From a linearized stability analysis of our general two-beam system we indeed find exactly two instabilities. Of course, in the general case the instabilities only arise for certain ranges of μ values.

3.2.3 Chaotic behavior

Both instabilities lead to chaos because of the anharmonic equations. Chaotic behavior arises when small differences between two different solutions grow exponentially. It is easy to see why α_1 and α_2 are pulled apart from each other. Let us consider the simpler case of a small initial asynchrony but same κ^2 . Let's write

$$\begin{aligned}\alpha_1 &= \alpha + \frac{\eta}{2} \quad , \\ \alpha_2 &= \alpha - \frac{\eta}{2} \quad ,\end{aligned}\tag{3.49}$$

where α respects $\ddot{\alpha} = -\kappa^2 \sin \alpha$. Taking the difference of the two equations one finds

$$\ddot{\eta} = -2\kappa^2 \cos \alpha \sin(\eta/2) \approx -(\kappa^2 \cos \alpha)\eta\tag{3.50}$$

In the normal hierarchy, when α is less than π the difference between α_1 and α_2 oscillates at a frequency $\kappa\sqrt{\cos \alpha}$. But as soon as the cosine becomes negative, the equation dictates an exponential growth. Figure 3.12 shows this exact behavior. We clearly see that whenever $\cos \alpha$ is above the difference between the two angles it oscillates and when it dips below the $\eta = 0$ line the two phases are pulled away from each other at an exponential rate. After every dip, the oscillations of the difference become larger and larger until finally, any obvious relation between the two phases is lost. Our observation was that even the minute shifts away from each other introduced by the numerical integration of the differential equations were enough to trigger a visible motion away from each other. A more general analysis was conducted in [41] by studying the stability of neighbouring

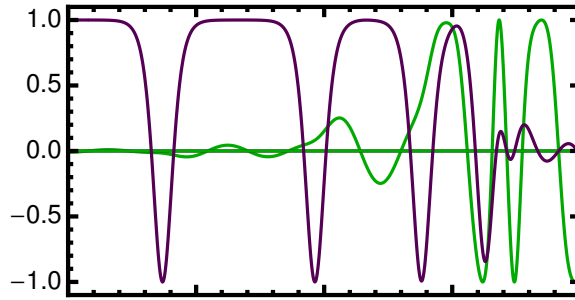


Figure 3.12: Evolution of $\sin \eta = \alpha_1 - \alpha_2$ (green solid line) and $\ddot{\eta}/\eta \approx \cos \alpha$ (red dashed line) using and initial difference of 1% .

trajectories using Lyapunov coefficients. They found the bipolar trajectory to be indeed unstable.

3.3 Summary

We presented in this chapter a simple model obtained by integrating out the dependence of the flavor content on the angular direction and on the position in space. This felt well-motivated for the study of a uniform, isotropic gas of neutrinos. We found full-amplitude oscillations akin to the motion of a pendulum and suppressable with a large ϵ asymmetry. This motion only happens if the relevant mass difference is of the IH type. It wouldn't happen therefore for the solar mass difference.

This difference between the two hierarchies became more nuanced as we studied collective flavor oscillations in a one-dimensional homogeneous and isotropic gas of neutrinos leads to an additional instability of the flavor state, resulting in large amplitude oscillation patterns in both hierarchies. This instability remains despite setting the lengths of the two velocity modes to the same value, i.e., imposing isotropy at the initial instant ($\vec{\mathbf{A}} = 0$ at $t = 0$). Despite this condition, in the NH the vector order parameter grows to a significant value.

In the next chapter we will start with the study of a perfectly isotropic and uniform gas of neutrinos and find that this MA mode does indeed play a major role in providing an instability for the flavor state in the NH. We will then study the instability of the flavor state in an escape from a SN in the last chapter. There, we will encounter again these two distinct instabilities: the bimodal (IH) and the MA (NH).

CHAPTER 4

Oscillations in a uniform isotropic ensemble

In the previous chapter we showed that collective oscillations can break flavor isotropy in a one-dimensional ensemble. In the NH, a situation with a zero net flavor current is not stable. Such a system in which its solutions do not respect individually the symmetry of the infinitesimal dynamics (the EoMs) is said to exhibit *spontaneous symmetry breaking*.

In the present chapter we address the full three-dimensional system of a uniform isotropic gas and study the conditions in which the state of maximal electron flavor becomes unstable. We will show that spontaneous symmetry breaking is present and that it is also related to the exponential growth of the flavor current.

4.1 Flavor evolution in a uniform neutrino fluid

Let us assume we are in a uniform system, i.e., the flavor content does not depend on the position in space: $\mathbf{P}(t, \vec{r}, \omega, \vec{v}) = \mathbf{P}(t, \omega, \vec{v})$. Then $d\mathbf{P}/dt = \partial_t \mathbf{P}$. The polarization vectors describing the flavor content of the uniform fluid evolve according to

$$\dot{\mathbf{P}}(t, \omega, \vec{v}) = \left[\omega \mathbf{B} + \lambda \mathbf{L} + \mu (\mathbf{D} - \vec{v} \cdot \vec{\mathbf{A}}) \right] \times \mathbf{P}(t, \omega, \vec{v}) \quad (4.1)$$

The equations only evolve in time. In the initial instant, all flavor vectors point in the positive z direction. In this situation, we have

$$\begin{aligned} \mathbf{P}(\omega, \vec{v}, 0) &= \mathbf{L}, \\ \mathbf{D}(0) &= \int \mathbf{P}_{\omega, \vec{v}}(0) d\Gamma = \epsilon \mathbf{L}, \\ \vec{\mathbf{A}}(0) &= \int \vec{v} \mathbf{P}_{\omega, \vec{v}}(0) d\Gamma = \left(\int \vec{v} d\Gamma \right) \mathbf{L} \equiv \vec{j} \mathbf{L}, \end{aligned} \quad (4.2)$$

The initial scalar part of the order parameter vanishes when neutrinos and anti-neutrinos are found in equal quantity in the ensemble. The initial vector part vanishes when the average direction of

flow vanishes. For a separable distribution $g(\omega, \vec{v}) = g(\omega) h(\vec{v})$, it is equal to

$$\vec{\mathbf{A}}(0) = \left(\int_{-\infty}^{+\infty} g(\omega) \int h(\vec{v}) \vec{v} d\vec{v} \right) \mathbf{L} = \epsilon \langle \vec{v} \rangle \mathbf{L}. \quad (4.3)$$

The scalar and vector parts match the definition of a density and of a current. If $\epsilon = 0$ then $\vec{j} = 0$. When the asymmetry is zero, both vanish¹. These are the cases which we studied in the previous chapter, in their unidimensional version. We found that even when there is a cancelation of the four components of the order parameter at the initial instant, and therefore $\dot{\mathbf{P}}$ does not depend on \mathbf{P} non-linearly, both hierarchies yield a pendulum-like behavior if the configuration is slightly disturbed.

We must now study the stability of this initial condition. As before, we write the polarization vectors as a perturbation near the fixed point: $\mathbf{P} = (p, P_z)$. Also,

$$\mathbf{R} = \mathbf{D} - \vec{v} \cdot \vec{\mathbf{A}} = (d, D_z) - \vec{v} \cdot (\vec{a}, \vec{A}_z), \quad (4.4)$$

with

$$\begin{aligned} d &= \int p(\omega, \vec{v}) d\Gamma, \\ \vec{a} &= \int \vec{v} p(\omega, \vec{v}) d\Gamma. \end{aligned} \quad (4.5)$$

Note that the second line defines a vector of three complex numbers of small amplitude, indicating three vectors on the xy plane. These correspond to the off-diagonal part of the density matrices. The terms in the EoMs (4.1) written in terms of the perturbations give, to first order

$$\begin{aligned} \mathbf{B} \times \mathbf{P} &= \begin{pmatrix} -P_y \cos 2\theta_0 + i(P_x \cos 2\theta_0 - P_z \sin 2\theta_0) \\ P_y \sin 2\theta_0 \end{pmatrix} \approx \begin{pmatrix} i(\cos 2\theta_0 p - \sin 2\theta_0) \\ P_y \sin 2\theta_0 \end{pmatrix}, \\ \mathbf{L} \times \mathbf{P} &= \begin{pmatrix} -P_y + iP_x \\ 0 \end{pmatrix} \approx \begin{pmatrix} ip \\ 0 \end{pmatrix}, \\ \mathbf{D} \times \mathbf{P} &= \begin{pmatrix} -D_z P_y + D_y D_z + i(D_z P_x - D_x P_z) \\ -D_y P_x + D_x P_y \end{pmatrix} \approx \begin{pmatrix} i(\epsilon p - d) \\ 0 \end{pmatrix}, \\ \vec{\mathbf{A}} \times \mathbf{P} &= \begin{pmatrix} -\vec{A}_z P_y + \vec{A}_y P_z + i(\vec{A}_z P_x - \vec{A}_x P_z) \\ -\vec{A}_y P_x + \vec{A}_x P_y \end{pmatrix} \approx \begin{pmatrix} i(\vec{j} p - \vec{a}) \\ 0 \end{pmatrix}, \end{aligned} \quad (4.6)$$

¹Unless the neutrinos and anti-neutrino have different velocity distributions, in which case the the vector parameter doesn't vanish.

We can now insert these approximations into the EoMs and get

$$\begin{aligned}\dot{p} &= i\omega (\cos 2\theta_0 p - \sin 2\theta_0) + i\lambda p + i\mu(\epsilon p - d - \langle \vec{v} \rangle p + \vec{a}), \\ &= i \left[\omega \cos 2\theta_0 + \lambda + \mu(\epsilon + \vec{v} \cdot \vec{j}) \right] p - i\omega \sin 2\theta_0 + i\mu(d - \vec{v} \cdot \vec{a}),\end{aligned}\quad (4.7)$$

which is affine in p . Since both d and \vec{a} are linear combinations of the many p modes, the whole equation is linear with an affine term $-i\omega \sin 2\theta_0$. The terms in this equation are easy to interpret. The part that multiplies p is an imaginary number which means it corresponds to a change perpendicular to p , that is, a rotation. It is therefore the precession rate induced by B_z , \mathbf{L} and R_z . The term $-i\omega \sin 2\theta_0$ encodes the continuous loss of P_y to the other components due to vacuum oscillations. The last term corresponds to the change in p due to the small off-diagonal parts of the order-parameter.

The coefficient $\omega \cos 2\theta_0$ should remind us of the co-rotating frame. In this case, all the modes precess with the common frequency $\bar{\lambda} \equiv \lambda + \epsilon\mu$. We can move to a frame of reference in flavor space which eliminates this inconsequential precession by observing that

$$\dot{p} - i(\lambda + \epsilon\mu)p = e^{-i(\lambda + \epsilon\mu)t} [\dot{q} - i(\lambda + \epsilon\mu)q] \quad (4.8)$$

with $q(t) \equiv \exp[i(\lambda + \epsilon\mu)t] p(t)$. The linearized EoMs in the co-rotating frame are

$$\dot{q} = i \left(\omega \cos 2\theta_0 + \mu \vec{v} \cdot \vec{j} \right) q - i\omega \sin 2\theta_0 e^{i\bar{\lambda}t} + i\mu(\delta - \vec{v} \cdot \vec{\alpha}), \quad (4.9)$$

where $\delta(t)$ and $\alpha(t)$ are defined analogously to $q(t)$:

$$\begin{aligned}\alpha(t) &\equiv \exp[i(\lambda + \epsilon\mu)t] \int p(t, \omega, \vec{v}) d\Gamma, \\ \vec{\delta}(t) &\equiv \exp[i(\lambda + \epsilon\mu)t] \int \vec{v} p(t, \omega, \vec{v}) d\Gamma.\end{aligned}\quad (4.10)$$

Because both λ and μ are much higher than the bulk of frequencies, the term $-i\omega \sin 2\theta_0 e^{i\bar{\lambda}t}$ averages to zero over a period of $2\pi/\bar{\lambda}$ which is much smaller than the typical scale of collective behavior. We recover hence our previous argument about the co-rotating frame. The averaged equations are now linear in $p(\omega, \vec{v})$. This high frequency also explains why our linearization scheme is self-consistent. The variation of P_z is

$$\dot{P}_z = \omega \sin 2\theta_0 P_y = \omega \sin 2\theta_0 \text{Im } p = \omega \sin 2\theta_0 \text{Im } q e^{-i\bar{\lambda}t}, \quad (4.11)$$

which also averages to zero over the very short period. We are left with the averaged EoMs

$$\dot{q} = i \left(\omega \cos 2\theta_0 + \mu \vec{v} \cdot \vec{j} \right) q + i\mu(\delta - \vec{v} \cdot \vec{\alpha}), \quad (4.12)$$

which is a set of infinite first-order linear differential equations. Their solutions are linear combinations of configurations which scale or rotate under the infinitesimal change described in equations (4.12). These equations can be rewritten as a differential matrix equation of infinite dimension

$$\dot{q}(\omega, \vec{v}) = \int K(\omega, \psi, \chi, \omega', \vec{v}') q(\omega', \vec{v}') d\Gamma \quad (4.13)$$

with the kernel (i.e., the continuous matrix)

$$K(\omega, \vec{v}, \omega', \vec{v}') = \frac{i}{g(\omega', \vec{v}')} \left(\omega \cos 2\theta_0 + \mu \vec{v} \cdot \vec{j} \right) \delta(\omega - \omega') \delta(\vec{v} - \vec{v}') + i\mu [1 - \vec{v} \cdot \vec{v}'] . \quad (4.14)$$

which contains a diagonal part – proportional to $\delta(\omega - \omega') \delta(\vec{v} - \vec{v}')$ – and a non-diagonal part.

Assuming that both μ and λ vary slowly compared to the rate of precession or growth of these eigenconfigurations, we can taken them for constants. In this case, the solutions of the system can be given as linear combinations of

$$q(\omega, \vec{v}, t) = Q_\Omega(\omega, \vec{v}) e^{i\Omega t}, \quad (4.15)$$

$Q_\Omega(\omega, \vec{v})$ are the eigenconfigurations of the kernel with corresponding eigenvalue Ω . Note that the variables ω, \vec{v} play the role of indexes, which is why the Q are functions of these variables (analogous to eigenvectors of a matrix) but the Ω aren't. These eigenconfigurations and eigenvalues are found from the study of the eigenvalue equation for the kernel, deduced from eq. 4.12 by inserting in it the definition of the eigenmodes (4.15)

$$i \left(\omega \cos 2\theta_0 - i\Omega + \mu \vec{v} \cdot \vec{j} \right) Q + i\mu \int (1 - \vec{v} \cdot \vec{v}') Q' d\Gamma = 0, \quad (4.16)$$

with $Q' = Q(\omega', \vec{v}')$.

Eq. (4.16) can be used to define the functional dependence of $Q(\omega, \vec{v})$:

$$Q(\omega, \vec{v}) = \frac{1}{\omega \cos 2\theta_0 - \Omega + \mu \vec{v} \cdot \vec{j}} \int (1 - \vec{v} \cdot \vec{v}') Q' d\Gamma' \equiv \frac{\Delta + \vec{v} \cdot \vec{C}}{\omega \cos 2\theta_0 - \Omega + \mu \vec{v} \cdot \vec{j}}. \quad (4.17)$$

Δ is the scalar component of the eigenconfiguration, whereas \vec{C} is the vector component. By inserting this form back into eq. (4.23), one gets

$$\Delta + \vec{v} \cdot \vec{C} = -\mu \int (1 - \vec{v} \cdot \vec{v}') \frac{\Delta + \vec{v}' \cdot \vec{C}}{\omega' \cos 2\theta_0 - \Omega + \mu \vec{v}' \cdot \vec{j}} d\Gamma' \quad (4.18)$$

This equation has four independent functional dependencies – scalar and vector – which must be verified independently:

$$\begin{aligned}\Delta &= -\mu \int \frac{\Delta + \vec{v} \cdot \vec{C}}{\omega \cos 2\theta_0 - \Omega + \mu \vec{v} \cdot \vec{j}} d\Gamma \\ \vec{C} &= \mu \int \vec{v} \frac{\Delta + \vec{v} \cdot \vec{C}}{\omega \cos 2\theta_0 - \Omega + \mu \vec{v} \cdot \vec{j}} d\Gamma,\end{aligned}\tag{4.19}$$

or in matrix form

$$\begin{pmatrix} 1 + I_{00} & -I_{01} & -I_{02} & -I_{03} \\ I_{10} & 1 - I_{11} & -I_{12} & -I_{13} \\ I_{20} & -I_{21} & 1 - I_{22} & -I_{23} \\ I_{30} & -I_{31} & 1 - I_{32} & 1 - I_{33} \end{pmatrix} \cdot \begin{pmatrix} \Delta \\ C_1 \\ C_2 \\ C_3 \end{pmatrix} = 0\tag{4.20}$$

where

$$I_{ij} = \mu \int \frac{g(\omega, \vec{v})}{\omega \cos 2\theta_0 + \mu \vec{v} \cdot \vec{j} - \Omega} v_i v_j d\Gamma,\tag{4.21}$$

The indices i and j run from 0 to 3. The zeroth component of the velocity is simply defined as 1. In order for the scalar component or the vector components of the eigenconfiguration to be non-trivial, i.e. $\Delta, \vec{C} \neq 0$, the determinant of this matrix must be zero. The eigenvalues are therefore determined by the equation

$$\det \begin{bmatrix} 1 + I_{00} & -I_{01} & -I_{02} & -I_{03} \\ I_{10} & 1 - I_{11} & -I_{12} & -I_{13} \\ I_{20} & -I_{21} & 1 - I_{22} & -I_{23} \\ I_{30} & -I_{31} & 1 - I_{32} & 1 - I_{33} \end{bmatrix} = 0\tag{4.22}$$

4.2 Stability of an isotropic distribution

We are now ready to address the most important question of this chapter: in a uniform isotropic gas of neutrinos, when does collective flavor conversion occur? For this we take $g(\omega, \vec{v}) = g(\omega)/4\pi$. The flavor difference current cancels, i.e. $\vec{j} = 0$, because all directions of flow present equal contributions. The eigenvalue equation becomes

$$i(\omega \cos 2\theta_0 - \Omega) Q + i\mu \int g(\omega') (1 - \vec{v} \cdot \vec{v}') Q' d\Gamma' = 0\tag{4.23}$$

The explicit dependence of Q on the angular variables is kept. In the last chapter we saw that neglecting this dependence in the one-dimensional case lead to incomplete results. Keeping the dependence on the velocity even though g does not depend on it allows for symmetry breaking instabilities to occur.

Because of the orthogonality of the trigonometric functions, many of the integrals I_{ij} evaluate

to zero. In fact in the matrix equation (4.20), only the diagonal terms remain. The matrix reveals its much simpler form

$$\begin{pmatrix} 1+I & 0 & 0 & 0 \\ 0 & 1-I/3 & 0 & 0 \\ 0 & 0 & 1-I/3 & 0 \\ 0 & 0 & 0 & 1-I/3 \end{pmatrix} \cdot \begin{pmatrix} \Delta \\ C_1 \\ C_2 \\ C_3 \end{pmatrix} = 0 \quad (4.24)$$

with

$$I = \mu \int_{-\infty}^{+\infty} \frac{g(\omega)}{\omega \cos 2\theta_0 - \Omega} d\omega \quad . \quad (4.25)$$

All the different modes – corresponding to the four different components of the eigenconfigurations Δ , C_1 , C_2 and C_3 – decouple, which means each of them behaves independently: the eigenconfigurations of the system *are* the scalar and vector parts of the initial configuration. The scalar part varies with the eigenvalue Ω_Δ determined by the eigenvalue equation $1 + I = 0$. The vector part with Ω_V obeying the eigenvalue equation $1 - I/3 = 0$. Note that the overall symmetry of the problem is preserved: we have three identical eigenvalue equations for each of the three-cartesian coordinates of the velocity. They all evolve with $\exp(i\Omega_V t)$. Spontaneous symmetry breaking happens because any linear dependence on the velocity the initial configuration may have gets blown to exponential proportions. In the nomenclature previously introduced, $I = -1$ defines the bipolar instability and $I = 3$ defines the MA instability. As you can see, the difference in sign implies the symmetry/anti-symmetry of the arrangement of the modes as discussed earlier; also, it means the behavior of one in one hierarchy is the behavior of the other in the other hierarchy.

To better understand these results, let's consider the case of a single frequency $\pm\omega_0$. As a direct consequence of the definition of $g(\omega) = -\delta(\omega + \omega_0) + (1 + \epsilon)\delta(\omega - \omega_0)$,

$$I = \mu \int_{-\infty}^{+\infty} \frac{g(\omega)}{\omega \cos 2\theta_0 - \Omega} d\omega = \mu \frac{1 + \epsilon}{\omega_0 \cos 2\theta_0 - \Omega} - \mu \frac{1}{-\omega_0 \cos 2\theta_0 - \Omega} \quad . \quad (4.26)$$

Thus the eigenvalue equations can be assembled into

$$\frac{1 + \epsilon}{\omega \cos 2\theta_0 - \Omega} - \frac{1}{-\omega_0 \cos 2\theta_0 - \Omega} = \frac{\alpha}{\mu} \quad (4.27)$$

with a parameter $\alpha = -1, 3$ for the scalar mode and the vector mode respectively. Ω is easy to compute from here

$$\Omega = -\frac{\epsilon\mu}{2\alpha} \pm \sqrt{\left(\frac{\epsilon\mu}{2\alpha} - \omega_0 \cos 2\theta_0\right)^2 - 2\frac{\mu}{\alpha}\omega_0 \cos 2\theta_0} \quad (4.28)$$

This last formula shows that there is always a precession term of frequency $-\epsilon\mu/2$ and $\epsilon\mu/6$ for the scalar and vector modes respectively. Taking into the account the precession of the co-rotating

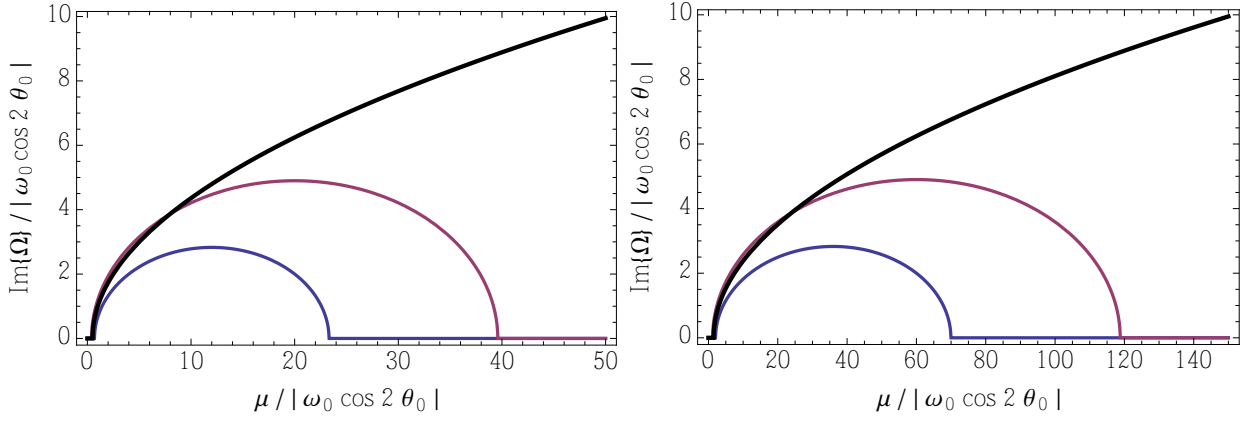


Figure 4.1: magnitude of the bipolar (*top*) and MZA (*bottom*) instabilities. The red and blue lines correspond respectively to $\epsilon = 0.5$ and $\epsilon = -0.5$. The thicker black curve is the value of the instability with zero asymmetry. It grows indefinitely, whereas for non-vanishing asymmetry they only act on a finite range of μ . Note that the plots are identical under a scale change of $\mu \rightarrow 3\mu$.

frame, they relate to the average interaction with the weakly charged background according to

$$\bar{\lambda} - \frac{\epsilon\mu}{2\alpha} = \lambda + \epsilon\mu \left(1 - \frac{1}{2\alpha}\right) = \sqrt{2}G_F \times \begin{cases} n_e - n_{\bar{e}} - \frac{1}{2}(n_{\nu_e} - n_{\bar{\nu}_e}) & \text{(scalar)}, \\ n_e - n_{\bar{e}} - \frac{5}{6}(n_{\nu_e} - n_{\bar{\nu}_e}) & \text{(vector)}. \end{cases} \quad (4.29)$$

This precession is unavoidable, even if there is an exponential growth of the transversal component of the flavor vectors. This growth comes from the square root term, when this one becomes imaginary. To find out the region where the term under the square root in eq.(4.28) is negative, we rewrite eq. (4.28) as

$$\frac{\Omega}{|\omega_0 \cos 2\theta_0|} = -\frac{\epsilon}{2} \frac{\mu}{|\alpha \omega_0 \cos 2\theta_0|} \text{sign}\{\alpha\} \pm \sqrt{\left(\frac{\epsilon}{2} \frac{\mu}{|\alpha \omega_0 \cos 2\theta_0|} \text{sign}\{\alpha\} - \text{sign}\{\omega_0 \cos 2\theta_0\}\right)^2 - 2 \frac{\mu}{|\alpha \omega_0 \cos 2\theta_0|} \text{sign}\{\alpha\} \text{sign}\{\omega_0 \cos 2\theta_0\}} \quad (4.30)$$

In this form, it becomes obvious that the signs α and $\omega_0 \cos 2\theta_0$ being identical is a prerequisite for the argument of the square root to be negative. Therefore, the scalar (bipolar) instability only occurs in the IH and the vector (MA) instability in the NH. Fig. 4.1 shows the magnitude of these instabilities for several values of ϵ .

4.3 Discretization of the angular distribution

One important issue remains to be addressed: how does the continuum limit come about as one makes a finer and finer gridding of the solid angle \vec{v} describes? Writing the velocity in spherical

coordinates

$$\vec{v} = (\sin \psi \cos \chi, \sin \psi \sin \chi, \cos \psi) \quad (4.31)$$

The issue may seem trivial, but consider that as one adds more and more angular bins – N_ψ and N_χ –, the kernel becomes a dimension $N_\psi \times N_\chi$ matrix (i.e., an $(N_\psi \times N_\chi) \times (N_\psi \times N_\chi)$ matrix) which evidently has $N_\psi \times N_\chi$ eigenvalues and eigenvectors. Yet somehow only two of these eigenvalues survive the process of reaching the continuum, the ones that respect the functional independence of ψ and χ .

We address this issue it is however easier to consider not the continuous uniform spectrum as a limit of the discrete uniform spectrum, but the discrete uniform spectrum as a particular realization of the general continuous spectrum in terms of dirac deltas:

$$g(\omega, \psi, \chi) = g(\omega) \times \frac{1}{N_\psi} \sum_{i=1}^{N_\psi-1} \delta\left(\psi - \frac{\pi i}{N_\psi - 1}\right) \times \frac{1}{N_\chi} \sum_{j=1}^{N_\chi} \delta\left(\chi - \frac{2\pi j}{N_\chi}\right) \quad (4.32)$$

The term $i - 1/2$ distributes evenly the values of ψ on the interval $[0, \pi]$. The same diligence isn't required for χ since its range is periodic. The average values $\langle \psi \rangle = 0$ and $\langle \chi \rangle = 0$ are in this way preserved and thus $\vec{j} = 0$. We can expand these spectra in trigonometric functions

$$\frac{1}{N_\psi} \sum_{i=1}^{N_\psi-1} \delta\left(\psi - \frac{\pi i}{N_\psi - 1}\right) = \frac{1}{\pi} \sum_{n=0}^{\infty} \cos(2N_\psi n \psi), \quad (4.33)$$

and

$$\frac{1}{N_\chi} \sum_{j=1}^{N_\chi} \delta\left(\chi - \frac{2\pi j}{N_\chi}\right) = \frac{1}{2\pi} \sum_{n=0}^{\infty} \cos(N_\chi n \chi). \quad (4.34)$$

These spectra must be inserted in the integrals in eq. (4.21). These integrals contain terms of the type

$$\int_0^\pi \cos(2N_\psi n \psi) \text{trig}(\psi) \sin \psi \, d\psi \quad \text{and} \quad \int_0^{2\pi} \cos(N_\chi n \chi) \text{trig}(\chi) \, d\chi, \quad (4.35)$$

where $\text{trig}(x) = 1, \cos x, \sin x$. Because of the orthogonality of the trigonometric functions all integrals in χ with $N_\chi > 2$ give the same behavior in the linear regime. The only non-vanishing integral for binnings greater than 2 is $n = 0$ and $\text{trig}(\psi) = 1$ which is trivially equal to 2π . The same is true for the integrals in ψ with $N_\psi > 2$ for $\text{trig}(\psi) = \sin \psi$ whose $n = 0$ term equals $\pi/2$. All the integrals with $\text{trig}(\psi) = \cos \psi$ vanish for any choice of N_ψ . However, the integrals with $\text{trig}(\psi) = 1$ remain finite up to any value of n no matter how high the N_ψ . Still, the coefficients for $n > 0$ decay rapidly with n and with N_ψ . It is generally enough to take $N_\psi > 5$ in which case all coefficients for $n > 0$ are smaller than 10^{-1} . The $n = 0$ coefficient evaluates to 2. Therefore one expects the matrix in eq. (4.24) to be approximately recovered for $N_\psi > 5$ and $N_\chi > 2$.

4.4 Expansion in spherical harmonics

The results of the previous section seem to indicate that, in the linear regime, that a few modes are enough to describe the complete system. In this section we will use spherical harmonics to describe the system of polarization vectors and find that actually the scalar and vector harmonics play a major role in the dynamics of the system². We will still assume an isotropic spectrum of the type $g(\omega, \psi, \chi) = g(\omega)/4\pi$. We now describe each component of the flavor vectors as a linear combination of spherical harmonics:

$$\mathbf{P}(\omega, \psi, \chi, t) = \sum_{l,m} \mathbf{c}_{lm}(\omega, t) Y_{lm}(\psi, \chi). \quad (4.36)$$

Note that $\mathbf{c}_{lm}(\omega, t)$ is written in bold-face because it is a three-dimensional vector of coefficients. The idea is to track the evolution of these coefficients instead of the polarization vectors directly. Our spherical harmonics respect³

$$\frac{1}{4\pi} \int_0^\pi \sin \psi \, d\psi \int_0^{2\pi} d\chi Y_{lm}(\psi, \chi) Y_{l'm'}^*(\psi, \chi). \quad (4.37)$$

The velocity can be written as

$$\vec{v} = \begin{pmatrix} v_x + j v_y \\ v_z \end{pmatrix} = \begin{pmatrix} \sin \psi e^{j\chi} \\ \cos \psi \end{pmatrix} = \frac{1}{\sqrt{3}} \begin{pmatrix} -\sqrt{2} Y_{11} \\ Y_{10} \end{pmatrix} \quad (4.38)$$

where j is the 90 degree rotation on the physical xy plane (not to be mistaken with i , the same rotation in flavor space). The order parameters become

$$\begin{aligned} \mathbf{D}(t) &= \int_{-\infty}^{+\infty} d\omega \frac{g(\omega)}{4\pi} \int_0^\pi \sin \psi \, d\psi \int_0^{2\pi} d\chi \sum_{l,m} Y_{lm}(\psi, \chi) \mathbf{c}_{lm}(\omega, t) \\ &= \int_{-\infty}^{+\infty} d\omega g(\omega) \mathbf{c}_{00}(\omega, t), \end{aligned} \quad (4.39)$$

$$\begin{aligned} \mathbf{A}_x(t) + j \mathbf{A}_y(t) &= \int_{-\infty}^{+\infty} d\omega \frac{g(\omega)}{4\pi} \int_0^\pi \sin \psi \, d\psi \int_0^{2\pi} d\chi \left(-\sqrt{\frac{2}{3}} \right) Y_{11} \sum_{l,m} Y_{lm}(\psi, \chi) \mathbf{c}_{lm}(\omega, t) \\ &= -\sqrt{\frac{2}{3}} \int_{-\infty}^{+\infty} d\omega g(\omega) \mathbf{c}_{11}(\omega, t), \end{aligned} \quad (4.40)$$

²For a similar calculation see [42]

³Defined therefore as $2\sqrt{\pi}$ times the usual spherical harmonics normalized to $4\pi \delta_{ll'} \delta_{mm'}$.

$$\begin{aligned}
\mathbf{A}_z(t) &= \int_{-\infty}^{+\infty} d\omega \frac{g(\omega)}{4\pi} \int_0^\pi \sin \psi d\psi \int_0^{2\pi} d\chi \frac{1}{\sqrt{3}} Y_{10} \sum_{l,m} Y_{lm}(\psi, \chi) \mathbf{c}_{lm}(\omega, t) \\
&= \frac{1}{\sqrt{3}} \int_{-\infty}^{+\infty} d\omega g(\omega) \mathbf{c}_{1,0}(\omega, t),
\end{aligned} \tag{4.41}$$

The previous equations should make the geometrical simplicity of the order parameters obvious: as expected, the scalar order parameter is a function of the coefficient of the scalar spherical harmonic, whereas the vector order parameter is a function of the coefficients of the vector spherical harmonics. For sake of concision, let's define:

$$\vec{\gamma}(\omega, t) = \begin{pmatrix} -\sqrt{2} \mathbf{c}_{1,1}(\omega, t) \\ \mathbf{c}_{1,0}(\omega, t) \end{pmatrix} \tag{4.42}$$

The EoMs can be rewritten as

$$\begin{aligned}
\sum_{l,m} Y_{lm}(\psi, \chi) \dot{\mathbf{c}}_{lm}(\omega, t) &= (\omega \mathbf{B} + \lambda \mathbf{L}) \times \sum_{l,m} Y_{lm}(\psi, \chi) \mathbf{c}_{lm}(\omega, t) \\
&+ \mu \int_{-\infty}^{+\infty} d\omega' g(\omega') \left[\mathbf{c}_{00}(\omega', t) - \frac{1}{\sqrt{3}} \vec{v} \cdot \vec{\gamma}(\omega', t) \right] \times \sum_{l,m} Y_{lm}(\psi, \chi) \mathbf{c}_{lm}(\omega, t).
\end{aligned} \tag{4.43}$$

The simplicity of these equations becomes all the more striking if one multiplies by $Y_{l'm'}^*$ and integrates over ψ and χ :

$$\begin{aligned}
\dot{\mathbf{c}}_{lm}(\omega, t) &= \left[\omega \mathbf{B} + \lambda \mathbf{L} + \mu \int_{-\infty}^{+\infty} d\omega' g(\omega') \mathbf{c}_{00}(\omega', t) \right] \times \mathbf{c}_{lm}(\omega, t) \\
&- \frac{1}{3} \left(\Upsilon_{lm}^{xy,+} \gamma_{xy}^* \times \mathbf{c}_{l+1,m} + \Upsilon_{lm}^{xy,-} \gamma_{xy}^* \times \mathbf{c}_{l-1,m} \right) \\
&- \frac{1}{3} \left(\Upsilon_{lm}^{z,+} \gamma_z \times \mathbf{c}_{l+1,m} + \Upsilon_{lm}^{z,-} \gamma_z \times \mathbf{c}_{l-1,m} \right).
\end{aligned} \tag{4.44}$$

and

$$\begin{aligned}
\Upsilon_{lm}^{xy,\pm} &= \int Y_{11} Y_{lm}^* Y_{l\pm 1,m} d\Gamma, \\
\Upsilon_{lm}^{z,\pm} &= \int Y_{10} Y_{lm}^* Y_{l\pm 1,m} d\Gamma.
\end{aligned} \tag{4.45}$$

In the EoMs as written in eq. (4.44), one recognizes the couplings 1 and -1/3 previously encountered in the stability analysis. If one neglects the vector interaction, the dynamics is completely given by the scalar modes \mathbf{c}_{00} whose EoMs, for a single energy

$$\begin{aligned}
\dot{\mathbf{c}}_{00}(+\omega_0, t) &= [+ \omega_0 \mathbf{B} + \lambda \mathbf{L} - \mu \mathbf{c}_{00}(-\omega_0, t)] \times \mathbf{c}_{00}(+\omega_0, t), \\
\dot{\mathbf{c}}_{00}(-\omega_0, t) &= [- \omega_0 \mathbf{B} + \lambda \mathbf{L} + (1 + \epsilon) \mu \mathbf{c}_{00}(+\omega_0, t)] \times \mathbf{c}_{00}(-\omega_0, t)
\end{aligned} \tag{4.46}$$

are identical to the EoMs deduced in the third chapter for the bipolar oscillations. The vector interaction works to couple modes to their neighbours: every harmonic of number l couples to the upper harmonic $l + 1$ and the lower harmonic $l - 1$.

4.5 Summary

This section studied the onset of flavor conversion due to non-linear refractive effects in a uniform, isotropic ensemble of neutrinos. Here are the main points we made:

- There is an instability that occurs in the IH called the bipolar instability (for a single frequency). It causes the scalar part of the order parameter \mathbf{D} to grow. In fact, the smaller ϵ is, the bigger the growth factor is. In other words, the smaller the initial condition for $\mathbf{D}(0)$ is, the faster the growth is.
- There is an instability that occurs in the IH called the MA instability (for a single frequency). It causes the vector part of the order parameter \mathbf{A} to grow.
- The results apply when resonant matter conversions are absent. In this regime, matter does not play a role in the onset of collective behavior. The eigenvalues Ω are independent of λ and as such the matter density cannot either enforce or prevent the instability. In the next chapter we will see that it is not always so when one introduces non-trivial angular distributions.

CHAPTER 5

Core-collapse supernovae

In this chapter, we introduce the relevant details of SN dynamics. Core-collapse SNe are one of the rare environments where collective flavor oscillations can take place. Its core – of dense nuclear matter – is one of the few places where neutrinos can be trapped and even reach thermal equilibrium. To become a neutron star, the core has to radiate its lepton number and gravitational binding energy. That radiation happens in the form of neutrinos. In fact, most of the change in the gravitational binding energy during the collapse is released in the form of neutrinos and anti-neutrinos of all species. The flux becomes so high that once they are released from the deep trapping volume – called the neutrino sphere – conditions are favorable for collective behavior. We will briefly go through the mechanism of the collapse, including the different phases that occur between the death of the progenitor and the birth of the neutron star. We will then present the reader with some basic information about the fluxes of neutrinos, of how they are produced in the core and of how they are emitted.

5.1 Collapse of the progenitor

During the life of a star, the high temperature resulting from its enormous mass fuses elements together. It burns hydrogen, a product of the Big Bang, into helium, in the deeper regions where the conditions are adequate to sustain the necessary reactions. This new element being heavier sinks to the core of the star. In heavier stars, the stellar body eventually contracts at the end of the hydrogen-burning cycle, thereby reheating the gas into the next stage of fusion. In the helium-rich core now, He nuclei are combined to form carbon. A new cycle of contraction happens and then carbon burns to form neon and oxygen and then silicon. In stars more massive than ten solar masses the process can produce iron from silicon fusion. This element is stabler than its neighbours of higher mass number, making iron the final product of the fusion chain. The iron core grows under an onion-like mantle of many elements distributed according to their densities, with heavier elements being produced in deeper regions. The age of the star reaches its final digit

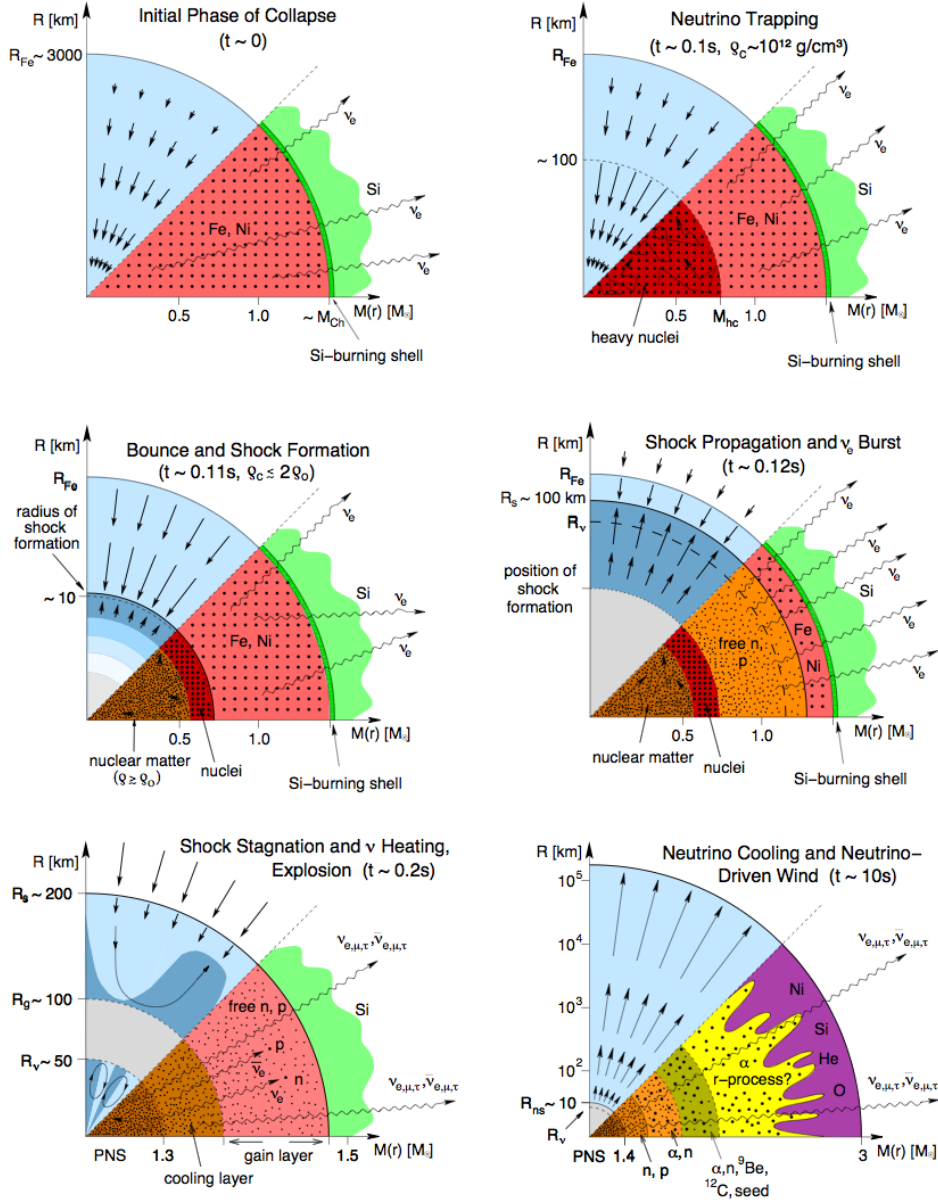


Figure 5.1: Schematic description of a core-collapse SN [43]. The hydrodynamics are shown in the upper half of each diagram, in the form of velocity vectors. The region of homologous (subsonic) and supersonic collapse are portrayed. The nuclear interactions and composition are shown in the lower half. The different phases are as described in the text. In the first panel ($t \sim 0$) one can see the collapse of the iron core of the star. In the second panel ($t \sim 0.1$ s), the formation of the neutrino sphere in the dense core. In the third panel ($t \sim 0.11$ s), the core of nuclear matter is formed on which the infalling matter bounces off to produce the shock wave. In the fourth panel ($t \sim 0.12$ s), the shock propagates photodissociating the iron content into free nucleons, leading to the emission of the prompt neutrino burst. In the fifth panel ($t \sim 0.2$ s), the accretion phase is depicted during which the shock stalls, convective currents form and there is an emission of all neutrino species; the neutron star begins to form. In the last panel ($t \sim 0.10$ s), the proto-neutron star cools down while the higher mantles containing heavier elements synthesized during the SN are blown out into space.

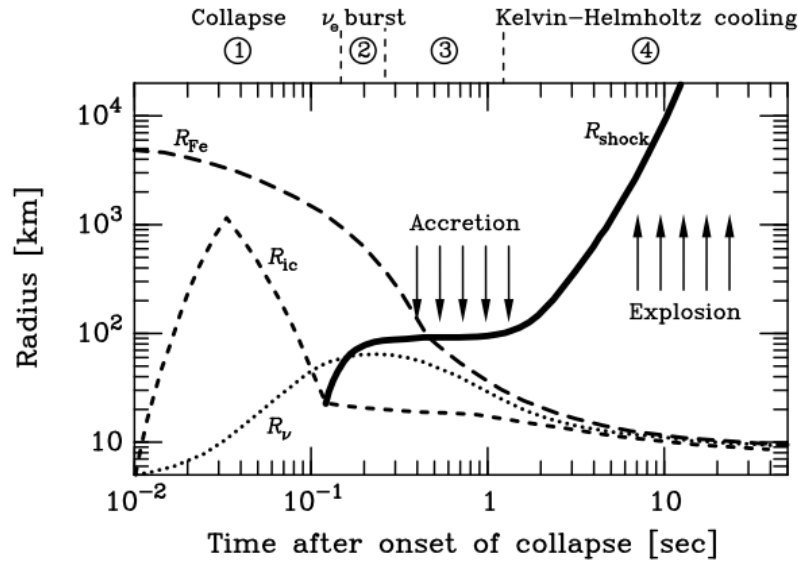


Figure 5.2: Schematic of description of different radii of relevance during the four periods of the collapse of a core-collapse SN [18]. R_{Fe} stands for the radius of the iron core, R_{ic} for that of the inner core, R_{shock} for the position of the shock front and R_{ν} . Of major interest to us in this figure is the neutrino sphere, the radius at which neutrino-matter collisions become inefficient and neutrinos stream out collisionlessly. This sphere reaches its peak during the early accretion phase, as the shock wave forms, when temperatures are highest and making conditions favorable for neutrino trapping. When the proto-neutron star is forming by cooling down of the neutron gas, the temperature decreases, making it easier for neutrinos to flee even the lower regions.

when balance is lost, that is, when an contraction of the iron core’s volume results in an insufficient pressure to sustain the consequent increase of the gravitational pull. Beyond this point the core becomes unstable and collapses¹. Several processes can serve as the origin of this pressure imbalance that brings about the instability. Iron core collapse happens when the pressure of the degenerate electron gas fails to support the core, which is inevitable if its mass reaches $M \gtrsim 1.4 M_{\odot}$. Other stars, such as the lighter kind O+Ne+Mg stars with $9\text{-}10M_{\odot}$ collapse because of electron capture in magnesium whereas much heavier stars $M > 140 M_{\odot}$ collapse because of e^+e^- pair production in nucleon collision or disintegration of nuclei by high energy gamma rays.

When this limit is overcome, the inert core of the star collapses onto itself. Matter falls in supersonically leaving the outer layers unaware of the internal catastrophe that is on-going. At the very center a region of subsonic infall is also present, where the densities are higher. These higher

¹Not all stars collapse however. Light stars simply burn all available material and cool down, trapping the heavy elements in their dead core.

densities now allow for electrons to be absorbed by the nuclei in processes of the type



This reaction reduces the pressure even further and accelerates the already on-going collapse. Progenitor stars also undergo photodissociation of their iron content:



This reaction is endothermic and thus also contributes to reducing the pressure.

Once the core reaches a density of about 10^{12} g cm⁻³ it becomes opaque to neutrinos. Thus begins the stage during which neutrinos are trapped in the core and reach thermal and β equilibrium ($p + e^- \leftrightarrow n + \nu_e$) with the surrounding matter. The equilibrium value of the lepton number per baryon is

$$Y_L \equiv Y_e + Y_\nu = \frac{n_{e^-} - n_{e^+}}{n_B} + \frac{n_\nu - n_{\bar{\nu}}}{n_B} \approx 0.35 \quad (5.3)$$

where n_B is the density of baryons. Once the core densities reach 10^{14} g cm⁻³, the degeneracy pressure is overcome and the neutrons and the nuclei present in the core begin to form the proto-neutron-star. The neutronization process causes the lepton number stored in the form of electrons to be converted into neutrinos which escape from a region at the edge of the core where β equilibrium is lost. This edge is called the *neutrino sphere*.

5.2 Core bounce and shockwave

The sudden increase in the pressure during the neutronization, due to the much stronger nuclear repulsion at short distance, sends out pressure waves that cluster in the region border between the subsonic and supersonic infalls, resulting in the formation of a shock wave which propagates outwards. The shock propagates as a discontinuity of pressure, density and temperature. It forms on the edge of the sub-sonic infall which happens nearer to the core. In the shock front, the conditions greatly enhance the cross-section of iron photodissociation. The later releases free protons which absorb the free electrons more easily than when they were bound in a nucleus. The resulting β reaction emits a great quantity of neutrinos, about 10^{54} erg s⁻¹ in what is known as the prompt neutrino burst, seen in the neutrino light curves as a sudden peak which lasts about 10 ms. Bipolar oscillations cannot happen during this phase because of the extremely high lepton number asymmetry ϵ of the neutrino radiation. Collective MSW conversions can however occur [44].

The large energy radiated away almost invariably (except for light progenitor O+Mg+Ne stars with 8-10 M_\odot) halts the propagation of the shock in the simulations performed so far. The front remains stalled at a certain distance or bounces back and forth before recollapsing. How the shock reacquires its momentum is the largest unresolved issue in core-collapse SNe, a gap which continues

to vex the researching community.

Recent results of 2D and 3D simulations have shown the shockwave to vibrate in a dipolar motion. This sloshing is known as the Standing Accretion Shock Instability (SASI). It was first witnessed in simulations [45] and then confirmed analytically [46]. This motion could leave imprints on the neutrino radiation by adding rapid oscillations to the fluxes [47, 48].

5.3 Neutrino sphere

Neutrino species in the core are in thermal and chemical equilibrium at a temperature of a few MeV. The thermalized neutrinos scatter back and forth between nucleons with a mean-free path of a few meters and for about a second before they are emitted from the neutrino sphere, the region of space outside of which neutrinos are more-or-less free to stream out. The great interest in SN neutrinos comes from the fact that they are emitted from the core and therefore could shed “light” into the events that occur deep there. The size of the neutrino sphere varies and different species have different neutrino spheres.

Muon and tau neutrinos share the same interactions in the SN. Their spectra, luminosities, emission and absorption rates are identical. Because of the massiveness of their charged partners – the muon and the tau – these neutrinos fall well-below the threshold for $n + \nu_{\mu,\tau} \rightarrow p + \mu, \tau$ and its inverse. They only interact through NCs which do not distinguish the flavor. The same applies to muon and tau anti-neutrinos. Therefore these species are the first to decouple and stream out from a deeper region. Electron neutrinos and anti-neutrinos, on the contrary, in addition to the NC interaction also interact via CC and therefore are emitted from higher regions.

5.4 Accretion phase

This phase lasts for a few hundred milliseconds after the initial burst. It corresponds to the period during which the shock is stalled and matter accretes in the core. The neutrino emission is dominated by the thermal processes such as $e^+e^- \rightarrow \nu\bar{\nu}$ and $n + p \rightarrow n + p + \nu\bar{\nu}$ which produce all flavors equally. Therefore ϵ is much lower during this phase, allowing for collective flavor conversion to potentially take place. We now list the key features of each neutrino flux.

Heavy-lepton neutrinos and antineutrinos Heavy lepton (anti)neutrinos’ energies are too low for effective charged current reactions such as $\nu_x(\bar{\nu}_X) + n \rightarrow p + X^-(X^+)$ (X denotes the corresponding heavy lepton). Therefore they are produced and absorbed in NC-driven processes, such as pair annihilation and creation $e^+e^- \leftrightarrow \nu_X\bar{\nu}_X$ and weak nucleon-nucleon bremsstrahlung $n + n \rightarrow n + n + \nu_X\bar{\nu}_X$. These processes are less efficient than the charged current reactions which contributes to a smaller heavy-lepton neutrinosphere (about 15 km). ν_X typically escape with energies of 13 - 16 MeV.

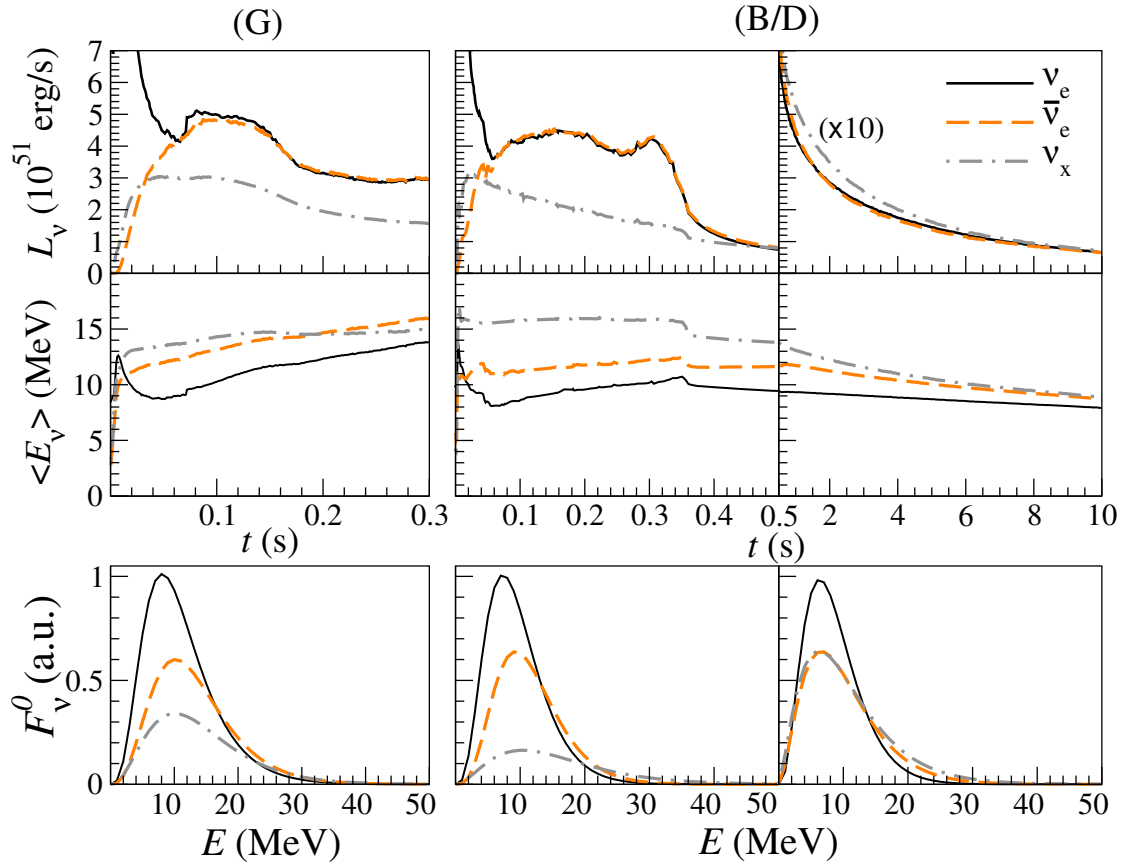


Figure 5.3: Luminosity and average energy for the different neutrino flavors as a function of time (upper panels), and the time-integrated spectrum (lower panels) [50]. The results come from two different groups: Garching ($15M_\odot$ progenitor) and Basel/Darmstadt ($18M_\odot$ progenitor). In the B/D simulation the cooling phase can be seen, starting at around 500 ms (right-most panels). The luminosity drops by an order of magnitude prior to this phase and keeps decreasing during it. In this phase, the usual flux hierarchy can be violated: in some simulations the flux of heavy-lepton neutrinos can overtake the other two, one of the reasons why a two-flavor analysis fails during the cooling phase.

Electron neutrinos The excess of electron neutrinos relative to the heavy-lepton ones comes mostly from the charged current process $e^- + p \rightarrow \nu_e + n$. The same is true for their absorption rate which comes mostly from the inverse process where a neutrino is absorbed in a free neutron, which are abundant in the protoneutron star atmosphere. It is the main contributor to the opacity of the deep core to ν_e . Thermal equilibrium is also reached through NC inelastic scattering on nuclei and especially on electrons. The cross-sections for these processes scale approximately with E_ν and thus, below a certain energy threshold, the neutrinos decouple from the gas. This region is called the “energy sphere”, where neutrinos last exchange energy with matter. The last diffusion happens at the so-called “neutrino sphere” and the two generally don’t match. The neutrino sphere of the

electrons is the largest because of the multitude of interaction channels it has with matter and the abundance of reactive elements in the core. It lets out free neutrinos with energies of 8 - 13 MeV.

Electron antineutrinos The production and absorption of neutrinos comes mostly from the reaction $\bar{\nu}_e + p \leftrightarrow e^+ + n$. The cross section of these processes are identical to the corresponding processes for the ν_e , though because the environment where the neutron star is forming is richer in neutrons than in protons, one should expect the overall production and absorption rates of electron antineutrinos to be smaller, yielding a lower anti-neutrino luminosity. Since the lower proton density allows them to escape earlier, they are emitted from a deeper region of higher temperature than the electron neutrinos. They typically escape from a smaller neutrino sphere with energies of 10 - 15 MeV.

Between the stalled shock and the PNS, there is a mantle of high temperature (tens of MeV) where electron-positron pairs are commonly produced. As indicated by simulations, between 100 to 250 ms, the lepton number develops a distributional asymmetry in this mantle which also results in an asymmetric emission of neutrinos vs. anti-neutrinos known as the LESA (Lepton-number Emission Self-sustained Asymmetry) [49].

5.5 Cooling

Finally, the period known as the Kelvin-Helmholtz cooling takes place. The shock by then has been somehow revived, eventually ejecting the elements² in higher layers into deep space. Meanwhile, the unsprayed matter near the core cools down by deleptonization to a soup of low leptonic number, of free neutrons, protons and electrons that soon will become a neutron star or a black hole. At this point there is a dramatic decrease in the luminosity of the neutrino radiation, though this signal is actually the longest lasting neutrino signal (lasting for seconds). The flux is equally distributed over all three species as most of the lepton number previously stored in the star has already been emitted. NC emission dominates. In this regime it has been shown that it is important to consider the full 3×3 flavor dynamics.

5.6 Summary

Many of these effects, their role in the explosion mechanism and interplay – collective oscillations, SASI, LESA, etc. – remain somewhat speculative. Because neutrinos play such a central role in the energy and lepton-number transfers inside the SN, a high statistics signal from a core-collapse SN would be highly desirable to settle some of these matters and rule out competing ideas. Low-energy detectors like Super-Kamiokande could witness about 10000 events if a core-collapse SN were to

²Actually it also ejects elements heavier than iron whose only chance of production is the SN itself, where conditions are reached that allow these products of unlikely fusions to come about.

happen in the 10 kiloparsec vicinity of Earth [23]. Other experiments such as SNO, KamLAND, LVD, MiniBooNE and Borexino could also detect signals, though with lesser event counts [51]. The SASI hypothesis could be tested in the rising background of IceCube which, even though the detector is optimized for much more energetic neutrinos, would allow one to observe the neutrino light curves.

Neutrinos decouple from the collapsing star long before photons do and from greater depths. If anything, this wide array of detectors [52] should in principle be capable of pin-pointing the source of the neutrino flux and act as a warning signal for astronomers to aim their telescopes at the location in the sky where a few hours later a beautiful exploding core-collapse supernova is supposed to appear.

The main points we have stressed in this chapter are:

- Neutrinos emerge from the core in three distinct phases: the prompt burst, the accretion-phase flux, and the cooling-phase flux. The first phase emits exclusively electron neutrinos. The second phase is less luminous but emits many species obeying $F_{\nu_e} > F_{\bar{\nu}_e} > F_{\nu_X} = F_{\bar{\nu}_X}$.
- Neutrinos emerge from a neutrino sphere located at tens of kilometers from the center of the progenitor star. This is the region when neutrinos decouple from the gas. The average energies respect $E_{\nu_e} < E_{\bar{\nu}_e} < E_{\nu_X} = E_{\bar{\nu}_X}$.
- The neutrino fluxes are high enough that the neutrino-neutrino interaction must be taken into account, possibly allowing collective flavor conversion to take place.

CHAPTER 6

Collective oscillations in supernovae

So far we have established a number of phenomena that can occur in collective flavor oscillations: bipolar oscillations, synchronized oscillations, spectral splits. We now address an environment in which these effects might come into play, in the contemporary universe: the inner regions of a core-collapse SN. The importance of the neutrino-neutrino refraction can be appreciated in figure 6.1 where one sees that the strength of the collective refractive effect comes close to the strength of the matter refraction.

In this chapter we investigate – in an astrophysical context – the onset of anharmonic behavior, by studying the linear stability of propagation in the flavor state. The main difference between this system and the homogeneous ensemble is the geometry of the problem. In such a system, we track the evolution of flavor as a function of distance instead of time. In a SN, neutrinos are emitted from the neutrino sphere and stream out from a spherically shaped object causing their flux to decrease with $1/r^2$. The angular distribution also varies with the distance travelled, narrowing the span of velocities and effectively decreasing the interaction between neutrinos as one moves away from the core. We will show that despite these peculiarities the instabilities described so far are recovered. We also discuss features unique to the SN case, such as the appearance of unphysical spurious modes which are absent in the isotropic uniform case.

6.1 Equations of motion for the flux of neutrinos

6.1.1 Stationarity

We study the stationary evolution of the neutrino radiation of a SN as it emitted from the neutrino sphere described in the previous chapter. Despite the fact that the emission, as we discussed before, is non-stationary, the variation of the fluxes are slow compared to the time it takes for the neutrinos to escape. When neutrinos are emitted from a spherical object of radius R , an instantaneous flash from the sphere will develop with distance into a shell of thickness R . Therefore, at a distance r from the neutrino sphere, the local interactions involve rays which were emitted in a window of

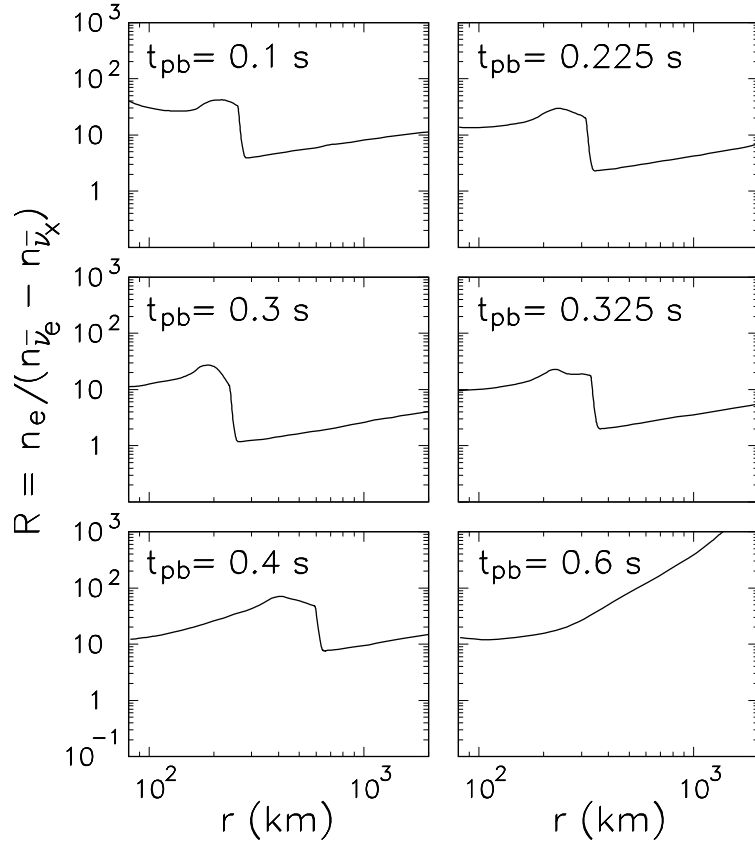


Figure 6.1: Plots of the ratio of the matter density to the anti-neutrino flavor difference flux for a 10.8 solar mass progenitor star, as a function of r , as produced from simulations of the Basel group, for various post-bounce time snaps [53]. The high plateau at low r corresponds to the homologous collapse. The sudden drop in the figure corresponds to the position of the shock front, the edge between the sub-sonic and super-sonic in-falls. The strength of the self-consistent refraction is maximal in the region just after the shock front, where the curve drops to its minimum. This is generally where the MAA instability occurs.

time of $2R/c$. When this length of time is much smaller than the time scale at which the initial conditions vary at the neutrino sphere, then it is a fair assumption that the emission is stationary, i.e., that all neutrinos interacting at a distance r and at time t were emitted in the same conditions and experienced the same histories. Since $R \sim 30$ km, meaning $2R/c \sim 100 \mu\text{s}$, this approximation is a safe assumption when compared with the typical time-scale of the emission ~ 100 ms. Even if there were a sudden change followed by a more stable phase, stationarity would be restored in a matter of microseconds. This means we can drop the explicit dependency of the density matrices on time, analysing each time snapshot as a case of its own:

$$\rho(\vec{r}, t, \vec{p}) = \rho(\vec{r}, \vec{p}). \quad (6.1)$$

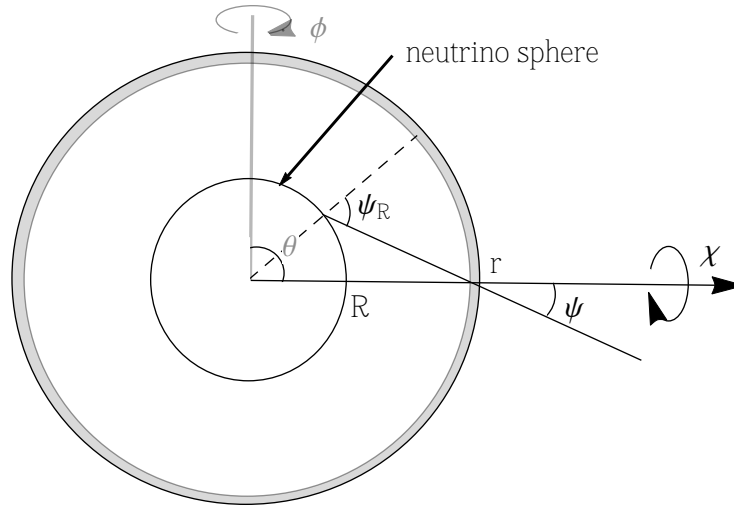


Figure 6.2: Schematic description of the geometry of the problem with definitions of the angles as described in the text.

Realistic analyses are done by obtaining a profile of matter and the flux of neutrinos at the neutrino sphere. These are taken to be static for as long as it takes for neutrinos to propagate out of the SN.

We also assume that all neutrinos stream away from the SN. This means that the radial velocity $v_r = \vec{v} \cdot \hat{r}$ is always positive. If ψ is the angle the velocity makes with the radial direction, then $0 < \psi < \pi/2$. This assumption is important to safeguard stationarity. If the back-scattered flux becomes too important then information may be carried downstream, meaning that one can no longer treat the dynamics as a function of r alone. This point will be further elaborated in the summary.

6.1.2 Isotropies

The continuity equations

$$\frac{\partial n_\nu(\vec{r}, \vec{p})}{\partial t} + \vec{v} \cdot \nabla n_\nu(\vec{r}, \vec{p}) = 0 \quad (6.2)$$

and

$$\frac{\partial f(\vec{r}, \vec{p})}{\partial t} + \vec{v} \cdot \nabla f(\vec{r}, \vec{p}) = 0 \quad (6.3)$$

for the density matrices

$$\rho(\vec{r}, \vec{p}) = \frac{1}{2} n_\nu(\vec{r}, \vec{p}) + \frac{1}{2} f(\vec{r}, \vec{p}) \mathbf{P}(\vec{r}, \vec{p}) \cdot \boldsymbol{\sigma} \quad (6.4)$$

as deduced in section 1.5 only apply in cases where $d\vec{p}/dt = 0$. This, as we stated, is a consequence of the assumption that refractive effects are the dominant effect. This condition is violated when one considers the early universe, for example, where collisional terms are significant. But in the case

of a SN, outside the neutrino sphere, the conservation of momentum is often a good approximation. However, a poor choice of coordinates can also violate this condition, if the coordinate system of the momentum depends on the position \vec{r} . Such is the case when one wants to analyse the density matrix of an ensemble of neutrinos at point \vec{r} and time t with momentum \vec{p} , as depicted in figure 6.2. The fact is that momentum is not conserved in this coordinate system because the number of neutrinos with velocity \vec{v} varies with the distance r to the center of the proto-neutron-star. This means the three equations for the total neutrino density $n_\nu(\vec{r}, \vec{p})$, the length of the polarization vector $f(\vec{r}, \vec{p})$ and the polarization vector $\mathbf{P}(\vec{r}, \vec{p})$ must be generalized to

$$\begin{aligned}\frac{dn_\nu}{dt}(\vec{r}, \vec{p}) &= \vec{v} \cdot \nabla n_\nu(\vec{r}, \vec{p}) + \frac{d\vec{p}}{dt} \cdot \frac{\partial n_\nu}{\partial \vec{p}}(\vec{r}, \vec{p}) = 0, \\ \frac{df}{dt}(\vec{r}, \vec{p}) &= \vec{v} \cdot \nabla f(\vec{r}, \vec{p}) + \frac{d\vec{p}}{dt} \cdot \frac{\partial f}{\partial \vec{p}}(\vec{r}, \vec{p}) = 0, \\ \frac{d\mathbf{P}}{dt}(\vec{r}, \vec{p}) &= \vec{v} \cdot \nabla \mathbf{P}(\vec{r}, \vec{p}) + \frac{d\vec{p}}{dt} \cdot \frac{\partial \mathbf{P}}{\partial \vec{p}}(\vec{r}, \vec{p}) = \mathbf{H}(\vec{r}, \vec{p}) \times \mathbf{P}(\vec{r}, \vec{p}),\end{aligned}\tag{6.5}$$

with

$$\frac{d\vec{p}}{dt} = \vec{v} \cdot \nabla \vec{p} = v_r \frac{\partial}{\partial r} + \frac{v_\theta}{r} \frac{\partial}{\partial \theta} + \frac{v_\phi}{p \sin \theta} \frac{\partial}{\partial \phi} = v_r \frac{\partial}{\partial r}.\tag{6.6}$$

Where θ and ϕ are the spherical coordinates that determine \vec{r} . In this last step we imposed isotropy of the SN. Throughout the rest of this section and in all studies performed so far, the SN and its neutrino radiation are always assumed to be spherically symmetric. Moreover, according to the local angular variables ψ and χ defined in figure 6.2, this variation of momentum is

$$\frac{d\vec{p}}{dt} \cdot \frac{\partial}{\partial \vec{p}} = \dot{p} \frac{\partial}{\partial p} + \frac{1}{p} \dot{\psi} \frac{\partial}{\partial \psi} + \frac{1}{p \sin \psi} \dot{\chi} \frac{\partial}{\partial \chi} = \frac{1}{p} \frac{\partial \psi}{\partial r} \frac{\partial}{\partial \psi}.\tag{6.7}$$

The momentum of each neutrino does not change in magnitude as the neutrino propagates. This comes from the assumption of collisionless propagation. Thus $\dot{p} = 0$. As for χ , this variable is defined by setting a local direction on the sphere of radius r that determines $\chi = 0$. This means one has the freedom to choose the vector field of $\chi = 0$ in such a way that in a given direction $\dot{\chi} = 0$. This limits the validity of our equations to this specific direction. However, as long as the isotropy of the SN is verified, i.e. the dynamics are identical for any distant observer, the results should apply in every direction.

6.1.3 Angular variables and spectra

Duan, Fuller and colleagues [54, 55] pointed out that, though the number of neutrinos with local velocity \vec{v} isn't conserved, the number of neutrinos that *were* emitted at a given angle ψ_R is. Therefore by studying the equations in terms of ψ_R instead of ψ one can simplify the continuity equations. The radial velocity at distance r can be determined unequivocally by r , R and ψ_R by

noting that

$$R \sin \psi_R = r \sin \psi \Rightarrow v_r = \cos \psi = \sqrt{1 - \frac{R^2}{r^2} u} \quad (6.8)$$

where we have introduced the new variable $u = \sin^2 \psi$. Since $0 < \psi < \pi/2$, at distance r , u is a one-to-one function of ψ . Hence,

$$\frac{d\vec{p}}{dt} \cdot \frac{\partial}{\partial \vec{p}} = \frac{1}{p} \frac{\partial \psi}{\partial r} \frac{\partial}{\partial \psi} = \frac{1}{p} \frac{\partial u}{\partial r} \frac{\partial}{\partial u} = 0. \quad (6.9)$$

because $\dot{u} = 0$. Going back to equations (6.5), we see that by defining the quantities in terms of u that

$$\begin{aligned} \frac{dn_\nu}{dt}(r, p, u, \chi) &= v_r \partial_r n_\nu(r, p, u, \chi) = 0 \Rightarrow n_\nu(r, p, u, \chi) = \text{constant}, \\ \frac{df}{dt}(r, p, u, \chi) &= v_r \partial_r f(r, p, u, \chi) = 0 \Rightarrow f(r, p, u, \chi) = \text{constant}. \end{aligned} \quad (6.10)$$

Both density and length with this set of variables are conserved along r . Indeed, one can verify that

$$\int_{-\infty}^{+\infty} p^2 dp \int_0^1 du \int_0^{2\pi} d\chi \rho(r, p, u, \chi) = 2 \frac{r^2}{R^2} \int v_r \rho(r, \vec{p}) d\vec{p} = \frac{2(2\pi)^3}{4\pi R^2} (\vec{J}_\nu \cdot \hat{r}) = \text{constant} \quad (6.11)$$

because the total flux escaping a sphere of radius r around the SN is conserved. Thanks to these conservation laws one can define the spectra according to the fluxes of neutrinos at the neutrino sphere, where the density matrices are diagonal. Since we assume the emission is spherically symmetric, we choose to write them in terms of the fluxes of neutrinos at the neutrino sphere $\Phi = 4\pi R^2 \rho$

$$n_\nu(p, u, \chi) = \frac{\Phi_{\nu_e}(R, p, u, \chi) + \Phi_{\nu_x}(R, p, u, \chi)}{4\pi R^2} \quad (6.12)$$

and

$$f(p, u, \chi) = \frac{\Phi_{\nu_e}(R, \vec{p}, u, \chi) - \Phi_{\nu_x}(R, \vec{p}, u, \chi)}{4\pi R^2}. \quad (6.13)$$

6.1.4 Equation of motion

In this section we deduce the EoMs in terms of the variables r , ω , u and χ . The third equation of (6.5) gives

$$\partial_r \mathbf{P}(r, \vec{p}, u, \chi) = \frac{1}{v_r} \mathbf{H}(\vec{r}, \vec{p}) \times \mathbf{P}(r, \vec{p}, u, \chi), \quad (6.14)$$

with

$$\mathbf{H}(\vec{r}, \vec{p}) = \omega \mathbf{B} + \sqrt{2} G_F n_e \mathbf{L} + \sqrt{2} G_F (\mathbf{N} - \vec{v} \cdot \vec{\mathbf{J}}). \quad (6.15)$$

The scalar coupling of the self-consistent refraction is

$$\begin{aligned}
\frac{1}{v_r} \mathbf{N} &= \frac{\sqrt{2} G_F}{v_r} \int \frac{d\vec{p}'}{(2\pi)^3} f(\vec{p}') \mathbf{P}(\vec{p}') \\
&= \frac{\sqrt{2} G_F}{v_r} \int_{-\infty}^{+\infty} p'^2 dp' \int_0^{\pi/2} d\psi' \int_0^{2\pi} d\chi' \frac{1}{(2\pi)^3} f(p', \psi', \chi') \mathbf{P}(p', \psi', \chi') \\
&= \frac{\sqrt{2} G_F}{v_r} \int_{-\infty}^{+\infty} d\omega' \int_0^1 du' \left| \frac{d \cos \psi'}{du'} \right| \int_0^{2\pi} d\chi' \left| \frac{\Delta m^2}{4\pi} \right|^3 \frac{1}{\omega'^4} f(\omega', u', \chi') \mathbf{P}(\omega', u', \chi') \\
&= \sqrt{2} G_F \int_{-\infty}^{+\infty} d\omega' \int_0^1 du' \int_0^{2\pi} d\chi' \left| \frac{\Delta m^2}{4\pi} \right|^3 \frac{1}{\omega'^4} \frac{R^2}{2r^2} \frac{1}{\sqrt{1 - \frac{R^2}{r^2} u}} \frac{f(\omega', u', \chi')}{\sqrt{1 - \frac{R^2}{r^2} u'}} \mathbf{P}(\omega', u', \chi') \\
&\approx \sqrt{2} G_F \int_{-\infty}^{+\infty} d\omega' \int_0^1 du' \int_0^{2\pi} d\chi' \left| \frac{\Delta m^2}{4\pi} \right|^3 \frac{1}{\omega'^4} \left(\frac{R^2}{2r^2} + \frac{u + u'}{2} \frac{R^4}{2r^4} \right) \times \\
&\quad \times f(\omega', u', \chi') \mathbf{P}(\omega', u', \chi')
\end{aligned} \tag{6.16}$$

where we used the large distance ($r \gg R$) approximation

$$\frac{1}{v_r} \left| \frac{d \cos \psi'}{du'} \right| = \frac{R^2}{2r^2} \frac{1}{\sqrt{1 - \frac{R^2}{r^2} u}} \frac{1}{\sqrt{1 - \frac{R^2}{r^2} u'}} \approx \frac{R^2}{2r^2} + \frac{u + u'}{2} \frac{R^4}{2r^4} + \mathcal{O}\left(\frac{R^6}{r^6}\right). \tag{6.17}$$

The vector coupling self-consistent refraction is

$$\begin{aligned}
\frac{1}{v_r} \vec{v} \cdot \vec{\mathbf{J}} &= \frac{\sqrt{2} G_F}{v_r} \int \frac{d\vec{p}'}{(2\pi)^3} \frac{\vec{v} \cdot \vec{p}'}{p'} f(\vec{p}') \mathbf{P}(\vec{p}') \\
&= \frac{\sqrt{2} G_F}{v_r} \int_{-\infty}^{+\infty} p'^2 dp' \int \frac{d\vec{v}'}{(2\pi)^3} (\vec{v} \cdot \vec{v}') f(p', \vec{v}') \mathbf{P}(p', \vec{v}') \\
&= \frac{\sqrt{2} G_F}{v_r} \int_{-\infty}^{+\infty} d\omega' \int_0^1 du' \left| \frac{d \cos \psi'}{du'} \right| \int_0^{2\pi} d\chi' \left| \frac{\Delta m^2}{4\pi} \right|^3 \frac{1}{\omega'^4} (\vec{v} \cdot \vec{v}') f(\omega', u', \chi') \mathbf{P}(\omega', u', \chi') \\
&\approx \sqrt{2} G_F \int_{-\infty}^{+\infty} d\omega' \int_0^1 du' \int_0^{2\pi} d\chi' \left| \frac{\Delta m^2}{4\pi} \right|^3 \frac{1}{\omega'^4} \left[\frac{R^4}{2r^4} + \cos(\chi - \chi') \sqrt{uu'} \frac{R^6}{2r^6} \right] \times \\
&\quad \times f(\omega', u', \chi') \mathbf{P}(\omega', u', \chi')
\end{aligned} \tag{6.18}$$

where we approximate

$$\begin{aligned}
\frac{1}{v_r} \left| \frac{d \cos \psi'}{du'} \right| (\vec{v} \cdot \vec{v}') &= \frac{1}{v_r} \left| \frac{d \cos \psi'}{du'} \right| \left(\frac{R^2}{r^2} \sqrt{uu'} \cos(\chi - \chi') + \sqrt{1 - \frac{R^2}{r^2} u} \sqrt{1 - \frac{R^2}{r^2} u'} \right) \\
&\approx \frac{R^2}{2r^2} + \cos(\chi - \chi') \sqrt{uu'} \frac{R^4}{2r^4} + \mathcal{O}\left(\frac{R^6}{r^6}\right).
\end{aligned} \tag{6.19}$$

When adding these two parts of the neutrino-neutrino refraction, the lower order terms cancel leaving us with an r^{-4} dependence

$$\frac{1}{v_r} \sqrt{2} G_F (\mathbf{N} - \vec{v} \cdot \vec{\mathbf{J}}) = \mu(r) \int_{-\infty}^{+\infty} d\omega' \int_0^1 du' \int_0^{2\pi} d\chi' \left[u + u' + 2 \cos(\chi - \chi') \sqrt{uu'} \right] \times \quad (6.20)$$

$$\times g(\omega', u', \chi') \mathbf{P}(\omega', u', \chi')$$

with the effective self-interaction strength defined as

$$\mu(r) \equiv \sqrt{2} G_F \frac{R^4}{r^4} \frac{\Phi_{\bar{\nu}_e}(R) - \Phi_{\nu_X}(R)}{4\pi R^2} \equiv \mu_R \frac{R^4}{r^4} \quad (6.21)$$

and the spectrum is given by

$$g(\omega, u, \chi) = \frac{1}{\Phi_{\bar{\nu}_e}(R) - \Phi_{\nu_X}(R)} \left| \frac{\Delta m^2}{4\pi} \right|^3 \frac{1}{\omega^4}. \quad (6.22)$$

The order parameters are defined as

$$\mathbf{D} = \int_{-\infty}^{+\infty} d\omega \int_0^1 du \int_0^{2\pi} d\chi g(\omega, u, \chi) \mathbf{P}(\omega, u, \chi), \quad (6.23)$$

$$\vec{\mathbf{A}} = \int_{-\infty}^{+\infty} d\omega \int_0^1 du \int_0^{2\pi} d\chi g(\omega, u, \chi) \vec{v} \mathbf{P}(\omega, u, \chi),$$

and with $g(\omega, u, \chi)$, the normalized spectrum, as defined before. At the neutrino sphere the order parameters are equal to

$$\mathbf{D}(R) = \epsilon \mathbf{L}, \quad (6.24)$$

$$\vec{\mathbf{A}}(R) = \vec{j} \mathbf{L}.$$

The two quantities ϵ and \vec{j} are now defined in terms of the total integrated fluxes

$$\epsilon = \frac{\Phi_{\nu_e}(R) - \Phi_{\bar{\nu}_e}(R)}{\Phi_{\bar{\nu}_e}(R) - \Phi_{\nu_X}(R)}, \quad (6.25)$$

$$\vec{j} = \int_{-\infty}^{+\infty} d\omega \int_0^1 du \int_0^{2\pi} d\chi g(\omega, u, \chi) \vec{v}.$$

In order to make an expansion in orders of R/r , we must first collect the complete r -dependent coefficients of each term in the EoMs. Reading from eq. (6.14), the linear terms of the Hamiltonian come multiplied by

$$\frac{1}{v_r} = \frac{1}{\sqrt{1 - \frac{R^2}{r^2} u}} \approx 1 + u \frac{R^2}{2r^2} + \mathcal{O}\left(\frac{R^4}{r^4}\right). \quad (6.26)$$

Note that we kept the first and second higher order terms for each part. Though keeping the higher

order term in R/r for each physical quantity is what matters, it may well happen that the higher order term does not play any role in the non-linear dynamics of the system, if it affects every mode in the same way, that is, if it doesn't explicitly depend on ω , u or χ . It will simply contribute to the precession of the co-rotating frame which we discussed before. Bearing that in mind, the vacuum term for large r/R is to higher order

$$\frac{1}{v_r} \omega \mathbf{B} \times \mathbf{P} \approx \omega \mathbf{B} \times \mathbf{P}. \quad (6.27)$$

The matter term becomes

$$\frac{1}{v_r} \sqrt{2} G_F n_e \mathbf{L} \times \mathbf{P} \approx \left(1 + u \frac{R^2}{2r^2}\right) \lambda \mathbf{L} \times \mathbf{P}. \quad (6.28)$$

We keep both orders of R/r because the first term $\sqrt{2} G_F n_e \mathbf{L} \times \mathbf{P}$ contributes in no way to the non-linear dynamics of the system. It simply adds to the common precession rate of all modes. Hence, the complete EoMs, for $r \gg R$, are

$$\partial_r \mathbf{P} = \left\{ \omega \mathbf{B} + \left[\sqrt{2} G_F n_e + u \lambda(r) \right] \mathbf{L} + \mu(r) \int \left[u + u' + 2\sqrt{uu'} \cos(\chi - \chi') \right] \mathbf{P}' d\Gamma' \right\} \times \mathbf{P}, \quad (6.29)$$

where

$$\begin{aligned} \lambda(r) &\equiv \sqrt{2} G_F n_e(r) \frac{R^2}{2r^2}, \\ \mu(r) &\equiv \mu_R \frac{R^4}{2r^4}, \\ d\Gamma &\equiv g(\omega, u, \chi) d\omega du d\chi. \end{aligned} \quad (6.30)$$

We recover the r^{-2} and r^{-4} mentioned before for the variation of the strength of the matter effects and of the neutrino effects respectively. The results with the Taylor expansion in terms of R/r were compared numerically with the results of the unexpanded equations. The unexpanded version has proven to not present any advantage in accuracy, as collective behavior tends to be suppressed near the neutrino sphere by the high electronic density.

6.2 General conditions for the stability of the flavor state

6.2.1 Eigenvalue equation

In the initial state, all polarization are at the zenith of the Bloch sphere. Like before, we want to study the stability of this configuration under small off-diagonal perturbations $p(\omega, u, \chi)$. Following

the same deduction done in the last chapter, we come to the linearized EoMs:

$$\begin{aligned}
\partial_r p &= i \left[\omega \cos 2\theta_0 + \sqrt{2} G_F n_e + u \lambda(r) \right] p + \omega \sin 2\theta_0 \\
&\quad + i \mu(r) \int \left[u + u' + 2\sqrt{uu'} \cos(\chi - \chi') \right] (p - p') d\Gamma' \\
&= i \left[\omega \cos 2\theta_0 + \sqrt{2} G_F n_e + u \bar{\lambda}(r) + w + 2\sqrt{u} (X \cos \chi - Y \sin \chi) \right] p + \omega \sin 2\theta_0 \\
&\quad - i \mu(r) \int \left[u + u' + 2\sqrt{uu'} \cos(\chi - \chi') \right] p' d\Gamma'
\end{aligned} \tag{6.31}$$

where

$$\begin{aligned}
\bar{\lambda}(r) &= \lambda(r) + \epsilon \mu(r), \\
w &= \int u d\Gamma, \\
X &= \int \sqrt{u} \cos \chi d\Gamma, \\
Y &= \int \sqrt{u} \sin \chi d\Gamma.
\end{aligned} \tag{6.32}$$

The terms $i \sqrt{2} G_F n_e p + i w p$ are common to all modes. We can move to the co-rotating frame by using the vectors $q(\omega, u, \psi) = p(\omega, u, \psi) e^{i(\sqrt{2} G_F n_e + w)r}$. In this frame the off-diagonal component of \mathbf{B} averages quickly out to zero:

$$\partial_r q = i \left[\omega + u \bar{\lambda} + 2\sqrt{u} (X \cos \chi - Y \sin \chi) \right] q - i \mu \int \left[u + u' + 2\sqrt{uu'} \cos(\chi - \chi') \right] q' d\Gamma'. \tag{6.33}$$

To prevent confusions arising from the many redefinitions, let us summarize:

$$\begin{aligned}
\omega &= \frac{\Delta m^2}{2E} \cos 2\theta_0, \\
\bar{\lambda}(r) &= \lambda(r) \frac{R^2}{2r^2} + \epsilon \mu(r) = \sqrt{2} G_F \frac{R^2}{2r^2} n_e(r) + \epsilon \mu(r), \\
\mu(r) &= \mu_R \frac{R^4}{2r^4} = \sqrt{2} G_F \frac{R^4}{2r^4} \frac{\Phi_{\bar{\nu}_e}(R) - \Phi_{\nu_X}(R)}{4\pi R^2}, \\
\epsilon &= \frac{\Phi_{\nu_e}(R) - \Phi_{\bar{\nu}_e}(R)}{\Phi_{\bar{\nu}_e}(R) - \Phi_{\nu_X}(R)}.
\end{aligned} \tag{6.34}$$

Assuming that the variation $\bar{\lambda}(r)$ and $\mu(r)$ vary over a distance much larger than the typical growth or precession rate of the system, these values can be taken as constant and the solutions in the linear regime are given by

$$q(\omega, u, \chi) = Q(\omega, u, \chi) e^{i\Omega r} \tag{6.35}$$

with the eigenvector equation

$$[\omega - \Omega + u\bar{\lambda} + 2\sqrt{u}(X \cos \chi - Y \sin \chi)] Q - \mu \int [u + u' + 2\sqrt{uu'} \cos(\chi - \chi')] Q' d\Gamma' = 0 \quad (6.36)$$

From which we deduce that Q is of the form

$$\begin{aligned} Q(\omega, u, \chi) &= \frac{\mu}{\omega - \Omega + u\bar{\lambda} + 2\sqrt{u}(X \cos \chi - Y \sin \chi)} \int [u + u' + 2\sqrt{uu'} \cos(\chi - \chi')] Q' d\Gamma' \\ &\equiv \frac{A + Bu + C\sqrt{u} \cos \chi + D\sqrt{u} \sin \chi}{\omega - \Omega + u\bar{\lambda} + 2\sqrt{u}(X \cos \chi - Y \sin \chi)} \end{aligned} \quad (6.37)$$

Following the same procedure as before we reinsert this form into the original equation (6.36) and find

$$\begin{aligned} &A + Bu + C\sqrt{u} \cos \chi + D\sqrt{u} \sin \chi \\ &- \mu \int [u + u' + 2\sqrt{uu'} \cos(\chi - \chi')] \frac{A + Bu' + C\sqrt{u'} \cos \chi' + D\sqrt{u'} \sin \chi'}{\omega' - \Omega + u'\bar{\lambda} + 2\sqrt{u'}(X \cos \chi' - Y \sin \chi')} d\Gamma', \end{aligned} \quad (6.38)$$

or in matrix form

$$\begin{pmatrix} I_1 - 1 & I_2 & I_{3/2}^c & I_{3/2}^s \\ I_0 & I_1 - 1 & I_{1/2}^c & I_{1/2}^s \\ -2I_{1/2}^c & -2I_{3/2}^c & -2I_1^{cc} - 1 & -2I_1^{sc} \\ -2I_{1/2}^s & -2I_{3/2}^s & -2I_1^{sc} & -2I_1^{ss} - 1 \end{pmatrix} \begin{pmatrix} A \\ B \\ C \\ D \end{pmatrix} = 0, \quad (6.39)$$

where

$$I_n^{c(s)} = \mu \int_{-\infty}^{+\infty} d\omega \int_0^1 du \int_0^{2\pi} d\chi \frac{u^n g(\omega, u, \chi)}{\omega + u\bar{\lambda} - \Omega} \cos \chi (\sin \chi). \quad (6.40)$$

Nontrivial solutions exist if the determinant of the matrix vanishes.

The uniform distribution

As a next step, we would like to study the stability of the system for a simple case. We simplify to $g(\omega, u, \varphi) \rightarrow g(\omega, u)/2\pi$ by assuming that the emission is isotropic around the radial direction. We maintain, for now, the possibility of an anisotropic spectrum on ψ_R . For such a distribution, $X = Y = 0$ and only the χ integrals with $\sin^2 \chi$ and $\cos^2 \chi$ in the matrix equation survive and yield $I_1^{cc} = I_1^{ss} = \frac{1}{2}I_1$ respectively, leaving us with

$$\begin{pmatrix} I_1 - 1 & I_2 & 0 & 0 \\ I_0 & I_1 - 1 & 0 & 0 \\ 0 & 0 & -(I_1 + 1) & 0 \\ 0 & 0 & 0 & -(I_1 + 1) \end{pmatrix} \begin{pmatrix} A \\ B \\ C \\ D \end{pmatrix} = 0. \quad (6.41)$$

This system has nontrivial solutions if

$$(I_1 - 1)^2 = I_0 I_2 \quad \text{or} \quad I_1 = -1, \quad (6.42)$$

where

$$I_n = \mu \int du d\omega \frac{u^n g(\omega, u)}{\omega + u\bar{\lambda} - \Omega}. \quad (6.43)$$

The previous system may be divided into two distinct solutions whose regions of instability are shown in figure 6.3 for the uniform distribution. The first of them is the solution of

$$\begin{pmatrix} I_1 - 1 & I_2 \\ I_0 & I_1 - 1 \end{pmatrix} \begin{pmatrix} A \\ B \end{pmatrix} = 0. \quad (6.44)$$

These equations determine how the system reacts to distributions of the type

$$Q = \frac{A + Bu}{\omega + u\bar{\lambda} - \Omega}. \quad (6.45)$$

These distributions are entirely independent of the peculiarities of the spectrum in χ . This means that all flavor vectors, no matter at what angle χ their respective beam comes in at, will evolve in the same way. So their distribution in χ is conserved, or more specifically, if the system is more or less symmetric in χ it will remain so under the influence of the dynamics induced by these equations. The instabilities arising from this term are all called multi-zenith angle (MZA) instabilities. When a single u -mode is used, the system behaves like the flavor pendulum introduced earlier and it is referred to in the literature as the bimodal instability.

The second equation allows for nonzero C and D , providing solutions with nontrivial χ dependence, unstable only in normal hierarchy, of the type:

$$Q = \frac{\sqrt{u}(C \cos \chi + D \sin \chi)}{\omega + u\bar{\lambda} - \Omega}. \quad (6.46)$$

A linear combination of $\cos \chi$ and $\sin \chi$ can always be recast into the form $\cos \chi$ by a proper shifting of χ , which means that these equations dictate the behavior of the dipolar moment of the flavor content in the velocity spectrum on the plane transversal to the radial direction. The instabilities that come from this equation are referred to as multi-azimuthal angle (MAA) instabilities. They always require several angular modes, as they induce spontaneous symmetry breaking of azimuthal isotropy.

To bring out the differences between the two instabilities (MZA and MAA), one may consider the unlikely case of $\lambda + \epsilon\mu = 0$ and assume the spectrum to factorize as $g(\omega, u) \rightarrow g(\omega)h(u)$. This relation between the matter density and the neutrino density is unphysical in SNe. In other words, it requires the neutrino fluid and the electron gas to have opposite lepton numbers. The point of

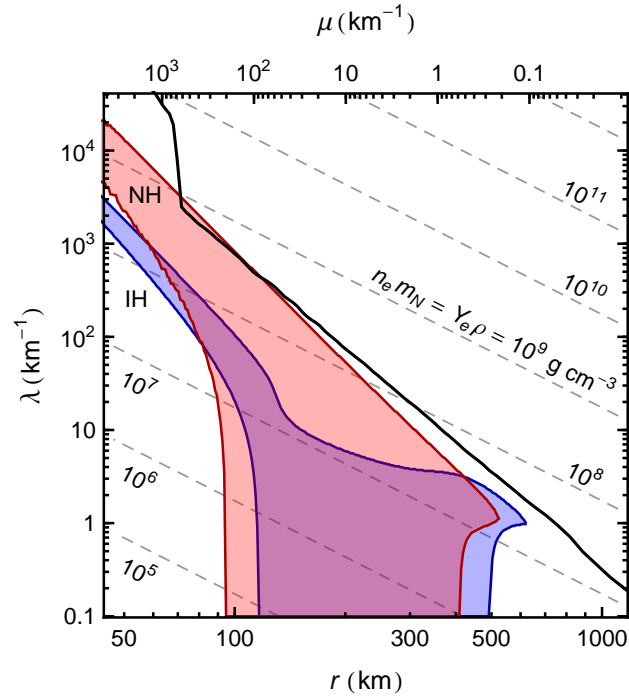


Figure 6.3: Region where $\kappa r > 1$ for IH (blue) and NH (red), depending on radius r and multi-angle matter potential λ for a uniform distribution in u . *Thick black line:* SN density profile. *Thin dashed lines:* Contours of constant electron density, where Y_e is the electron abundance per baryon.

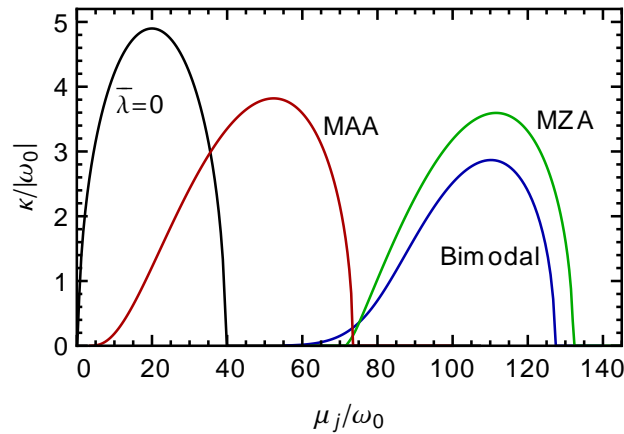


Figure 6.4: Growth rate κ for blackbody-like zenith distribution, single energy $\pm\omega_0$, and $\epsilon = 1/2$. *Black line:* All cases for $\bar{\lambda} = \lambda + \epsilon\mu = 0$ (no matter effect). *Other lines:* Indicated unstable cases for $\bar{\lambda} = 300|\omega_0|$.

this calculations is merely to perceive the difference between the various instabilities in a case where an analytical formula is available. If $\bar{\lambda} = 0$ then the denominator of (6.43) is independent of u :

$$I_n = \mu \int \frac{g(\omega)}{\omega - \Omega} d\omega \int u^n h(u) du = I \langle u^n \rangle \quad (6.47)$$

with $I = \mu \int d\omega g(\omega)/(\omega - \Omega)$, Eqs. (6.42) are

$$(\langle u \rangle I - 1)^2 = \langle u^2 \rangle I^2 \quad \text{or} \quad \langle u \rangle I = -1 \quad (6.48)$$

These equations can be solved for I . The second-order polynomial leads to

$$I = \frac{1}{\langle u \rangle \pm \langle u^2 \rangle^{1/2}} \quad (6.49)$$

Therefore, the three equations can be cast into the compact form

$$I^{-1} = h_i \equiv \begin{cases} \langle u \rangle + \langle u^2 \rangle^{1/2} > 0 & \text{(bimodal)}, \\ \langle u \rangle - \langle u^2 \rangle^{1/2} < 0 & \text{(MZA)}, \\ -\langle u \rangle < 0 & \text{(MAA)}, \end{cases} \quad (6.50)$$

The solutions of these equations are shown in figure 6.4. Note that, since $0 \leq u \leq 1$ is positive and $\langle u \rangle < \sqrt{\langle u^2 \rangle}$, I^{-1} is positive in the first case, and negative in the second and third. The hierarchy of masses plays an important role here. We illustrate its importance with a simple example and consider the usual single frequency spectrum $g(\omega) = -\delta(\omega + \omega_0) + (1 + \epsilon) \delta(\omega - \omega_0)$. The integral I becomes

$$\frac{I}{\mu} = \frac{1 + \epsilon}{\omega_0 - \Omega} - \frac{1}{-\omega_0 - \Omega} = \frac{(1 + \epsilon)\omega_0 + \epsilon\Omega}{\omega_0^2 - \Omega^2} \quad (6.51)$$

Equation (6.50) is now equivalent to the quadratic equation

$$I^{-1} = \frac{\omega_0^2 - \Omega^2}{2\omega_0 + \epsilon(\omega_0 + \Omega)} = \mu h_i \equiv \mu_i, \quad (6.52)$$

where $\mu_i = \mu(\langle u \rangle \pm \langle u^2 \rangle^{1/2})$ or $-\mu\langle u \rangle$. The solutions are

$$\Omega_i = \frac{1}{2} \left(-\epsilon \mu_i \sqrt{(2\omega_0 - \epsilon \mu_i)^2 - 8\omega_0 \mu_i} \right). \quad (6.53)$$

Exponentially growing solutions ($\kappa = \text{Im } \Omega > 0$) can only exist when $\omega_0 \mu_j > 0$. This condition is valid for

- IH: $\omega_0 > 0$ which requires $\mu_j > 0$ for there to be an instability; this happens exclusively for $j = \text{bimodal}$;

- NH: $\omega_0 < 0$ which requires $\mu_j < 0$ and thus $j = \text{MZA, MAA}$.

The system is unstable for μ_i between the limits $2\omega_0/(\sqrt{1+\epsilon}\pm 1)^2$. The maximum growth rate obtains for $\mu_i = 2\omega_0(2+\epsilon)/\epsilon^2$ and is $\kappa_{\text{max}} = 2|\omega_0|\sqrt{1+\epsilon}/\epsilon$. Therefore, a typical growth rate is a few times the vacuum oscillation frequency. For $\epsilon = 1/2$ we find $\kappa_{\text{max}} = 2\sqrt{6}|\omega_0| \approx 4.90|\omega_0|$.

6.2.2 Spontaneous symmetry breaking in numerical simulations

The phenomenon of azimuthal symmetry breaking as predicted from our linear stability analyses has been investigated in simulations [53,56]. Using a 10.8 solar mass iron-core progenitor, the symmetry breaking instability was observed for certain time shots during the accretion phase. In general, the much higher electronic density before the shock front suppresses MAA flavor conversion. In the time shots for which non-linear behavior was observed, the $\lambda \sim \mu$ after the abrupt drop in matter density at the shock does allow for the excitation of the MAA mode.

For $\lambda = 0$, a comparison between figures 6.5 shows the onset of flavor conversion happens at the peak of the instability for all cases. This simple connection becomes somewhat blurred when one introduces the matter effect because the value of the growth rate shrinks to much smaller values and is confined to the region visible in figure 6.1 where the ratio λ/μ is minimal. The growth factor being so small, flavor conversion tends to be entirely prevented or at least delayed by about ~ 100 km. This is because the number of e-foldings required to grow the minute off-diagonal terms to a point where non-linear dynamics set in is too large for the short window where the growth factor is non-zero. The situation becomes entirely hopeless when a realistic angular distribution – forward-peaked – is introduced. In this case, the instability is so highly suppressed that no non-trivial dynamics were observed in any of the cases.

Still, the simulations do confirm that symmetry breaking can happen and that one must be careful not to do away negligently with the azimuthal angular dependence. However, once one introduces more detailed spectra and matter effects, the growth of the symmetric vector order parameter seems to be highly susceptible to suppression, much more than the MZA instability [53].

6.3 Spurious instabilities

In the last chapter we saw that instabilities of a continuous uniform distribution were accurately predicted by a system with a relatively small number of discrete angular modes. It turns out that the peculiar mixings between the scalar and vector part of the non-linear refraction and the angular dependence of the matter effects induced by the non-trivial geometry of the SN, result in very distressing failures when simulating multi-angle effects numerically with a handful of modes. Actually, all the way back to the earliest simulations [55], a peculiar phenomenon haunted the results: single u-angle simulations and high- N_u simulations in the IH and at low electronic densities yielded similar results, but few mode simulations were entirely inaccurate. The case gets even worse

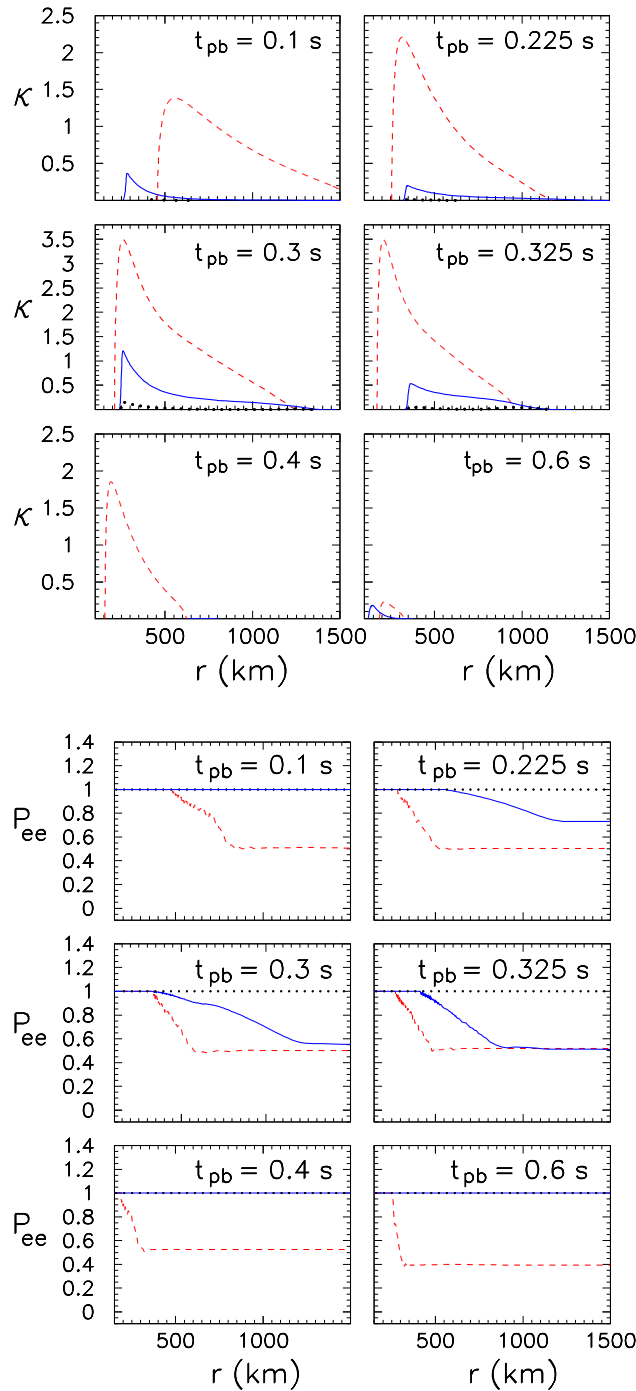


Figure 6.5: Multiangle, single frequency simulations in the NH during the accretion phase of a type II SN of a 10.8 solar mass iron-core progenitor star for various post-bounce time snaps. The left panel shows the strength of $\kappa = \text{Im}\Omega$ as a function of r [53]. The sharp increase of the instability at low r is related to the sudden drop in the matter density as witnessed in figure 6.1. The right panel shows the results of the simulation for $P_z =$ survival probability for $e \rightarrow e$ as a function of r . In both plots, the red dashed line shows the results for a uniform u spectrum at $\lambda = 0$; the blue solid line shows the case of a uniform u distribution with $\lambda = \lambda(r)$ and finally the black dotted curve corresponds to a realistic u spectrum with $\lambda = \lambda(r)$. We see that whenever κ is too small and short lived, non-linear behavior fails to start.

for high density media, where thousands of modes might be needed to get reasonable predictions. In this section we will explain this peculiar phenomenon for the MZA instability from the point of view of the dynamics in the linear regime, following the results of [57].

6.3.1 Single-angle vs. uniform distribution

We proceed with the analysis of a single frequency system, as it was already argued that it captures the qualitative features of a more general system. Moreover, if the neutrino sphere emits as a black body, then the emission is uniform in u that is,

$$g(\omega, u) = [(1 + \epsilon)\delta(\omega - \omega_0) - \delta(\omega - \omega_0)]. \quad (6.54)$$

The instability for this spectrum must be computed numerically as there is no formula for it in terms of common analytical functions. The eigenconfigurations of this system are of the form

$$Q(\pm\omega_0, u) = \frac{A + B u}{\pm\omega_0 - \Omega + u \bar{\lambda}} \quad (6.55)$$

These eigenconfigurations correspond to arcs of circles on the complex plane whenever Ω is complex. We can compare it to the instability as computed with the single-angle spectrum taken at the mid-value of the u -scale

$$g(\omega, u) = [(1 + \epsilon)\delta(\omega - \omega_0) - \delta(\omega - \omega_0)] \delta(u - 0.5). \quad (6.56)$$

In this case there is an available analytic formula for the eigenvalue:

$$\Omega = -\frac{\epsilon\mu}{2} \pm \sqrt{1 - (2 + \epsilon)\mu + \left(\frac{\epsilon\mu}{2}\right)^2} \quad (6.57)$$

Figure 6.6 shows these two instabilities. We see that, though the single-angle fails to predict exactly the range of μ -values for which the system becomes unstable, the general picture seems to be maintained. It however misses altogether the small MZA instability found in the NH for the uniform spectrum which is a suppressed version of the instability found in chapter 3.

6.3.2 Discrete approximation of the uniform spectrum

We study the spectrum

$$g(\pm\omega_0, u) = [(1 + \epsilon)\delta(\omega - \omega_0) - \delta(\omega - \omega_0)] \sum_{i=1}^{N_u} \delta(u - u_i) \quad (6.58)$$

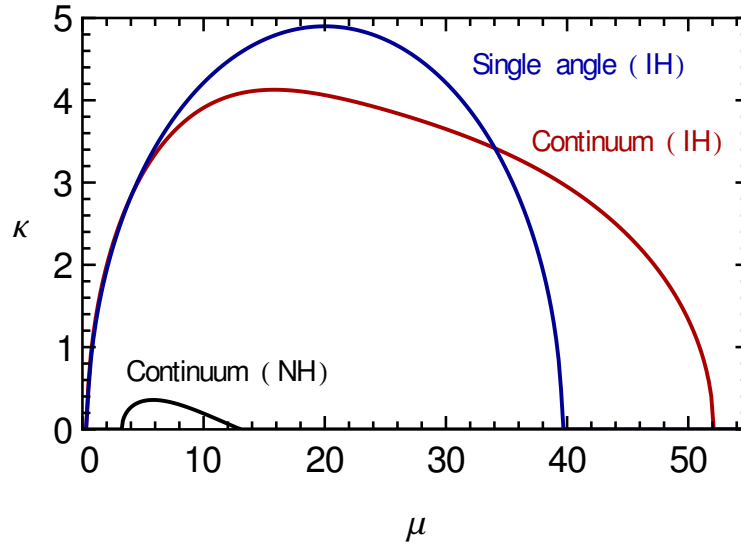


Figure 6.6: The bimodal, MZA (in IH and NH) and MAA instabilities as a function of μ for a single frequency, shown as a plot of the growth rate κ vs. μ for $\lambda = 0$ and $\epsilon = 0.5$.

with the u_i spaced evenly on from 0 to 1. The integral eigenvalue equation becomes a matrix equation

$$\begin{pmatrix} (\omega_0 - \Omega + \bar{\lambda} u_j) \delta_{ij} - \mu(1 + \epsilon)(u_i + u_j) g_j & -\mu(u_i + u_j) g_j \\ \mu(1 + \epsilon)(u_i + u_j) g_j & (-\omega_0 - \Omega + \bar{\lambda} u_j) \delta_{ij} + \mu(u_i + u_j) g_j \end{pmatrix} \begin{pmatrix} Q_j^+ \\ Q_j^- \end{pmatrix} = 0 \quad (6.59)$$

The total eigenvector is a combination of the two eigenvectors of positive and negative frequency which are of the type:

$$Q_i^\pm = \frac{A + B u_i}{\pm \omega_0 + \bar{\lambda} u_i - \Omega} \quad (6.60)$$

Each entry of this vector gives the position on the transversal plane (as a complex number) of each mode of frequency $\pm \omega_0$ and zenith angle u_i . This matrix equation is easily generalizable to more energy modes. Alternatively, one can determine the eigenvalues Ω by computing the discrete approximation of the integrals

$$I_n = \mu(1 + \epsilon) \sum_{i=0}^{N_u} \frac{u_i^n g_j}{-\omega_0 + \bar{\lambda} u_i - \Omega}, \quad (6.61)$$

and solving for A and B and Ω in eq. (6.44). The two techniques are equivalent. When either of them is solved, one encounters an instability which approaches the continuum instability the larger N_u becomes. However, one also encounters a growing number of other complex eigenvalues whose imaginary part is of similar order to the continuum instability. As one adds bins to the variable

u , these spurious instabilities grow in number but move to higher μ , that is, higher self-coupling strengths are required to excite this instability. These spurious instabilities are what causes the unphysical predictions of few-bins simulations. As one can see, the region of instability can be unphysically extended to ten- or even hundred-fold range of μ values because of these spurious imaginary eigenvalues. The situation becomes far worse when one includes matter effects, as the physical instability is suppressed whereas the spurious ones virtually aren't. For this case, thousands of modes may be required to isolate the real instability.

Though no actual analytical explanation exists for the presence of the spurious instabilities, a bit more insight into their nature can be gained by looking at the eigenvectors of the spurious instabilities versus the physical one. As said, the eigenfunctions of the uniform distribution are arcs of circle. The physical eigenvector describes a set of points that neatly fall on these arcs of circle. On the other hand, the unphysical eigenvectors span almost the complete circle, as shown in figure 6.7. This extreme behavior is best picture on the plot of the norm of the eigenvectors vs. u . The norm of a point on the circle gives a curve that looks like a resonance curve. The difference between the physical and the unphysical instabilities is that the peak falls within the region of u between 0 and 1, while it remains outside this window for the physical eigenvector. Also, the real part of the unphysical eigenvalues appears to be always of opposite sign to that of the physical one.

Further concrete understanding of this phenomenon is lacking. We tried to discretize the equations in terms of Legendre polynomials instead of discrete values of u , yet it lead to very similar results and it seems that the number of modes required to decantate the physical instability is almost identical. Thus no improvement came of it. Whether an appropriate scheme of discretization exists that could avoid these spurious phenomena is a question that remains open.

Furthermore, these spurious modes are not an exclusive phenomenon of discretization. Empirically one finds that spectra with sharp edges tend to produce these effects. One can use instead of spikes a collection of boxes. Again spurious instabilities appear, that require higher and higher μ 's the narrower we make the spaces between them. The same is true for a spectrum where a sudden increase happens. In this case, the instabilities migrate to higher μ 's as one smoothes the step. For some reason, descending steps do not produce spurious configurations, only ascending ones. The realistic spectra are nevertheless smooth spectra which tend to peak at lower u 's, so no physical instabilities of this type should exist. Any such spurious phenomena should be due to effects of the discretization scheme used to simulate the dynamics of the non-linear system.

6.4 Summary

In this chapter, we concluded a long walk towards the study of flavor evolution in the strong neutrino flux escaping the core of a SN. We studied the evolution not in time but in radius and found similar results to the uniform case, with some more complicated features. We summarize them here:

- The analysis is done assuming stationarity and isotropy around the SN;

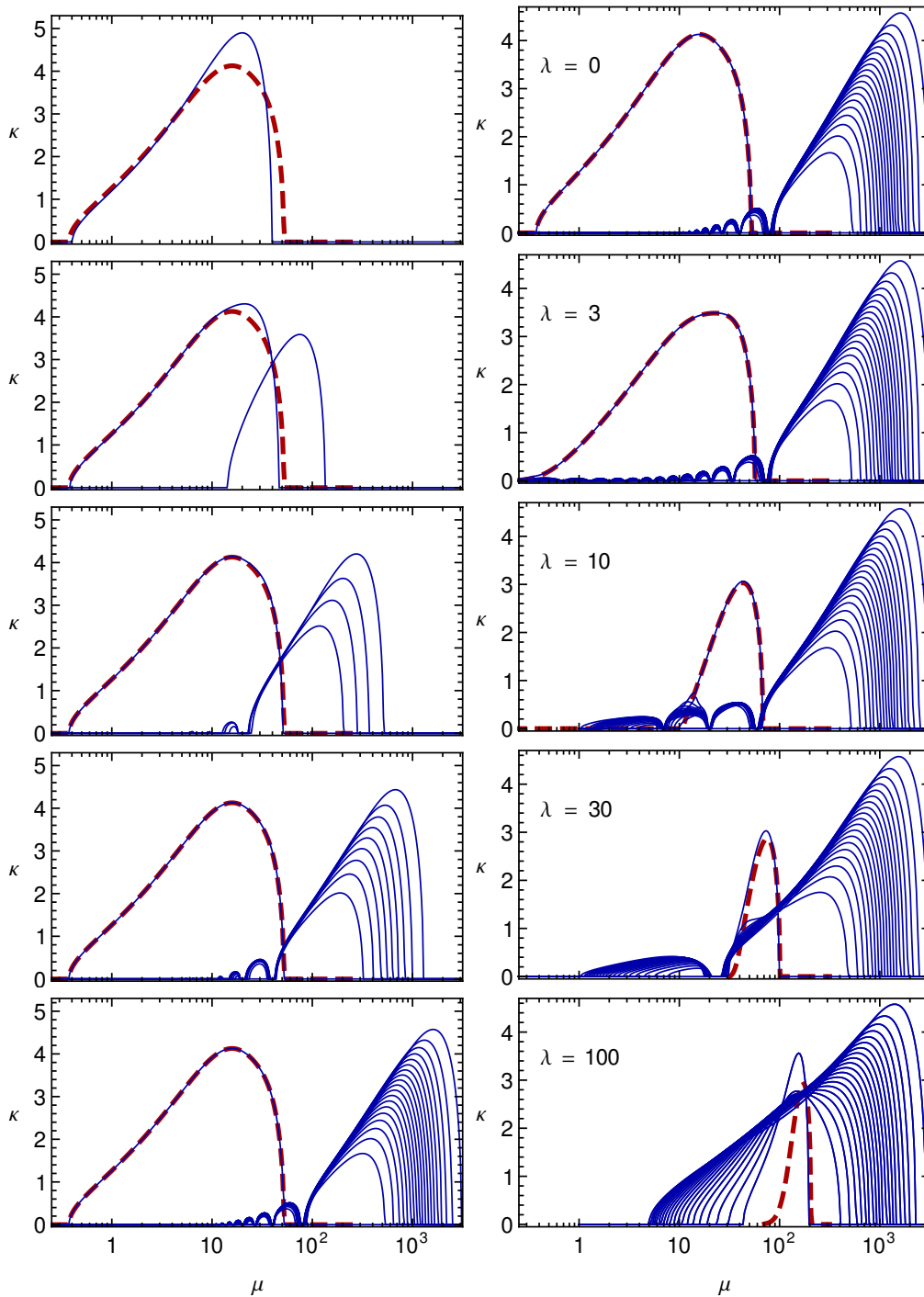


Figure 6.7: *Left panel:* κ vs. μ for a growing number of zenith angular bins $N_u = 1, 2, 5, 10, 20$, for $\lambda = 0$ and $\epsilon = 0.5$, in the IH (MZA) [57]. The red dashed curve shows the continuum limit. The spurious instabilities are seen to appear at high μ and migrate to the right as one increases the binning but never dim in strength.

Right panel: The last case of the left panel ($N_u = 20$) for increasing values of λ . When the matter density becomes too high, the continuum limit is buried under the barely-susceptible-to-matter spurious modes. In these cases hundreds, even thousands of u values may be required to separate the physical instability from the spurious ones.

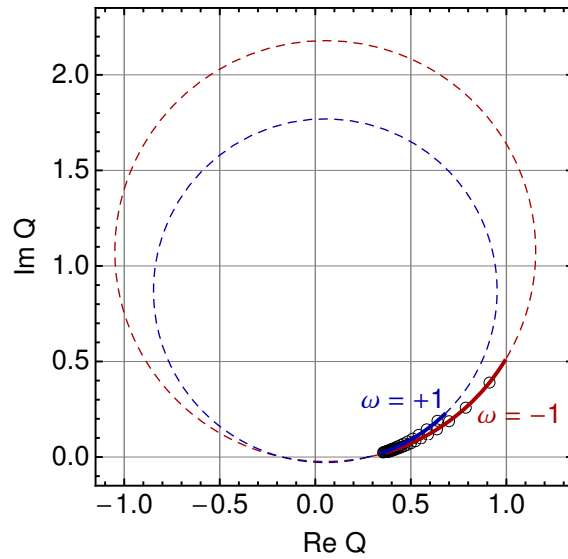


Figure 6.8: The physical eigenconfigurations $Q(\omega = \pm 1, u)$ of the uniform distribution (red and blue solid lines) and their discretized homologi with $N_u = 20$, at $\mu = 50$, $\lambda = 0$ and $\epsilon = 0.5$ [57]. The dashed circles correspond to the full range of u if it were allowed to vary beyond its physical interval of $[0, 1]$.

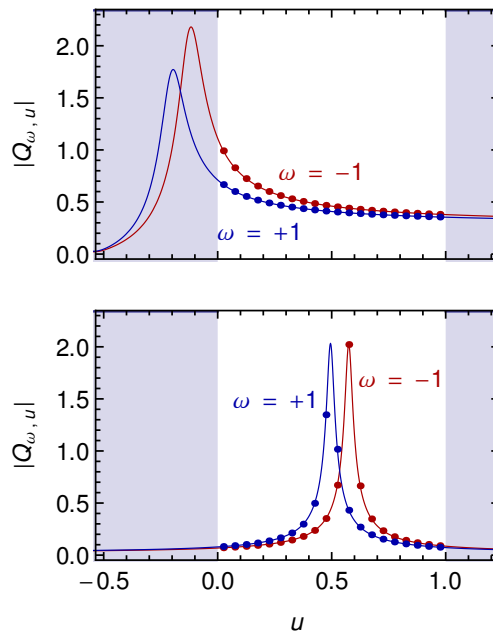


Figure 6.9: Amplitude of the complex numbers $Q(\omega = \pm 1, u)$ for the same case [57]. In addition to the physical configuration we show the spurious ones too. For these, the configuration can span the whole circle as can be seen by the presence of an amplitude resonance in the range $0 < u < 1$.

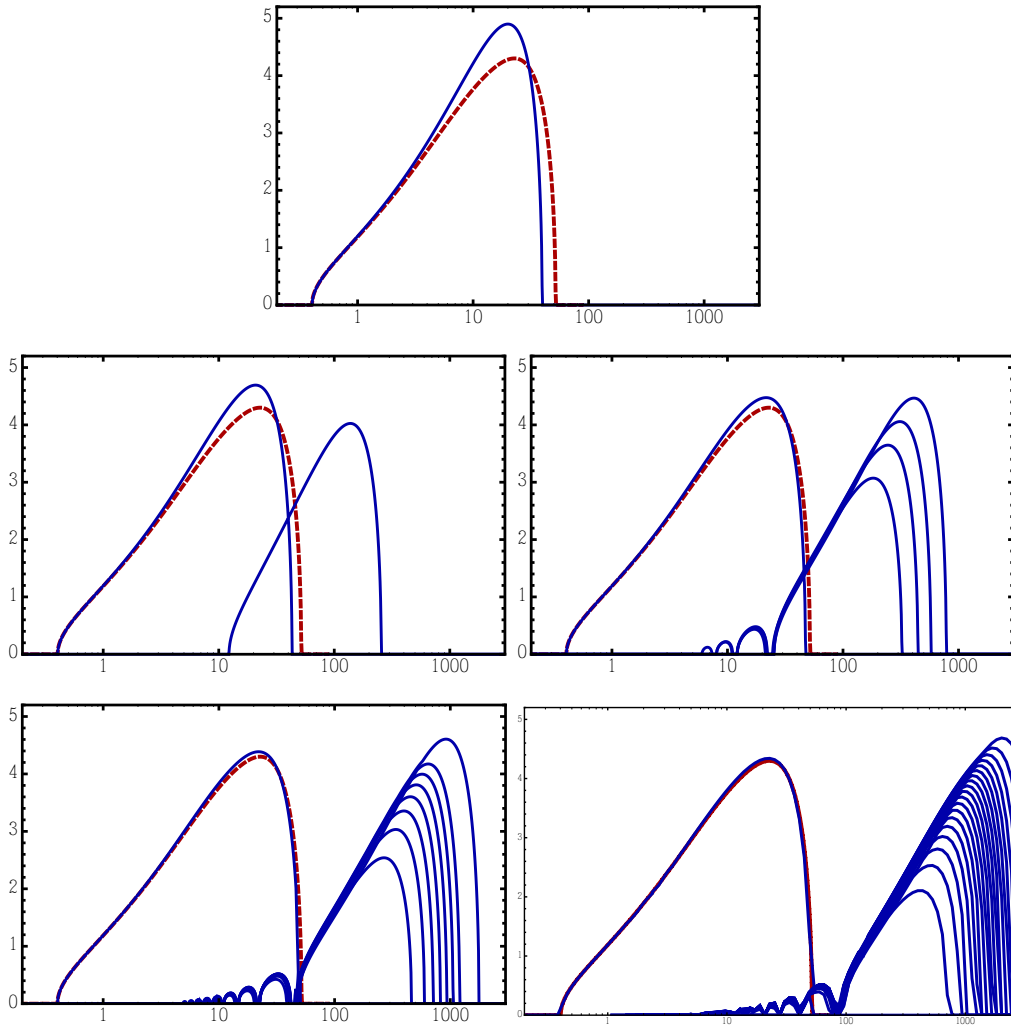


Figure 6.10: κ vs. μ for a growing number of zenith angular bins $N_u = 1, 2, 5, 10, 20$, for $\lambda = 0$ and $\epsilon = 0.5$, in the NH (MAA). The red dashed curve shows the continuum limit. The spurious instabilities are seen to appear at high μ and migrate to the right as one increases the binning but never dim in strength.

- because of the projection of the vacuum and matter oscillation patterns on the radial direction of study, there are angle-dependent matter effects. These can suppress the instabilities and prevent the onset of flavor conversion, unlike the uniform isotropic case where the instabilities were independent of the matter background;
- the scalar non-linear term of the previous chapter also becomes angle-dependent because of the projection on the radial direction; it mixes with the zenith angle term of the vector part of the order parameter, leading to an MZA instability of peculiar properties. This instability is stronger in IH but can also leave small traces for low λ in the NH.

- a vector non-linear term mode of growth of the type encountered in chapter five is preserved around the radial axis, called the MAA instability. If symmetry in the spectrum at the neutrino sphere around this axis is assumed, then this term leads to symmetry breaking like we discussed in the last chapter. This phenomenon only happens in the NH.

The prediction of symmetry breaking from the study of the linear stability was confirmed in simulations, though the instability was shown to be very susceptible to matter suppression and in realistic cases entirely absent. In general, a parametric understanding of these instabilities is still incomplete. There is little understanding on the characteristics that determine the shape of the unstable region in parameter space. Empirically, one finds that forward-peaked spectra tend to suppress the instability even more.

We also discussed how the MZA instability reacts to discretization of the u variable. It turns out that spurious modes, instabilities which are entirely absent in the continuous case, show up, often making numerical simulations very demanding in computing power, especially at high λ . An analytical understanding of these spurious instabilities is still lacking, and whether a discretization scheme of u exists that could avoid them altogether.

There is another matter which requires some attention. Far away from the neutrino sphere where all neutrino rays become parallel, the ambient halo of scattered neutrinos becomes of relevance since it has a much broader, in fact uniform, angular distribution. It has been shown [58] that this can lead to an extension of the parameter space where the MZA instability occurs. For the MAA instability, it was found to be irrelevant. However, these studies make the assumption of stationarity, and this assumption becomes doubtful for these cases. That is because a reflected beam carries information in the opposite direction from the one the equations are being evolved. When doing so, the sign of the vacuum term is flipped because of the $1/v_r < 0$ coefficient, making a neutrino look like an anti-neutrino. If an instability occurs at some distance it could be carried back to lower distances by these backward streaming modes. Preliminary simulations of the interaction of two head-on beams appear to hint at non-trivial behavior. Further work is required to put one's mind at peace.

Conclusions

The quest to understand the behavior of neutrinos in the presence of each other is one which continues to yield new effects. We introduced the known effects of flavor oscillations in the chapters 1 to 3 and deduced the multi-dimensional partial differential equations which describe collective oscillations. But until supercomputers are put to process these multi-dimensional partial differential equations, we will have to rely on our physical intuition to find the right simplifications to elucidate the characteristics of this self-refractive system. Real experimental data would be the most desired commodity in this field, as it would allow us to test our ideas, thereby distinguishing the simple ones from the simplistic ones. Many detectors exist nowadays which are sensitive to the range of energy of supernova neutrinos, and many more are to come. In the future, the deployment of large water, scintillator and argon detectors might allow us to collect individual neutrino events from the Local Group of galaxies [59]. Core-collapse supernova events are relatively rare – once every 2 to 3 decades within the observation range of our neutrino detectors – leading to a lack of data. Right now, the only available observations are of SN1987A, out of which little information beyond the duration and energy of the signal can be extracted.

In the meantime, work is being done to predict the neutrino signal to be seen some day in these experiments. And, sometimes, seemingly sound assumptions are made in order to achieve a more manageable system, both analytically and numerically. The importance of this thesis lies in investigating a common assumption in most of the preceding literature, that an isotropic distribution of flavor is stable under the EoMs, and establishing that in many cases it is not. The first time this phenomenon was observed was in a study of a homogeneous gas of neutrinos [42], where it was observed that an initially isotropic distribution of flavor would excite higher-order multipoles of the distribution. However, it was not until a study of linear stability in the context of supernovae [60] that the full extent of the implications of this work was appreciated. In supernovae, one tracks the stationary evolution of flavor in the radial direction. Until then, it was generally assumed that if this direction is an axis of symmetry of the outgoing neutrino radiation, then the dependence of the equations on the position around this axis could be dropped. In our initial work [60], we showed how this was an incorrect simplification, since the symmetry of the distribution was unstable under the evolution of the system. This is a case of spontaneous symmetry breaking, when the dynamics of the system do not possess the symmetry of the infinitesimal evolution. As a consequence, we

predicted that a region of parameter space where the system remained in the flavor eigenstate under the imposition of symmetry in the normal hierarchy would in fact exhibit non-linear behavior if this imposition is relaxed. This prediction was later confirmed in numerical simulations [53]. In the latter work, it was also shown that the multi-azimuthal-angle instability was more prone to being suppressed by the refractive effects of matter than the axially-symmetric instability of the inverted hierarchy. In any case, the findings were enough to convince the community that from now on that the parameter space had to be scanned for instabilities in both hierarchies and that axial-symmetry should not be imposed. Until the ordering of the neutrino masses is established by measurement, one will have to keep track of the possibility of non-linear motion in both cases. These results were discussed in chapter 6.

To better understand the origin of this spontaneous breakdown of symmetry, the simplest possible model was investigated in an ensemble of opposite moving beams [61] and described in chapter 3. We successfully isolated the crucial ingredient in a one-dimensional model by showing that the non-linear behavior arises in the inverted hierarchy from an exponential growth of a symmetric mode $\mathbf{P}_{\vec{v}} \leftrightarrow \mathbf{P}_{-\vec{v}}$ while in the normal hierarchy it comes from a growth of an anti-symmetric mode $\mathbf{P}_{\vec{v}} \leftrightarrow -\mathbf{P}_{-\vec{v}}$. Physically, this means it is the scalar interaction $\sqrt{2} G_F [\rho_\nu, \rho'_\nu]$ between neutrinos that feeds the anharmonic behavior in the inverted hierarchy, whereas in the normal hierarchy, it is the vector interaction $-\sqrt{2} G_F \vec{v} \cdot \vec{v}' [\rho_\nu, \rho'_\nu]$. Any imposition of directional symmetry prevents the vector interaction in the sub-space of the symmetry, which is why the multi-azimuthal instability was missed in the earlier calculations. On the other hand, because the geometry of the neutrino radiation of a supernova is naturally zenith-angle asymmetric, the multi-zenith-angle instability was accurately predicted in both hierarchies.

Much is left to be done. The discovery of spontaneous symmetry breaking somehow took a blow at the confidence the community had on many of the other simplifications. Stationarity and uniformity [62], absence of spin-flip [9] and the mean-field approximation [29] are some of the examples of the many assumptions that are now under critical scrutiny. The long list of assumptions is one of the reasons why the community is in such dire need of experimental evidence to guide its intuition.

At the same time, even the simplest models of collective oscillations call for a scanning of the many supernova simulations in order to ascertain the onset of anharmonic oscillations with a linear stability analysis as presented in chapter 6. Here, one also faces another source of doubt, the fact that fully-trustworthy simulations of supernova explosions are still inexistent, due to the recollapse of the shockfront in three-dimensional models. In any case, the simulations – despite being unsuccessful at detonating the star – do capture many expected features. They also seem to indicate that the neutrino radiation in the accretion phase is highly anisotropic [49]. If it is so, accurate prediction of the flavor evolution of neutrinos will have to take into account the direction of streaming. Given the additional complication, hard to capture analytically, large-scale numerical simulations might be necessary. We have shown in chapter 6 that spurious instabilities can appear

in multi-angle simulations, demanding tens, hundreds or even thousands of angular bins to avoid them [57]. More analytical insight might be vital before these numerical studies can be undertaken. In this field, numerics and analytics work hand in hand for the improvement of each other.

On the more theoretical side, many questions remain to be answered. A stability analysis of the dynamical fixed point of the EoMs as considered in the context of spectral splits is still lacking. So is an analytical expression for the adiabatic invariants of a general system of many polarization vectors. Such an expression would greatly simplify the calculations of flavor in a system of slowly decreasing $\nu - \nu$ interaction. Finally, a parallelism can be drawn between some effects in the theory of superconductivity and the interplay of different modes of energy in collective flavor oscillations, a parallelism which still waits to be investigated (see references [36, 63]).

The above discussion should be regarded as proof of the vibrant phase the field of collective neutrino flavor oscillations is going through. Much is left to be explored in this recent area of physics where a simple calculation can still yield very significant results. The time we live now is at the transition from a time when the parameters of neutrinos are the focus of studies to an era in which they become a familiar particle whose role in many natural phenomena becomes the centrepiece. Neutrinos may one day be used not as an item of study in itself, but as a probe into the astrophysics of supernovae and of the collision of neutron stars.

Bibliography

- [1] B. Pontecorvo, *Mesonium and anti-mesonium*, Zh. Eksp. Teor. Fiz. 33, 549, 1957; Zh. Eksp. Teor. Fiz. 34, 247, 1958.
Z. Maki, M. Nakagawa, S. Sakata, *Remarks on the Unified Model of Elementary Particles*, Prog. Theor. Phys. 28, 870, 1962.
- [2] E. Kh. Akhmedov, *Neutrino Physics*, Lectures given at Trieste Summer School in Particle Physics, June 7 – July 9, 1999 (arXiv:hep-ph/0001264)
- [3] F. P. An *et al.*, *Observation of electron-antineutrino disappearance at Daya Bay*, Phys. Rev. Lett. 108, 171803, 2012 (arXiv:1203.1669).
- [4] J. Beringer *et al.* (Particle Data Group), *Review of Particle Physics*, Phys. Rev. D 86, 010001, 2012.
- [5] X. Qian, W. Wang, *Reactor neutrino experiments: θ_{13} and beyond*, Mod. Phys. Lett. A 29, 1430016, 2014 (arXiv:1405.7217).
- [6] E. Akhmedov, *Do charged leptons oscillate?*, JHEP 0709, 116, 2007 (arXiv:0706.1216).
- [7] E. Majorana, *Teoria simmetrica dell'elettrone e del positrone*, Nuovo Cimento 5, 171, 1937.
- [8] C. Aalseth *et al.*, *Neutrinoless double beta decay and direct searches for neutrino mass*, summary report of the APS Multidivisional Neutrino Study, 'The Neutrino Matrix' (arXiv:hep-ph/0412300).
- [9] A. Vlasenko, G.M. Fuller, V. Cirigliano, *Prospects for Neutrino-Antineutrino Transformation in Astrophysical Environments*, arXiv:1406.6724.
- [10] V. Cirigliano, G.M. Fuller, A. Vlasenko, *A New Spin on Neutrino Quantum Kinetics*, arXiv:1406.5558.
- [11] A. de Gouvea, S. Shalgar, *Transition Magnetic Moments and Collective Neutrino Oscillations: Three-Flavor Effects and Detectability*, JCAP 1304, 018, 2013 (arXiv:1301.5637).

- [12] R. N. Cahn, D. A. Dwyer, S. J. Freedman, W. C. Haxton, R. W. Kadel, Yu. G. Kolomensky, K. B. Luk, P. McDonald, G. D. Orebi Gann, A. W. P. Poon, *White Paper: Measuring the Neutrino Mass Hierarchy*, White paper prepared for Snowmass-2013 (arXiv:1307.5487).
- [13] W. Winter, *Neutrino mass hierarchy determination with IceCube-PINGU*, Phys. Rev. D 88, 013013, 2013 (arXiv:1305.5539).
- [14] R. Davis, *A review of the Homestake solar neutrino experiment*, Prog. Part. Nucl. Phys. 32, 13 1994).
- [15] D. Vignaud (for the GALLEX Collaboration), *The GALLEX solar neutrino experiment*, Nucl. Phys. B - Proc. Sup., 60, 20, 1998.
- [16] L. Stodolsky, *When the Wavepacket is Unnecessary*, Phys. Rev. D 58, 036006, 1998 (arXiv:hep-ph/9802387).
- [17] B. Dasgupta, G. Raffelt, I. Tamborra, *Triggering collective oscillations by three-flavor effects*, Phys. Rev. D 81, 073004, 2010 (arXiv:1001.5396).
- [18] G. Raffelt, *Stars as Laboratories for Fundamental Physics*, The University of Chicago Press, 1996.
- [19] B. Dasgupta, A. Mirizzi, I. Tamborra, R. Tomás, *Neutrino mass hierarchy and three-flavor spectral splits of supernova neutrinos*, Phys. Rev. D 81, 093008, 2010 (arXiv:1002.2943).
- [20] H. Murayama, *Lecture Notes on Spin*, in Quantum Mechanics I Course, University of California, Berkeley, 2001 (<http://hitoshi.berkeley.edu/221a/spin.pdf>).
- [21] L. Wolfenstein, Phys. Rev. D 17, 2369, 1978; L. Wolfenstein, Phys. Rev. D 20, 2634, 1979; S. P. Mikheyev and A. Yu. Smirnov, Yad. Fiz. 42, 1441, 1985 [Sov. J. Nucl. Phys. 42, 913 (1985)]; S. P. Mikheyev and A. Yu. Smirnov, Nuovo Cimento 9C, 17, 1986.
- [22] A. Bellerive, *Review of Solar Neutrino Experiments*, Int. J. Mod. Phys. A 19, 1167, 2004 (arXiv:hep-ex/0312045).
- [23] C.W. Walter, *The Super-Kamiokande Experiment*, in “Neutrino Oscillations: Present Status and Future Plans”, J. Thomas and P. Vahle editors, World Scientific Publishing Company, 2008 (arXiv:0802.1041).
- [24] N. Jelley, A. B. McDonald, R.G. Hamish Robertson, *The Sudbury Neutrino Observatory*, Annu. Rev. Nucl. Part. Sci. 59, 431, 2009.
- [25] K. Eguchi *et al.* (Kamland Collaboration), *First results from KamLAND: Evidence for reactor antineutrino disappearance* Phys. Rev. Lett. 90, 021802, 2003; Araki, T. *et al.*

- (Kamland Collaboration), *Measurement of neutrino oscillation with KamLAND: Evidence of spectral distortion* Phys. Rev. Lett. 94, 081801, 2005.
- [26] Amol S. Dighe, Alexei Yu. Smirnov, *Identifying the neutrino mass spectrum from a supernova neutrino burst*, Phys. Rev. D 62, 033007, 2000 (arXiv:hep-ph/9907423).
- [27] R. Tomás, M. Kachelriess, G. Raffelt, A. Dighe, H.-T. Janka, L. Scheck, *Neutrino signatures of supernova shock and reverse shock propagation*, JCAP 0409, 015, 2004 (arXiv:astro-ph/0407132).
- [28] G. Sigl, G. Raffelt, *General kinetic description of relativistic mixed neutrinos*, Nucl. Phys. B 406, 423, 1993.
- [29] E. Kh. Akhmedov, J. Kopp, M. Lindner, *Decoherence by wave packet separation and collective neutrino oscillations*, arXiv:1405.7275.
- [30] C. Volpe, D. Väänänen, C. Espinoza, *Extended evolution equations for neutrino propagation in astrophysical and cosmological environments*, Phys. Rev. D 87, 113010, 2013 (arXiv:1302.2374).
- [31] A. Esteban-Pretel, A. Mirizzi, S. Pastor, R. Tomás, G. Raffelt, P. D. Serpico, G. Sigl, *Role of dense matter in collective supernova neutrino transformations*, Phys. Rev. D 78, 085012, 2008.
- [32] S. Pastor, G. Raffelt, D. V. Semikoz, *Physics of Synchronized Neutrino Oscillations Caused by Self-Interactions*, Phys. Rev. D 65, 053011, 2002 (arXiv:hep-ph/0109035).
- [33] G. Raffelt, A.Y. Smirnov, *Self-induced spectral splits in supernova neutrino fluxes*, Phys. Rev. D 76, 081301, 2007; Erratum-ibid. D 77, 029903, 2008 (arXiv:0705.1830).
- [34] G. Raffelt, A. Yu. Smirnov, *Adiabaticity and spectral splits in collective neutrino transformations*, Phys. Rev. D 76, 125008, 2007 (arXiv:0709.4641).
- [35] S. Sarikas, Doctoral Thesis *Neutrino Oscillations at High Densities: Cosmological and Astrophysical Aspects*, University of Naples "Federico II", 2011 (http://www.fedoa.unina.it/8573/1/Sarikas_srdjan24.pdf).
- [36] G. Raffelt, *N-mode coherence in collective neutrino oscillations*, Phys. Rev. D 83, 105022, 2011 (arXiv:1103.2891).
- [37] S. Hannestad, G. G. Raffelt, G. Sigl, Y. Y. Y. Wong, *Self-induced conversion in dense neutrino gases: Pendulum in flavour space*, Phys. Rev. D 74, 105010, 2006; Erratum-ibid. D 76, 029901, 2007 (arXiv:astro-ph/0608695).

- [38] S. Raghavan, A. Smerzi, S. Fantoni, S. R. Shenoy, *Coherent oscillations between two weakly coupled Bose-Einstein condensates: Josephson effects, p oscillations, and macroscopic quantum self-trapping*, Phys. Rev. A 59, 620, 1999.
- [39] M. Albiez, R. Gati, J. Fölling, S. Hunsmann, M. Cristiani, M.K. Oberthaler, *Direct Observation of Tunneling and Nonlinear Self-Trapping in a Single Bosonic Josephson Junction* Phys. Rev. Lett. 95, 010402, 2005.
- [40] H. Duan, G.M. Fuller, Y.-Z. Qian, *Collective neutrino flavor transformation in supernovae*, Phys. Rev. D 74, 123004, 2006 (arXiv:astro-ph/0511275).
- [41] R. S. Hansen, S. Hannestad, *Chaotic flavor evolution in an interacting neutrino gas*, Phys. Rev. D 90, 025009, 2014 (arXiv:1404.3833).
- [42] G. Raffelt, G. Sigl, *Self-induced decoherence in dense neutrino gases*, Phys. Rev. D 75, 083002, 2007 (arXiv:hep-ph/0701182).
- [43] H.-T. Janka, K. Langanke, A. Marek, G. Martinez-Piñedo, B. Müller, *Theory of Core-Collapse Supernovae*, Phys. Rept. 442, 38, 2007 (arXiv:astro-ph/0612072).
- [44] B. Dasgupta, A. Dighe, A. Mirizzi, G. Raffelt, *Spectral split in prompt supernova neutrino burst: Analytic three-flavor treatment*, Phys. Rev. D 77, 113007, 2008.
- [45] H.-T. Janka, L. Scheck, K. Kifonidis, E. Müller, T. Plewa, in ASP Conf. Ser. 332, 2005, *The Fate of the Most Massive Stars*, ed. R. Humphreys and K. Stanek (San Francisco: ASP), 372.
- [46] J. M. Blondin, A. Mezzacappa, *The Spherical Accretion Shock Instability in the Linear Regime*, ApJ 642, 401, 2006.
- [47] I. Tamborra, F. Hanke, B. Müller, H.-T. Janka, G. Raffelt, *Neutrino signature of supernova hydrodynamical instabilities in three dimensions*, Phys. Rev. Lett. 111, 121104, 2013 (arXiv:1307.7936).
- [48] T. Lund, A. Marek, C. Lunardini, H.-T. Janka, G. Raffelt, *Fast time variations of supernova neutrino fluxes and their detectability*, Phys. Rev. D 82, 063007, 2010 (arXiv:1006.1889).
- [49] I. Tamborra, F. Hanke, H.-T. Janka, B. Müller, G. Raffelt, A. Marek, *Self-sustained asymmetry of lepton-number emission: A new phenomenon during the supernova shock-accretion phase in three dimensions*, Astr. J. 792, 96, 2014 (arXiv:1402.5418).
- [50] E. Borriello, S. Chakraborty, A. Mirizzi, P. D. Serpico, I. Tamborra, *(Down-to-)Earth matter effect in supernova neutrinos*, Phys. Rev. D 86, 083004, 2012 (arXiv:1207.5049).
- [51] K. Scholberg, *Supernova neutrino detection*, Ann. Rev. of Nucl. and Part. Sci. Vol. 62, 81, 2012 (arXiv:1205.6003).

- [52] K. Scholberg, *Supernova Early Warning System*, proceedings of "Hotwiring the Transient Universe 2007", eds. A. Allan, J. S. Bloom, R. Seaman, Astron. Nachr. vol. 329, March 2008 (arXiv:0803.0531).
- [53] S. Chakraborty, A. Mirizzi, N. Saviano, D. de Sousa Seixas, *Suppression of the multi-azimuthal-angle instability in dense neutrino gas during supernova accretion phase*, Phys. Rev. D 89, 093001, 2014 (arXiv:1402.1767).
- [54] H. Duan, G.M. Fuller, J. Carlson, Y.-Z. Qian, *Coherent Development of Neutrino Flavor in the Supernova Environment*, Phys. Rev. Lett. 97, 241101, 2006 (arXiv:astro-ph/0608050).
- [55] H. Duan, G.M. Fuller, J. Carlson, Y.-Z. Qian, *Simulation of Coherent Non-Linear Neutrino Flavor Transformation in the Supernova Environment I: Correlated Neutrino Trajectories*, Phys. Rev. D 74, 105014, 2006 (arXiv:astro-ph/0606616).
- [56] S. Chakraborty, A. Mirizzi, *Multi-azimuthal-angle instability for different supernova neutrino fluxes*, Phys. Rev. D. 90, 033004, 2014 (arXiv:1308.5255).
- [57] S. Sarikas, D. de Sousa Seixas, G. Raffelt, *Spurious instabilities in multiangle simulations of collective flavor conversion*, Phys. Rev. D 86, 125020, 2012 (arXiv:1210.4557).
- [58] S. Sarikas, I. Tamborra, G. Raffelt, L. Hüdepohl, H.-T. Janka, *Supernova neutrino halo and the suppression of self-induced flavor conversion*, Phys. Rev. D 85, 113007, 2012 (arXiv:1204.0971).
- [59] S. Ando, J.F. Beacom, H. Yüksel, *Detection of Neutrinos from Supernovae in Nearby Galaxies*, Phys. Rev. Lett. 95, 171101, 2005 (arXiv:astro-ph/0503321).
- [60] G. Raffelt, S. Sarikas, D. de Sousa Seixas, *Axial symmetry breaking in self-induced flavor conversion of supernova neutrino fluxes*, Phys. Rev. Lett. 111, 091101, 2013 (arXiv:1305.7140).
- [61] G. Raffelt, D. de Sousa Seixas, *Neutrino flavor pendulum in both mass hierarchies*, Phys. Rev. D 88, 045031, 2013 (arXiv:1307.7625).
- [62] G. Mangano, A. Mirizzi, N. Saviano, *Damping the neutrino flavor pendulum by breaking homogeneity*, Phys. Rev. D 89, 073017, 2014 (arXiv:1403.1892).
- [63] E. A. Yuzbashyan, *Normal and anomalous solitons in the theory of dynamical Cooper pairing*, Phys. Rev. B 78, 184507, 2008 (arXiv:0807.3181).

Acknowledgements

If one life lesson can be learned from the study of non-linear dynamics, it is that in real life it is very hard to single out the contribution of each discrete agent. Therefore, I would like to restrict my acknowledgement to people without whom this thesis would not exist. I should, of course, thank my parents for supporting me and, well, having me. Without me, this thesis would definitely not exist. But in that case I should also thank my friends for making my life enjoyable during these four years. And maybe their parents too for raising them to be the lovely people they are. That can't have been easy. And my grandparents too. Without them, this thesis would not exist. And, though we have only just began and there are many more people to mention, I sort of get already the impression that down this road of generous acknowledgements, there is a little cell who – by splitting and starting all life on Earth – is going to take the credit for this whole thesis. I can't have that. No ancient cell is snatching from my hands a posthumous honorary PhD.

The people I really need to thank are those whom I do not have a better way of thanking than this one. No other person deserves more my heartfelt thanks than my supervisor, Georg Raffelt. His insights have, no doubt, shaped my way of thinking more than he knows and, probably, more than I know myself. He taught me how to put to practice the pleasure of searching simple answers to complex problems. But most of all, without his olympic patience I would have failed this PhD a numerable number of times. I am truly thankful for having been his student.

My colleagues, Sovan Chakraborty, Srdjan Sarikas, Javier Redondo and Ignacio Izaguirre also deserve a very strong thank you. They put up with me. A lot.

I must also acknowledge and give thanks to all the Portuguese people for their efforts to preserve and support the Fundação para a Ciência e a Tecnologia which awarded me the needed funding in a time of great need. You may all add me on facebook.